A Fundamental Study of Self-association Behavior of Highly Polar Molecules in Solution

A doctoral thesis

by

Shunzo Takabatake

Submitted to

Department of Symbiotic Science of Environment and Natural Resources

United Graduate School of Agricultural Science

Tokyo University of Agriculture and Technology

2017

Acknowledgements

The author would like to express the deepest appreciation to Professor Toshiyuki Shikata for his insightful comments, constructive suggestions and warm encouragement.

The author is indebted to Horiba Ltd. (Kyoto) for their kind permission to use the XploRA Plus confocal Raman microscope installed in an application center at their Tokyo office. The author is also indebted to Miss Tomoko Numata of Horiba for her kind technical support in the Raman spectrum measurements and her fruitful discussion on the data obtained in this study (Chapter 4).

The author would like to thank Professor Takayuki Okayama, Professor Natsuki Kasuya, Professor Masao Takayanagi and Professor Shinso Yokota for useful discussion.

The author is grateful to the late Professor Hideharu Ushiki for his guidance and encouragement.

Shunzo Takabatake

A Fundamental Study of Self-association Behavior of Highly Polar Molecules in Solution

Chapter 1 General Introduction

1.1. Overview

Much of the current research including pharmacology, medicine, biology and environmental science requires the knowledge on dissolving behaviors of solute molecules such as the structures of solutions, solute–solvent interactions, solvent–solvent interactions, solute-solute interactions and chemical equilibria.

In particular, intermolecular association behavior is often observed in solutions of various kinds of polar compounds. As the concentration of solute molecule increases, dimers and other higher order intermolecular associations may form in the solution. The susceptibility of the association formation also depends on its molecular structure, kinds of solvents, temperature and pressure, and the association phenomena strongly influence physico-chemical characteristics of the solutions.

The molecular interactions in solutions, however, are so complicated and intricate that it is practically impossible to investigate them individually. In addition, the effects of the molecular interactions may be observed in different ways, depending on the method of investigation. Hence, comprehensive assessment by comparing the data obtained by the various kinds of methods is necessary to achieve an overall understanding of the system.

As a result of numerous experimental studies, the aggregation or association constants have been determined for a number of dyes and pigments,[1–9] alcohols,[10–15] carboxylic acids,[16] 2-pyrrolidinone,[17–22] aldehydes,[23,24] amides,[25,26] amino acid,[27] indole derivative,[28] hydrophosphorous acid,[29] nitrile compounds[30,31] and some other aromatic compounds[32–34] in solution using various methods including absorption and fluorescence spectroscopy, nuclear magnetic resonance (NMR) spectroscopy, infrared (IR) spectroscopy, Raman spectroscopy and dielectric spectroscopic measurements. Nevertheless, in self-association phenomena, the effect of dipole–dipole interaction has not been paid enough attention compared with that of hydrogen bond, and the details of the contribution of dipole–dipole interactions to intermolecular association still remain as open questions necessary for further discussion.

In this thesis, self-association behavior, in particular anti-parallel dimerization behavior of some highly polar low mass compounds in solution was investigated to not only quantitatively evaluate the anti-parallel dimer formation but also to elucidate dynamics controlling the association phenomena, providing valuable information on the structure formed by the intermolecular

associations, which will be useful to improve solution properties for practical application.

Chapter 2 shows principles of experimental techniques and their details used in this thesis.

Chapter 3 describes anti-parallel dimer formation of liquid crystal forming (5CB and 8CB) and also not forming (3CB and 4CB) 4-cyano-4′-alkylbiphenyls (*n*CB) in isotropic cyclohexane solution.

Chapter 4 describes the chemical equilibrium for the anti-parallel dimer formation of ethylene carbonate (EC) in solution of pure solvents, such as benzene (Bz) and dimethyl carbonate (DMC).

Chapter 5 discusses the formation dynamics and the solvent dependence of anti-parallel dimers of EC in solutions of Bz and DMC in detail.

Chapter 6 briefly summarizes all of the discussion in this thesis.

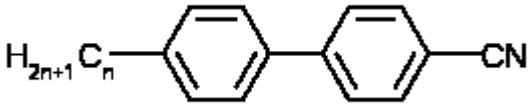

*n*CB: 4-cyano-4′-alkylbiphenyl (*n* = 3, 4, 5 and 8)

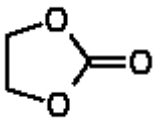

EC: ethylene carbonate

Fig.1.1. Compounds investigated

1.2. References

[1] Y. Lu and A. Penzkofer, *Chem. Phys.*, 1986, **107**, 175.

[2] F. L. Arbeloa, P. R. Ojeda and I. L. Arbeloa, *J. Chem. Soc., Faraday Trans. 2*, 1988, **84**, 1903.

[3] K. Kemnitz and K. Yoshihara, *J. Phys. Chem.*, 1991, **95**, 6095.

[4] C. T. Lin, A. M. Mahloudji, Li Li and M. W. Hsiao, *Chem. Phys. Lett.*, 1992, **193**, 8.

[5] P. Bojarski, A. Matczuk, C. Bojarski, A. Kawski, B. Kukliński, G. Zurkowska and H. Diehl, *Chem. Phys.*, 1996, **210**, 485.

[6] F. Würthner, S. Yao, T. Debaerdemaeker and R. Wortmann, *J. Am. Chem. Soc.*, 2002, **124**, 9431.

[7] A. Ghanadzadeh, A. Zeini, A. Kashef, and M. Moghadam, *J. Mol. Liq.*, 2008, **138**, 100.

[8] H. Sun, Y. Zhao, Z. Huang, Y. Wang and F. Li, *J. Phys. Chem. A*, 2008, 112, 11382.

[9] A. Ghanadzadeh Gilani, M. Moghadam, S.E. Hosseini and M.S. Zakerhamidi, *Spectrochim. Acta A*, 2011, **83**, 100.

[10] P. Bordewijk, P. Kunst and A. Rip, *J. Phys. Chem.*, 1973, **77**, 548.

[11] G. Brink and L. Glasser, *J. Phys. Chem.*, 1978, **82**, 1000.

[12] M. Kunst, D. van Duijn and P. Bordewijk, *Ber. Bunsenges. Phys. Chem.*, 1979, **83,** 840.

[13] M. Kunst, D. van Duijn and P. Bordewijk, *Z. Natureforsch*, 1979, **34**a, 369.

[14] G. M. Førland, Y. Liang, O. M. Kvalheim, H. Høiland and A. Chazy, *J. Phys. Chem. B*, 1997, **101**, 6960.

[15] M. A. Czarnecki and K. Orzechowski, *J. Phys. Chem. A*, 2003, **107**, 1119.

[16] J.O. Jenkins and J. W. Smith, *J. Chem. Soc. B: Phys Org.*, 1970, 1538.

[17] J. A. Walmsely, E. J. Jacob and H. B. Thompson, *J. Phys. Chem.*, 1976, **80**, 2745.

[18] J. A. Walmsley, *J. Phys. Chem.*, 1978, **82**, 2031.

[19] J. Jadzyn, J. Malecki and C. Jadzyn, *J. Phys. Chem.*, 1978, **82**, 2128.

[20] D. P. McDermott, *J. Phys. Chem.*, 1986, **90**, 2569.

[21] K. De Smet, P. Kedziora, J. Jadzyn and L. Hellemans, *J. Phys. Chem.*, 1996, **100**, 7662.

[22] H. Yekeler, A. Gaven and R. Ozkan, *J. Comput. Aided Mol. Des.*, 1999, **13**, 589.

[23] N. Karger, A. M. Amorim da Costa and P. J. A. Ribeiro-Claro, *J. Phys. Chem. A*, 1999, **103**, 8672.

[24] A. G. Gilani, M. Mamaghani and L. Anbir, *J. Sol. Chem.*, 2003, **32**, 625.

[25] M. M. Kopecni, R. J. Laub and D. M. Petkovic, *J. Phys. Chem.*, 1981, **85**, 1595.

[26] P. Kędziora and J. Małecki, *Adv. Mol. Relax. Processes*, 1980, **17**, 141.

[27] J. Huang, T. C. Stringfellow and L. Yu, *J. Am. Chem. Soc.*, 2008, **130**, 13973.

[28] J. A. Walmsley, *J. Phys. Chem.*, 1981, **85**, 3181.

[29] J. A. Walmsley, *J. Phys. Chem.*, 1984, **88**, 1226.

[30] T. Takagi, H. Fujiwara and Y. Sakai, *Bull. Chem. Soc. Jpn.*, 1984, **57**, 1299.

[31] M. Banno, A. Kotani, K. Ohta and K. Tominaga, *Bull. Chem. Soc. Jpn.*, 2014, **87**, 470.

[32] D. B. Davies, L. N. Djimant and A. N. Veselkov, *J. Chem. Soc., Faraday Trans.*, 1996, **92**, 383.

[33] A. J. Charlton, A. L. Davis, D. P. Jones, J. R. Lewis, A. P. Davies, E. Haslamc and M. P. Williamson, *J. Chem. Soc., Perkin Trans.2*, 2000, 317.

[34] D. Rudan-Tasic, C. Klofutar and M. Bešter-Rogač, *Monatsh. Chem.*, 2011, **142**, 19.

Chapter 2 Fundamentals of Experimental Techniques

2.1. Dielectric relaxation

Dielectric relaxation measurements are very useful techniques for the investigation of dynamics of molecules that have dipole moments, and therefore for the characterization of intermolecular interactions such as solute–solute and solvent–solute intermolecular interactions. Valuable information on the origins and strength of intermolecular interactions can be determined by using dielectric relaxation measurements.

2.1.1. Static electric polarization

When an electric field applied to polar molecules which have permanent dipole moments like water molecule, slight displacement of electrons is induced, resulting in electronic polarization in the molecule. In addition, the permanent dipole of molecules responds to the electric field and causes macroscopic polarization (orientational polarization). After defining the static permittivity in this part, we will discuss time (or frequency) dependent responses of tested polar molecules to the applied electric field in the following part.

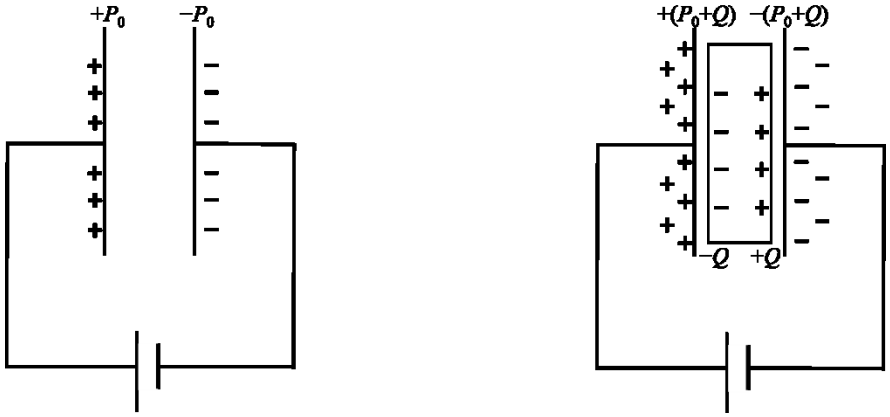

Fig. 2.1. (a) A charged parallel plate capacitor in vacuum; (b) a charged parallel plate capacitor with an insulator between the plates.

Consider two parallel electrode plates separated in vacuum as shown in Fig. 2.1(a), which are applied with a static electric field $\boldsymbol{E}$. The electric field applied to these plates causes a surface charge density $\boldsymbol{P}_0$ that is proportional to $\boldsymbol{E}$. $\boldsymbol{P}_0$ is the macroscopic dipole moment per unit volume and therefore is given by $\boldsymbol{P}_0 = \varepsilon_v \boldsymbol{E}$, where ε_v denotes the electrical permittivity of vacuum. If the electrode plates are now filled with a perfect insulator as shown in Fig. 2.1(b), another charge

density $\boldsymbol{Q}$ is newly introduced on the electrode surfaces to neutralize the polarization caused by the insulator. A quantity called electric displacement, $\boldsymbol{D}$, is defined as $\boldsymbol{D} \equiv \boldsymbol{P}_0 + \boldsymbol{Q}$, which is the total charge density on the electrode surface. $\boldsymbol{D}$ and $\boldsymbol{E}$ satisfy the following relationship:

$$\boldsymbol{D} = \boldsymbol{P}_0 + \boldsymbol{Q} = \varepsilon_v(1+\chi)\boldsymbol{E} = \varepsilon_r\varepsilon_v\boldsymbol{E} \tag{2.1.1}$$

where χ is the dielectric susceptibility meaning a proportional constant of $\boldsymbol{Q}$ to $\boldsymbol{E}$, and ε_r means the relative permittivity of an inserted dielectric substance (the insulator), which quantifies a material dependent characteristics demonstrating how much the dielectric substance causes polarization charge density relative to vacuum under the application of the static electric field. The value of ε_r is a numerical number greater than unity. Then, all the materials store more electric energy than vacuum space when they are subjected to an electric field.

2.1.2. Frequency dependency of a dielectric permittivity

Now, supposing application of a dynamic electric field given by $E(\omega) = E_0\cos\omega t$, where ω is the angular frequency, to the electrode plates filled with the perfect dielectric substance or insulator, the response of electric displacement $D(\omega)$ can be written as

$$D(\omega) = \varepsilon_r\varepsilon_v E_0 \cos\omega t \tag{2.1.2}$$

without phase delay. However, in general cases, the substance inserted in electrode plates is not perfect insulator but slightly conductive material. Then, $D(\omega)$ can be given as

$$D(\omega) = D_0 \cos(\omega t - \delta), \tag{2.1.3}$$

where D_0 is the amplitude of electric displacement and δ is the phase difference between $D(\omega)$ and $E(\omega)$. The quantity δ is constant for a given frequency, but depends on the frequency. $D(\omega)$ is split into orthogonal parts:

$$D(\omega) = D_0 \cos(\omega t - \delta) = D_0 \cos\delta\cos\omega t + D_0 \sin\delta \sin\omega t\,. \tag{2.1.4}$$

As an in-phase component and a 90° phase lag (or out-of-phase) component, the dielectric constant, ε', and the dielectric loss, ε'', are defined as follows, respectively:

$$\varepsilon' = \frac{D_0\cos\delta}{\varepsilon_v E_0} \quad , \quad \varepsilon'' = \frac{D_0\sin\delta}{\varepsilon_v E_0}\,. \tag{2.1.5}$$

For the mathematical convenience, the applied electric field can be expressed in terms of a complex number as

$$E^* = E_0 \exp(i\omega t) = E_0(\cos\omega t + i\sin\omega t)\,. \tag{2.1.6}$$

Then the electric displacement can be also given by

$$\begin{aligned} D^* &= D_0 \exp[i(\omega t - \delta)] = D_0 \exp(-i\delta)\exp(i\omega t) \\ &= D_0(\cos\delta - i\sin\delta)(\cos\omega t + i\sin\omega t) \\ &= (\varepsilon' - i\varepsilon'')\varepsilon_v E_0(\cos\omega t + i\sin\omega t) \end{aligned} \quad . \qquad (2.1.7)$$

Equivalently this relation can be written as the same form as eqn (2.1.1)

$$\boldsymbol{D}^*(\omega) = \varepsilon^* \varepsilon_v \boldsymbol{E}^*(\omega), \qquad (2.1.8)$$

where

$$\varepsilon^* = \varepsilon' - i\varepsilon''. \qquad (2.1.9)$$

The real part of the complex dielectric constant, ε', represents the ability of a material to store electrical energy of the applied electric field. On the other hand, the imaginary part of the complex dielectric constant, ε'', refers to the loss of energy of the electric field in the material, which is converted into heat. Dependence of complex permittivity, ε^*, on frequency, ω, is sometimes called dielectric dispersion.

Dielectric relaxation techniques are quite useful methods to investigate rotational motion of polar molecules because the rotation of permanent dipole moments of polar molecules is none other than that of the polar molecules themselves.

Relationship between dielectric constant and index of refraction

In the frequency range of optics, it is convenient to define a complex index of refraction (or a complex refractive index):

$$n^* = n - i\kappa. \qquad (2.1.10)$$

Here, n is the refractive index which contributes to the phase effect (time delay or variable velocity), and is a measure for how much the speed of light is reduced inside the medium. The value κ is the extinction coefficient (or the absorption constant) which indicates the amount of absorption loss. At optical frequencies there is a simple relationship between dielectric constant and refractive index in a non-magnetic material discussed in this thesis:

$$\begin{aligned} n^* &= \sqrt{\varepsilon^*} = \sqrt{\varepsilon' - i\varepsilon''} \\ \varepsilon' &= n^2 - \kappa^2 \\ \varepsilon'' &= 2n\kappa \\ n^2 &= \frac{1}{2}\left[\sqrt{\varepsilon'^2 + \varepsilon''^2} + \varepsilon'\right] \\ \kappa^2 &= \frac{1}{2}\left[\sqrt{\varepsilon'^2 + \varepsilon''^2} - \varepsilon'\right] \end{aligned} \quad . \qquad (2.1.11)$$

2.2. Steady-state fluorescence spectroscopy

Fluorescence is widely used in many research fields involving biochemistry, medicine and basic chemistry due to its high sensitivity and selectivity. Fluorescence spectroscopy, mainly used for measuring compounds in solution, is a type of electromagnetic spectroscopy that measures the intensity of photons emitted from a sample after it has absorbed photons.

Steady-state fluorescence spectroscopy measures the long-term average fluorescence of a sample, and both excitation spectrum (the light absorbed by a sample) and/or emission spectrum (the light emitted by the sample) can be measured. Fluorescence emission spectra are recorded at the fixed wavelength of the excitation light, and the fluorescence emission is scanned as a function of wavelength. On the other hand, excitation spectra are recorded at the fixed emission light wavelength, and excitation light is scanned as a function of wavelength. The excitation spectra generally resemble to the absorption spectra of measured sample.

2.2.1. The origin of fluorescence

Fluorescence is the emission of light from a substance that has absorbed light or other electromagnetic radiation, and occurs from electronically excited states.

The energy of photon is supplied and absorbed by a fluorescent substance (fluorophore), generating an electronically excited state when the energy of photon is equal to energy gap between the ground state and the excited state of the fluorophore. These transitions typically occur in the time scale of about 10^{-15} s. This time scale is too short for displacement of nuclei included in fluorophores (Frank-Condon principle).

Following excitation light absorption, fluorophores that has been exited to some higher vibrational levels of S_n (n: quantum number and $n > 1$ for excited states) rapidly relax to the lowest vibrational level of S_1 within about 10^{-12} s. This process is called internal conversion. Because the part of exciting energy is dissipated as heat to the matrix or solvent in the relaxation process, the emitted light has a longer wavelength than the absorbed light. Since fluorescence lifetimes of aromatic molecules bearing π-electron systems are typically 10^{-9}–10^{-8} s, the molecules reach equilibrium states within their fluorescence lifetimes. Fluorescence emission is a luminous transition from this state to the ground Frank-Condon state.

In the case of aromatic hydrocarbons, since fluorophores relax to some vibrational levels belonging to the ground state, fine vibrational structures are often observed in fluorescence emission spectra. Fluorescence emission spectra are generally independent of excitation wavelength

so long as all the fluorescence is emitted from the lowest excited singlet state.

2.2.2. Excimers

Interactions between molecules in the excited singlet state and other molecules in the ground state cause another fluorescence emission anew such as excimer emission on occasions.

An excimer, the term *excimer* is an abbreviation for an excited-state dimer and was introduced by Stevens and Hutton in 1960[1] to describe D^*, is an excited complex formed by the association of excited and unexcited monomer molecules which have a definite fluorescence lifetime.[2]

Possible luminous reactions of monomers and excimers in solution are summarized in Table 2.1.[3,4] M and D represent monomer and dimer molecules respectively, an asterisk denotes excited state, and c necessary in the mode (iii) means the concentration in moles per liter.

Table.2.1. Reaction Scheme

	Modes reactions	Rate parameter (sec^{-1})	Process
(i)	$M^* \rightarrow M + h\nu_M$	k_{fM}	fluorescence of M^*
(ii)	$M^* \rightarrow M$	k_{iM}	internal quenching of M^*
(iii)	$M^* + M \rightarrow D^*$	$k_{DM}\,c$	excimer formation
(iv)	$D^* \rightarrow M + M + h\nu_D$	k_{fD}	fluorescence of D^*
(v)	$D^* \rightarrow M + M$	k_{iD}	internal quenching of D^*
(vi)	$D^* \rightarrow M^* + M$	k_{MD}	regenerating of M^* from dissociation of D^*

2.3. Time-resolved fluorescence spectroscopy

Time-resolved fluorescence spectroscopy is one of extensions of steady-state fluorescence spectroscopy. Here, the fluorescence of a sample is monitored as a function of an elapse time after excitation by use of a pulse shape excitation light source. Fluorescence lifetimes, which are characteristic quantities for each fluorophore, can be determined from fluorescence decay curves observed in extraordinary short time domains ranged from picoseconds to nanoseconds.

2.3.1. Determination of fluorescence lifetime

Now, we consider excitation of a sample containing the fluorophore by using an infinitely sharp

(δ-function type) pulse of light. This yields an initial population (n_0) in the excited state. The decay of the excited-state population is described by the next equation using a rate $k_r + k_{nr}$,

$$\frac{dn(t)}{dt} = -(k_r + k_{nr})n(t), \qquad (2.3.1)$$

where $n(t)$ is the number of excited molecules at time t, k_r is the radiative transition rate, and k_{nr} is the non-radiative transition rate. Since emission occurs randomly, and each excited molecule has the same probability of emitting in a given period of time, the decay of the excited population is described by an exponential decay law:

$$n(t) = n_0 \exp(-t/\tau), \qquad (2.3.2)$$

where the fluorescence lifetime, τ, is the reciprocal of the total decay rate, $\tau = (k_r + k_{nr})^{-1}$.

In fluorescence experiments the number of excited molecules is not observed, but fluorescence intensity, which is proportional to $n(t)$, is directly observed. Hence, eqn(2.3.1) can also be written in terms of the time-dependent fluorescence intensity $I(t)$. Integration of eqn(2.3.1) yields the expression for a single exponential decay as

$$I(t) = I_0 \exp(-t/\tau), \qquad (2.3.2)$$

where I_0 is the fluorescence intensity at the time $t = 0$. The fluorescence lifetime τ is recognized to be the time for fluorescence intensity to decrease down to the value of $1/e$ (e is the base of natural logarithm) or ~37% of the initial intensity.

The fluorescence quantum yield, Φ, which is defined as the ratio of photons emitted to photons absorbed, is related to the fluorescence lifetime τ as given by

$$\Phi = \frac{k_r}{k_r + k_{nr}} = k_r \tau . \qquad (2.3.3)$$

Although the decay behavior is based on the first order kinetics in general, practically observed fluorescence decays are sometimes more complicatedly influenced by the chemical composition of environments for the tested systems. Many additional processes like quenching, charge transfer, solvation dynamics also have an effect on the decay kinetics and can lead to multi- or non-exponential decay behavior. For more complex systems like heterogeneous environments, fluorescence decay function $I(t)$ is often represented by a multi-exponential model:

$$I(t) = \sum_i \alpha_i \exp(-t/\tau_i), \qquad (2.3.4)$$

where the values of α_i and τ_i are the pre-exponential factors and the decay times for each mode, respectively. Relationship between the steady-state and time-resolved measurements is given by the

relationship

$$I_{ss} = \int I_0 \exp(-t/\tau) dt = I_0 \tau \,, \tag{2.3.5}$$

where I_{ss} is the steady-state fluorescence intensity.

The impulse response function $I(t)$ given in eqn 2.3.2 is what would be observed only for pulse excitation light source using instruments possessing δ-function type quick response. In practice, the impulse response function cannot be measured directly because the excitation pulse is not δ-function type, and in addition, instruments have a certain characteristic response time. This is quantified by the instrument response function (IRF), $L(t)$, which is individually determined as a particular response of each instrument to a scattered excitation pulse instead of the sample. Then, an excitation pulse is assumed to be the summation of a series of δ-functions with different amplitudes. Each of these δ-functions excites an impulse response from the sample, whose intensity is proportional to the height of the δ-function. The measured response is the sum of all these impulse responses which start with different amplitudes and at different times. In brief, the measured fluorescence decay, $N(t)$, is the convolution of decay functions responding to a δ-function type excitation pulse characterized by the detection system given by

$$N(t) = \int_0^t L(t') I(t - t') dt' \,, \tag{2.3.6}$$

where $I(t - t')$ denotes the fluorescence intensity from the sample at time t, originating as a response to a δ-function type excitation pulse at time t'.[5] For convenience replacing t' with dummy variable of integration, $t - \mu$, so that the convolution integral is expressed as

$$N(t) = \int_0^t L(t - \mu) I(\mu) d\mu \,. \tag{2.3.7}$$

Here, our task is the determination of the best matching fluorescence decay function $I(\mu)$ to the experimental data.

Goodness of the fit procedure is evaluated by using the value of reduced chi-square χ_R^2 given by

$$\chi_R^2 = \frac{\chi^2}{n - p} = \frac{\chi^2}{v} \,, \tag{2.3.8}$$

where n is the number of datapoints, p is the number of floating parameters, $v = n - p$ is the number of degrees of freedom. The value χ^2 is goodness-of-fit parameter, which is given by

$$\chi^2 = \sum_{k=1}^{n} \frac{1}{\sigma_k^2} [N(t_k) - N_c(t_k)]^2 = \sum_{k=1}^{n} \frac{[N(t_k) - N_c(t_k)]^2}{N(t_k)} \quad , \tag{2.3.9}$$

where $N_c(t_k)$ is the calculated decay and σ_k is the standard deviation of each datapoint at time t_k. If only random errors contribute to χ_R^2, then this value is expected to be near unity.

2.3.2. Streak cameras

Streak cameras can simultaneously provide two-dimensional fluorescence information: time and wavelength, at high time resolution of several ps.[6–15] A streak camera consists of a vacuum tube (streak tube) which transfers a fluorescence signal distributed as a function of wavelength (wavelength axis) by using a polychromator into a two-dimensional detector (time axis) converting single-photon detection at the high time resolution.

Figure 2.2 shows the operating principle of the streak camera. The details are as follows. The fluorescence light signal dispersed according to wavelengths passes through an incident slit and is projected on the surface of photocathode. The incident light on the photocathode is converted into a number of electrons proportional to the intensity of the light. Then, after passing through a pair of accelerating electrodes, they pass through a pair of sweep electrodes where serrate pulse voltage is applied at a synchronized timing to the incident light. The electrons dispersed by the electrodes are bended perpendicularly to the length of the incident slit there and enter the micro-channel plate (MCP). The electrons are multiplied by several thousands of times passing through the MCP, after which they are converted into optical image again on a surface of a phosphor screen. On the phosphor screen, the phosphor images are arranged in sequential order from top to bottom in accordance with the arrival time. Hence, the streak camera can provide simultaneous measurements

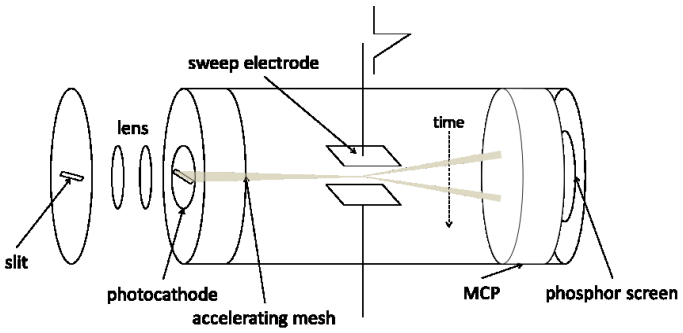

Fig. 2.2. Operating principle of the streak tube.

of both wavelength and time-resolved decays.

2.4. Raman spectroscopy

The Raman spectroscopy detects the vibrational motions occurring in molecules like the infrared (IR) spectroscopy. The physical method of observing the vibrations is, however, different from the IR spectroscopy. In Raman spectroscopy one measures the light scattering while the IR spectroscopy is based on absorption of photons. Since their selection rules are different from each other, the Raman spectroscopy and IR spectroscopy can be treated complementarily. They are widely used to obtain information relating to chemical structures, and to identify substances from the characteristic spectral patterns. In Raman spectroscopy samples can be examined in a whole range of physical states; for example, as vapors, liquids, solutions or solids, in vacuum or under high pressure, in hot or cold states, or as surface layers in a nondestructive manner.

Classical description of the Raman phenomenon is shown as follows:

Consider a molecule without a permanent dipole moment. An oscillating electric field, $\boldsymbol{E}$, induces a dipole moment, $\boldsymbol{p}$:

$$\boldsymbol{p} = \boldsymbol{\alpha} \cdot \boldsymbol{E}, \tag{2.4.1}$$

which can also be expressed

$$\begin{pmatrix} p_x \\ p_y \\ p_z \end{pmatrix} = \begin{pmatrix} \alpha_{xx} & \alpha_{xy} & \alpha_{xz} \\ \alpha_{yx} & \alpha_{yy} & \alpha_{yz} \\ \alpha_{zx} & \alpha_{zy} & \alpha_{zz} \end{pmatrix} \begin{pmatrix} E_x \\ E_y \\ E_z \end{pmatrix}. \tag{2.4.2}$$

The quantity $\boldsymbol{\alpha}$ is the polarizability tensor. The polarizability varies with every vibrational motion of the molecule. An oscillating dipole moment emits an electromagnetic wave with the frequency of the incident field, $\boldsymbol{p}(\nu_0)$, (Rayleigh scattering) in phase with the incident field, ν_0. In addition, the molecule radiates electromagnetic waves with two frequencies: positive and negative shifted ones by the frequency of the molecular vibration, ν (Raman scattering). The Raman scattered light has a lower frequency than the incident light, $\boldsymbol{p}(\nu_0 - \nu)$, (Stokes-Raman scattering) or a higher frequency, $\boldsymbol{p}(\nu_0 + \nu)$, (anti-Stokes-Raman scattering).

According to the classical theory of the electromagnetism, the Raman-scattering intensity for an optically isotropic sample is given by

$$I = \frac{\pi^2 N_i}{\varepsilon_0^2 c^4} (\nu_0 \pm \nu)^4 I_0 \left\langle \left(\alpha_{\rho\sigma}^R \right)^2 \right\rangle, \tag{2.4.3}$$

where ε_0 is the electric permittivity of a vacuum, I_0 is the intensity of incident light, N_i is the number of molecules in the initial state i and the brackets < > denotes the ensemble average. $\alpha^{R}_{\rho\sigma}$ is the Raman tensor, which is given by

$$\alpha^{R}_{\rho\sigma} = \frac{1}{2}\left(\frac{\partial \alpha_{\rho\sigma}}{\partial Q}\right)_0 Q^0, \tag{2.4.4}$$

where $\alpha_{\rho\sigma}$ (ρ, σ: x, y, z) is the $\rho\sigma$ component of the polarizability tensor, Q is the reference coordinate system, Q^0 is the amplitude of the reference vibration, and the subscript character 0 denotes the differential calculus at the equilibrium position of nuclei.

Raman scattering is observed as long as one or more components of the derived polarizability tensor has non-zero value:

$$\left(\frac{\partial \alpha_{\rho\sigma}}{\partial Q}\right)_0 \neq 0 \quad (\rho,\sigma : x,y,z) \tag{2.4.5}$$

In Raman spectra, fundamental tone of fundamental vibration associated with changes in polarizability is observed.

2.5. References

[1 B. Stevens and E. Hutton, *Nature*, 1960, **186**, 1045

[2] J. B. Birks, Excimers, *Rep. Prog. Phys.*, 1975, **38**, 903.

[3] J. B. Birks and L. G. Christophorou, *Spectrochim. Acta*, 1963, **19**, 401.

[4] J. B. Birks and L. G. Christophorou, *Proc. R. Soc. Lond. Ser. A Math. Phys. Eng. Sci.*, 1963, **274**, 552.

[5] M. G. Baeda and L. Brand, *Methods Enzymol*, 1971, **61**, 378.

[6] T. M. Nordlund, Streak camera for time-domain fluorescence, In *Topics in fluorescence spectroscopy*, Vol. 1: *Techniques*, pp. 183–260, ed. J. R. Lakowicz, Plenum Press, New York, 1991.

[7] N. H. Schiller, Picosecond streak camera photonics, In *Semiconductors probed by ultrafast laser spectroscopy*, Vol. 2, pp. 441–458, Academic Press, New York, 1984.

[8] A. J. Campillo, S. L. Shapiro, *IEEE J. Quantum Electron.*, 1983, **19**, 585.

[9] W. Knox and G. Mourou, *Opt. Commun.*, 1981, **37**, 203.

[10] P. P. Ho, A. Katz, R. R. Alfano and N. H. Schiller, *Opt. Commun.*, 1985, **54**, 57.

[11] Y. Tsuchiya and Y. Shinoda, *Proc. SPIE*, 1985, **533**, 110.

[12] K. Kinoshita, M. Ito and Y. Suzuki, *Rev. Sci. Instrum.*, 1987, **58**, 932.

[13] M. Watanabe, M. Koishi and P. W. Roehrenbeck, *SPIE Proc.*, 1993, **1885**, 155.

[14] A. Wiessner and H. Staerk, *Rev. Sci. Instrum.*, 1993, **64**, 3430.

[15] U. Graf, C. Bühler, M. Betz, H. Zuber and M. Anliker, *SPIE Proc.*, 1994, **2137**, 204.

Chapter 3 Anti-parallel Dimer Formation of 4-Cyano-4′-alkylbiphenyls in Isotropic Cyclohexane Solution

3.1. Introduction

Because much of modern technology contains at least one liquid crystalline (LC) component, LC materials are of vast importance to our daily lives. LC materials have been incorporated into the displays of a broad range of everyday tools, including television sets, personal computers, and mobile phones. As a result, information technologies have been established so that society conveniently communicates better.[1–5] Despite this importance, LC phase formation occurs in materials that possess particular structural characteristics, and the mechanism for this change is not completely understood.

4-Cyano-4′-alkylbiphenyls (*n*CBs), such as 4-cyano-4′-pentylbiphenyl (5CB) and 4-cyano-4′-octylbiphenyl (8CB), are well-known LC materials and are widely used in LC displays.[6,7] 5CB is a thermo-tropic LC substance that demonstrates an isotropic to nematic LC phase transition at $T_{I–N}$ = 35 °C and a nematic LC phase to solid phase transition (melting point) at T_m = 22.5 °C.[7] 8CB possesses transition temperatures at $T_{I–N}$ = 40 °C, $T_{N–S}$ = 32.5 °C and T_m = 22 °C for the isotropic to nematic LC, the nematic LC to smectic LC and the smectic LC to solid phase transitions, respectively.[7] In the smectic LC phase of 8CB occurring in the temperature range between $T_{N–S}$ and T_m, formation of anti-parallel dimers has been confirmed using scattering experimental techniques[8–10] and scanning tunneling microscopic (STM) observations on a graphite surface.[11] The formed dimers are arranged in a particular direction (uni-axial director) due to strong dipole–dipole interactions between the dipolar cyano groups. Moreover, Smith *et al.*[12] reported that the solid phase structure of some longer *n*CBs ($n \geq 8$) deposited on flat graphite surfaces showed two-dimensional molecular arrangements made of anti-parallel dimers. Thus, an anti-parallel dimer $(8CB)_2$ is an essential element forming the smectic LC phase in 8CB. Because the nematic LC phase has a simpler structure than the smectic LC phase and possesses only a uni-axial director and none of the periodically arranged layers observed in the smectic LC phase, it is possible that anti-parallel dimers are not essential elements of the nematic LC phase for all *n*CBs. Leadbetter *et al.*[10] claimed that a local bilayer structure made of anti-parallel dimers was present in the nematic LC phase of 5CB using X-ray diffraction techniques. Shorter alkyl chain-having homologous series ($n < 5$), on the other hand, does not exhibit LC phase under general conditions. 3CB and 4CB, which are usually considered non-mesogenic compounds, are known for monotropic LC substances.

They exhibit very unstable nematic LC phase only in a temperature-lowing process.[13–15] Although 3CB (T_m = 67.4 °C) and 4CB (T_m = 48.6 °C) demonstrate respective isotropic to nematic phase transitions at $T_{I–N}$ = 30.7 °C and 16.5 °C, the difficulty lies in obtaining nematic phases of these compounds.[15] In 1983, Vani[16] studied the crystal and molecular structure of 4CB using X-ray diffraction technique. The results confirmed that 4CB molecules packed in a sheet-like arrangement, with nearest neighbor oriented anti-parallel to each other.

More than a decade ago, the formation of excimers, *i.e.*, excited dimers including excited ground state dimers, in pure, neat 5CB, 6CB and 8CB, was investigated using steady-state fluorescence spectroscopy and time-resolved fluorescence lifetime measurements over a range of temperatures spanning the isotropic to crystalline states.[17–19] Although the monomer fluorescence intensity was much stronger than the excimer intensity in the crystalline state, excimer fluorescence emission became much stronger than the monomer emission at temperatures higher than T_m, regardless of other transition temperatures, *i.e.*, $T_{I–N}$ and $T_{N–S}$.[17] Because excimers are excited dimers, they possess characteristic spacing and directionality between the two constituent monomers. Thus, it is possible that excimers formed by *n*CB molecules are identical to the anti-parallel dimers detected previously. If so, a substantial increase in excimer fluorescence emission would reveal the presence of anti-parallel dimers ((*n*CB)$_2$) not only in the smectic LC phase but also in the nematic LC and isotropic phases. These considerations lead to speculation that anti-parallel dimers (*n*CB)$_2$ may be the essential basic elements for the formation of nematic LC phases in *n*CB systems.

Molecular dynamics (MD) simulations are useful and reliable tools to investigate intermolecular conformations formed by a test system. Fukunaga *et al.*[20] carried out MD calculations employing a coarse-grained model and clarified both the static structure and some dynamic properties of 5CB in a nematic LC phase. They concluded that anti-parallel intermolecular associations are formed locally.

Dielectric relaxation (DR) measurements are useful methods for investigating the magnitude of dipole moments and their orientational dynamics in experimental systems.[21–24] The *n*CB molecules bear cyano (–C≡N) groups with a large intrinsic permanent dipole moment of 4.1–4.75 D[24,25] fixed at the ends of the molecules parallel to the biphenyl group. Thus, a Kirkwood factor (g_K), defined as the ratio of the square of the apparent dipole moment (μ_{app}^2) to the square of the intrinsic dipole moment (μ_0^2), quantitatively demonstrates the magnitude of the orientational correlation between the dipole moments (and also the molecular axes) in samples.[26] There are three possible outcomes: (i) when $g_K > 1$, the dipole moments in the sample tend to be aligned parallel to each other, (ii)

when $g_K = 1$, the dipole moments have no orientational correlation, and (iii) when $g_K < 1$, the dipole moments tend to be aligned anti-parallel to each other. In addition, because the dipole moments in the *n*CBs are a result of the dipolar cyano groups that are fixed parallel to the biphenyl groups, the DR modes observed in the *n*CB systems are easily assigned to the molecular motions that are relevant to changes in molecular orientation.

Shikata and Minamoto[24] have investigated the formation of 5CB and 8CB anti-parallel dimers in isotropic benzene solution (*n*CB–Bz) using dielectric techniques. Fast and slow relaxation modes were observed at *ca.* 120 and 400 ps, and the strength of the slow mode remarkably increased with an increase in *n*CB concentration. Additionally, the Kirkwood factors observed in the isotropic solution were less than unity and substantially decreased with an increase in concentration. Thus, they concluded that anti-parallel dimers exist, even in isotropic solution, for both 5CB and 8CB in the work. The fast relaxation mode was assigned to rotation of the monomeric *n*CB molecules, and the slow mode was assigned to dissociation of the anti-parallel dimers $(nCB)_2$.[24] However, more evidently, quantitative additional experimental results other than the dielectric techniques should be necessary to establish the presence of the anti-parallel dimers in isotropic *n*CB solution even under dilute conditions other than the dielectric techniques.

More than a decade ago, Shabatina *et al*.[27] used infrared (IR) absorption spectroscopy in a wavenumber (WN) range from 2200 to 2250 cm^{-1} to monitor the C≡N stretching vibration mode and found that the peak wavenumber was slightly altered upon formation of anti-parallel dimers. Thus, IR measurements in this WN range can be used to evaluate the mole fractions of *n*CB molecules forming the anti-parallel $(nCB)_2$ dimers. In the previous work,[24] the formation of anti-parallel dimers of 5CB and 8CB in the isotropic *n*CB–Bz system was also confirmed using the IR techniques proposed by Shabatina *et al*.[27] A reasonable agreement between equilibrium constants for anti-parallel dimer formation evaluated using IR and DR data strongly suggests that anti-parallel dimers are present, thereby validating their analysis.[24]

In this study, in addition to DR relaxation measurements over a frequency range up to 50 GHz, steady-state and time-resolved fluorescence emission (FE) experiments in the wavelength range from 290 to 500 nm were employed to confirm evidently the formation of *n*CB (n = 3, 4, 5 and 8) anti-parallel dimers in isotropic cyclohexane (cH) solutions. Bz was not used as a solvent because of its relatively strong absorption between 230 and 270 nm and fluorescence emission from 270 to 320 nm.[28] On the other hand, cH does not fluoresce and can dissolve *n*CB molecules to relatively high concentrations needed to clearly recognize LC phases.[25] Based on the obtained DR and FE

data, the dynamics of the *n*CB molecules and the chemical equilibrium between monomeric *n*CB molecules and anti-parallel $(nCB)_2$ dimers in the isotropic *n*CB–cH system were discussed in detail as a function of *n*CB concentration. The results were compared with those obtained for non-mesogenic compound systems, 3CB–cH and 4CB–cH.

3.2. Experimental

Materials

3CB (> 97%), 4CB (>97%), 5CB (> 97%) and 8CB (> 97%) were purchased from Wako Pure Chemical Industries Ltd. (Osaka) and were used without any further purification. Highly purified cyclohexane, cH, (> 98%) was purchased from Kanto Chemical Co., Inc. (Tokyo) and was used without purification. 3CB, 4CB, 5CB and 8CB were dissolved in cH at several concentrations (c) ranging from 7.92×10^{-6} to 4.80×10^{-1} mol L^{-1} (M), 9.79×10^{-6} to 1.75 M, 1.01×10^{-6} to 1.30 M and 1.10×10^{-6} to 1.24 M (2.25×10^{-4} to 13.2 wt%, 2.96×10^{-4} to 34.3 wt%, 3.26×10^{-5} to 37.6 wt% and 4.10×10^{-5} to 41.6 wt%), respectively. In the dielectric experiments, only solutions from 0.15 to 0.48 M, 0.19 to 1.27 M, 0.16 to 1.30 M, 0.16 to 1.24 M were used, respectively.

Methods

Dielectric relaxation, DR, measurements were carried out at 25 °C in a frequency (ν) range from 1 MHz to 50 GHz using two measuring systems. In the low frequency range from 1 MHz to 3 GHz, an RF LCR METER 4287A (Agilent Technologies, Santa Clara, USA) equipped with a home-made electrode cell with a vacant electric capacitance of C_0 = 660 fF was used. In this measuring system, real and imaginary components (ε' and ε'') of the electric permittivity were calculated using the relationships $\varepsilon' = CC_0^{-1}$ and $\varepsilon'' = (G - G_{dc})(\omega C_0)^{-1}$, where C, G, G_{dc}, and ω are the electric capacitance of the sample, the electric conductance of the sample, the direct current conductance of the sample due to the presence of ionic impurities, and the angular frequency given by $\omega = 2\pi\nu$, respectively. In the high frequency range from 50 MHz to 50 GHz, a dielectric probe kit 8507E consisting of a network analyzer N5230C, an ECal module N4693A and a performance probe 05 (Agilent Technologies) was used for the DR measurements. A three-point calibration procedure using *n*-hexane, 3-pentanone, and water as standard materials was carefully performed prior to sample measurements. In this system, ε' and ε'' were automatically calculated using pre-installed software in the dielectric probe system. The calibration procedure is described in detail elsewhere.[22,23] Temperature of the sample solutions was kept at 25 °C using thermostating

equipment controlled by Peltier devices in both the dielectric measuring systems.

Steady-state fluorescence spectra of the *n*CB–cH system were recorded at room temperature (*ca.* 25 °C) using a spectrofluorimeter FP-777 (JASCO, Tokyo). Because absorption and fluorescence emissions were so strong in the moderate to concentrated regime, most of the excitation light was absorbed in front of the quartz cell, and fluorescence emission also occurred there. Thus, a regular rectangular (1 cm × 1 cm) quartz cell could not be used. Instead, the author used a screw capped quartz cell with an optical length of 1 mm, allowing the sample to be sealed to avoid evaporation of the cH solvent. The quartz cells were fixed at a 45° angle position relative to the incident excitation light so that the excitation light reflected away from the monochromator is used to analyze the FE to reduce errors introduced by the strong reflection of the excitation light.

Time-resolved fluorescence spectra and decays of the *n*CB–cH system were measured with a picosecond fluorescence lifetime measurement system (Fig. 3.1) at room temperature (*ca.* 25 °C). A streak scope C4334–01 (Hamamatsu Photonics K.K., Hamamatsu), equipped with spectrograph C5094 (Hamamatsu Photonics K.K.; grating 150g/mm, resolution approx. 1.5 nm), was operated in photon counting mode at a sweep repetition rate of 1 MHz. The streakscope enables a wide range of fluorescence lifetime measurement from ps to ms with a temporal resolution of < 15 ps. A pulsed diode laser PLS270 (PicoQuant GmbH, Berlin, Germany) (wavelength λ = 271 nm, full width at half-maximum (FWHM) < 460 ps, repetition rate up to 8 MHz) was used as an excitation light source with a control unit PDL200–B (PicoQuant GmbH), and the timing for the sweep of the

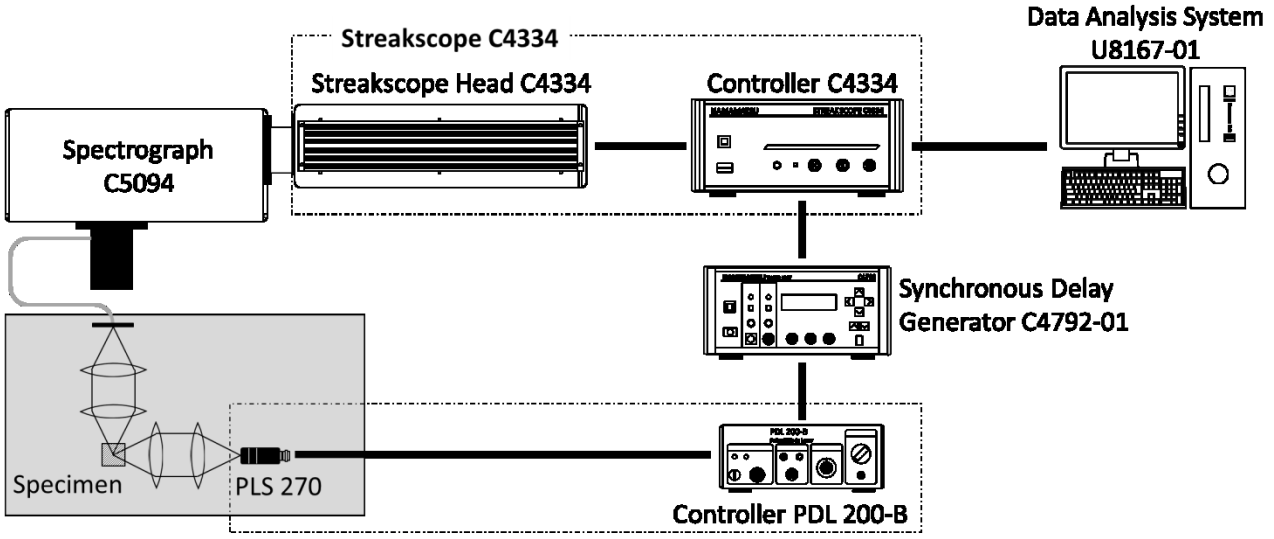

Fig. 3.1. Picosecond fluorescence lifetime measurement system.

streak scope and the excitation pulse light was set using synchronous delay generator C4792–01 (Hamamatsu Photonics K.K.). The FWHM value of the instrument response function (IRF) was < ~ 870 ps with the temporal resolution not worth than several hundred ps through deconvolution processing. The sample solution was placed into a screw capped quartz cell with an optical length of 1 mm, and the quarts cells were fixed at the same angular position as the steady-state measurements for the reason mentioned above. Fluorescence decay curves were fitted using Hamamatsu U8167-01 module. The goodness of the fit procedure was judged by the value of reduced chi square, χ_R^2. If only random errors contribute to χ_R^2, then this value is expected to be near unity. The χ_R^2 values were ranged from 0.962–1.534 for the fitted decays.

3.3. Results and discussion

3.3.1. Dielectric behavior

Figure 3.2(a) and (b), (c) and (d) show the dielectric spectra of 5CB–cH at $c = 2.03 \times 10^{-1}$ M (6.4 wt%) and 1.30 M (37.6 wt%), and 8CB–cH at $c = 2.37 \times 10^{-1}$ M (8.7 wt%) and 1.24 M (41.6 wt%), respectively, as typical experimental results. Two sets of Debye-type relaxation functions

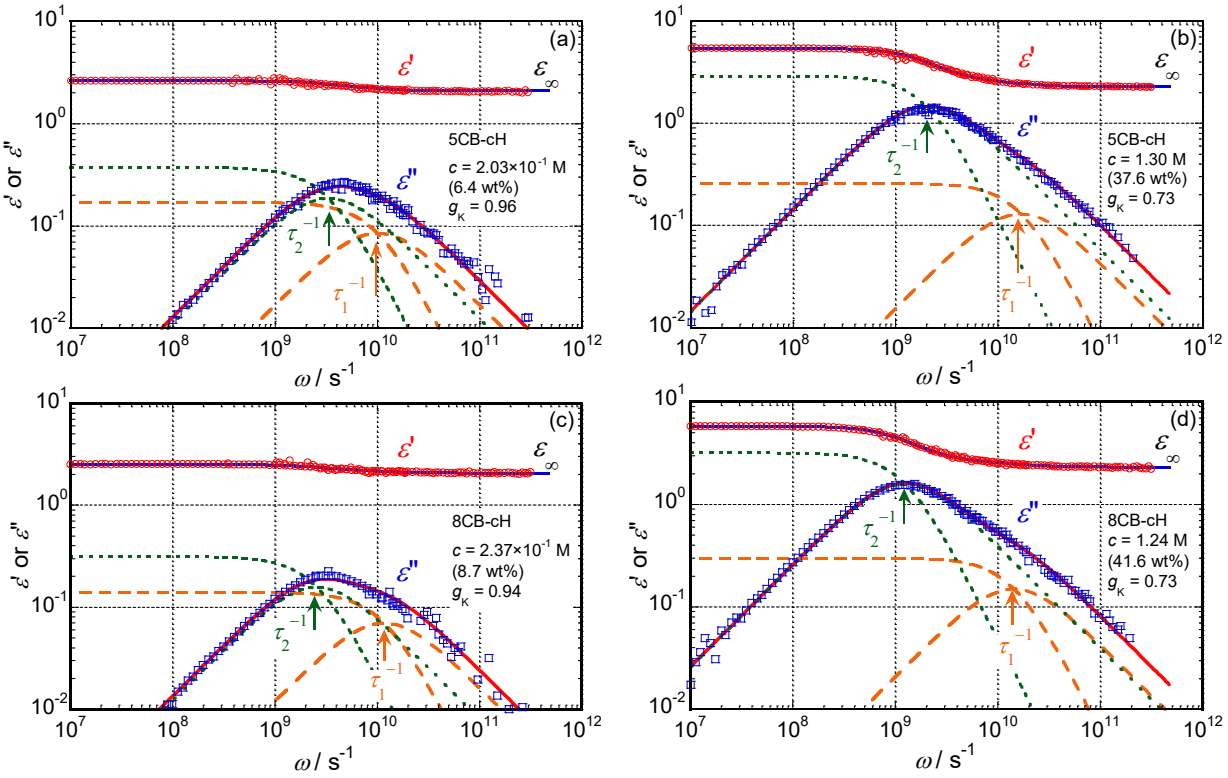

Fig. 3.2. Dielectric spectra, ε' and ε'' vs. ω, of 5CB–cH at $c = 2.03 \times 10^{-1}$ (a) and 1.30 M (b), and 8CB–cH at $c = 2.37 \times 10^{-1}$ (c) and 1.24 M (d).

given by eqn (3.1) with four parameters (relaxation time (τ_j) and strength (ε_j), j = 1 and 2) were necessary to describe the obtained dielectric spectra.

$$\varepsilon' = \sum_{j=1}^{2} \frac{\varepsilon_j}{1+\tau_j{}^2\omega^2} + \varepsilon_\infty, \quad \varepsilon'' = \sum_{j=1}^{2} \frac{\varepsilon_j \tau_j \omega}{1+\tau_j{}^2\omega^2} \tag{3.1}$$

Solid lines in the figures represent the summation of the constituent Debye-type relaxations, and the broken and dotted lines represent the two-component relaxation modes for j = 1 and 2, respectively.

The dependence of ε_j and τ_j (j = 1 and 2) on c for the 5CB–cH and 8CB–cH systems is shown in Fig. 3.3(a) and (b), Fig. 3.4(a) and (b) , respectively. Similar dependence was observed for the 3CB–cH and 4CB–cH systems. Because the fast relaxation mode j = 1 was found to be independent of the concentration for all the *n*CB species examined, this mode was attributed to the rotational relaxation mode of the monomeric *n*CB molecules.[24] Similar experimental results were obtained in *n*CB benzene solution.[24] Although the macroscopic viscosity of benzene (*ca.* 0.6 mPa s at 25 °C) was slightly lower than that of cyclohexane (*ca.* 0.9 mPa s at 25 °C), the τ_1 value of benzene solution (*ca.* 1.5×10^{-10} s) is slightly longer than that of cyclohexane solution (*ca.* 0.9×10^{-10} s). Then, the author speculates that the microscopic viscosity experienced by monomeric *n*CB molecules in solution is not controlled by the macroscopic viscosity of a used solvent, but other factors at the molecular (or nano) level such as an affinity between *n*CB and solvent molecules, and solvation effects. On the other hand, the slow mode j = 2 was observed most clearly at moderate to high concentrations, and it abruptly increased with an increase in the concentration. Neither the fast

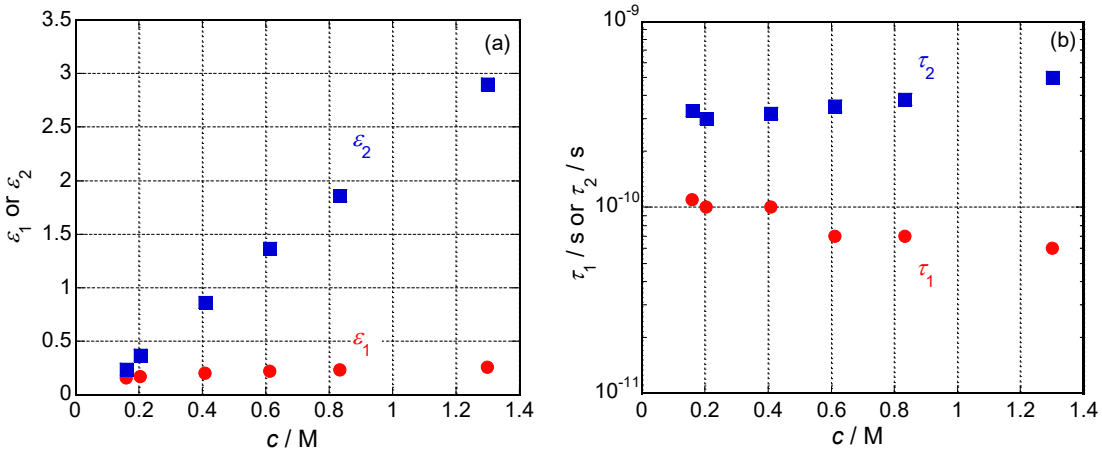

Fig. 3.3. Dependence of relaxation strength, ε_1 and ε_2 (a), and times, τ_1 and τ_2 (b), on the concentration, c, for the 5CB–cH system.

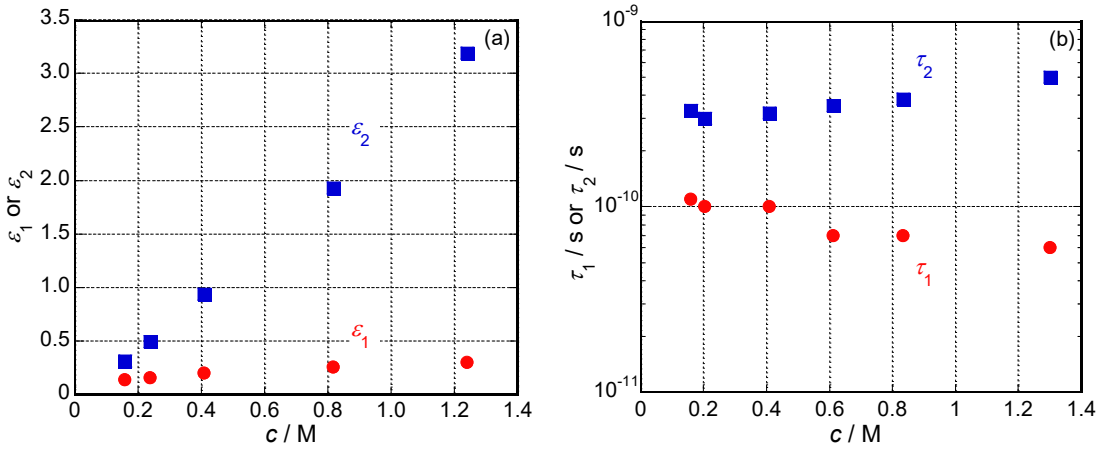

Fig. 3.4. Dependence of ε_1 and ε_2 (a) and τ_1 and τ_2 (b) on c for the 8CB–cH system.

nor the slow modes observed in the *n*CB data could be assigned to rotation about the long molecular axis of the *n*CB molecules; instead, these modes were assigned to monomer rotation and anti-parallel dimer dissociation $(n\mathrm{CB})_2$, as discussed in the previous study.[24] The Kirkwood factor, g_K, is defined as a ratio of the square of an apparent dipole moment, μ_{app}^2, to the square of the intrinsic dipole moment, μ_0^2, of a tested substance, $g_K = \mu_{app}^2 \mu_0^{-2}$. This parameter is a quantitative measure of the orientational correlation between two dipoles using the molecular axes of the *n*CB molecules described in the Introduction. According to Kirkwood and Fröhlich, the square of apparent dipoles, μ_{app}^2, is given by

$$\mu_{app}^{\ 2} = \frac{9(\varepsilon_0 + \varepsilon_\infty)(2\varepsilon_0 + \varepsilon_\infty)\varepsilon_v k_B T}{\varepsilon_0(\varepsilon_\infty + 2)^2 c N_A}, \qquad (3.2)$$

where ε_0, ε_v, k_BT, and N_A represent the electric permittivity at $\omega = 0$ ($\varepsilon_0 = \varepsilon_1 + \varepsilon_2 + \varepsilon_\infty$ for Fig. 3.2(a) and (b)), the electric permittivity of a vacuum, the product of the Boltzmann constant and the absolute temperature, and Avogadro's number, respectively. The value of the intrinsic dipole moment has been reported to be $|\mu_0| = 4.75$ D for 5CB.[24,25,29] The evaluated g_K values noted in Fig. 3.2(a) and (b) assuming $|\mu_0| = 4.75$ D were close to unity, suggesting a weak orientational correlation between dipoles. Consequently, independent of the alkyl chains, the *n*CB molecules demonstrated a dielectric process related to the rotational mode around the shorter molecular axes governed by free rotations, which resulted in $g_K = 1$ for the extremely dilute conditions. The concentration dependence of the g_K values for the *n*CB–cH systems assuming $|\mu_0| = 4.75$ D is shown in Fig. 3.5. The g_K value decreased with an increase in c from unity at $c = 0$ down to *ca.* 0.7 at $c =$ 1.27, 1.30 and 1.24 M for 4CB, 5CB and 8CB, respectively. Similar behavior was shown for 3CB–cH system though its degree of liquidation was low. The c dependence of g_K was also observed for

the 5CB–Bz and 8CB–Bz systems.[24] Ghanadzadeh and Beevers[25] also observed g_K values of less than 0.7 in 6CB–cH and 7CB–cH systems using static dielectric constant measurements, and they concluded that anti-parallel dimers are formed in these systems. The obtained g_K values are substantially less than unity and serve as strong evidence for the formation of anti-parallel dimers in the *n*CB–cH systems, especially at moderate to high concentrations. Urban *et al.*[29] also reported a g_K value less than unity for pure 5CB in an isotropic state, and they discussed the presence of anti-parallel dimers, $(5CB)_2$. Kundu *et al.*[30] also considered the contribution of anti-parallel $(5CB)_2$ dimers to the DR behavior. Similar dielectric behavior as shown in Fig. 3.5, *i.e.*, g_K values less than unity, has also been observed in tetrachloromethane (CCl_4) solutions of dimethylsulfoxide (DMSO), which has a relatively large dipole moment of *ca.* 4.0 D and a strong tendency to form anti-parallel dimers.[31]

According to the previous study,[24] the author proposes a simple model to describe the *c* dependence of g_K values based on a simple chemical reaction between monomeric *n*CB and anti-parallel dimers, $(n\mathrm{CB})_2$, governed by an equilibrium constant (K_d) as schematically depicted in Fig. 3.6.[24,31–33] The equilibrium constant can be calculated using the concentration of monomeric *n*CB ([M]) and anti-parallel dimeric $(n\mathrm{CB})_2$ ([D] = $(c - [\mathrm{M}])/2$)

$$K_d = \frac{[\mathrm{D}]}{[\mathrm{M}]^2} = \frac{c - [\mathrm{M}]}{2[\mathrm{M}]^2} \tag{3.3}$$

The fast dielectric relaxation mode j = 1 has been assigned to rotations of monomeric *n*CB molecules because this motion is the fastest dielectrically active mode.[24] The values of τ_1 seem to range from 70 to 100 ps independent of the concentrations and species of *n*CB, as observed in Figs. 3.3(b) and 3.4(b). On the other hand, the slow mode j = 2 was assigned to dissociation of the anti-parallel dimers, $(n\mathrm{CB})_2$, governed by the lifetime of the dimers (τ_{life}).[24] Because (perfectly) anti-parallel dimers possess no dipole moments, rotations of the anti-parallel dimers are dielectrically inert, as schematically described in Fig. 3.6. After the dissociation process, the two monomeric *n*CB molecules that are generated are capable of the quick rotation having a dielectric relaxation with a characteristic time of τ_2 ($\sim\tau_{life}$). According to this model,[24] the lifetime, τ_2, of anti-parallel dimers, $(8CB)_2$, in cH does not look so different from that of $(5CB)_2$.

Here, the author considers the relationship $\varepsilon_1 = \alpha_M[\mathrm{M}]$, where α_M is a proportionality constant obtained by assuming $\mu_{app}^2 = \mu_0^2$ and g_K = 1 for the monomeric *n*CB and [M] = *c*, *i.e.*, [D] = 0, in eqn (3.2).[24] By use of α_M, eqn (3.3) is rewritten as

$$K_d = \frac{\alpha_M{}^2 (c - \varepsilon_1/\alpha_M)}{2\varepsilon_1{}^2}. \qquad (3.3')$$

Eqn (3.3′) permits the calculation of K_d at each examined concentration, c, from the dielectric relaxation data. In addition, the ratio of the concentration of anti-parallel dimer to that of monomer [D]/[M] (= $(c - \varepsilon_1/\alpha)(2\varepsilon_1/\alpha)^{-1}$) was also obtained. The obtained K_d values are plotted as a function of the concentration for the *n*CB–cH (n = 3, 4, 5 and 8) systems in Fig. 3.7(a)–(d), respectively. K_d increased with an increase in c irrespective of the *n*CB species. This observation clearly suggests that anti-parallel dimer formation is remarkably enhanced by increasing c, even in an isotropic cH solution, and this increase is especially pronounced at low c. Large amounts of the *n*CB molecules form anti-parallel dimers at a high c, as shown in the molar fraction of $(n\text{CB})_2$ ($f_D = 1 - [M]c^{-1}$) in Fig. 3.7(a)–(d). It seems that most of the 4CB, 5CB and 8CB molecules in the system (greater than 0.9 by molar fraction) form anti-parallel dimers at $c \geq 0.8$ M. The dependence of K_d on c observed in Fig. 3.7 suggests that longer alkyl chains have a stronger tendency to form anti-parallel dimers at low c. The K_d values for 5CB and 8CB in isotropic Bz solution[24] were significantly lower than those in cH solution over the entire c range examined. These differences in the K_d values seem to be the result of the differences in solubility of the *n*CB molecules in Bz and cH.

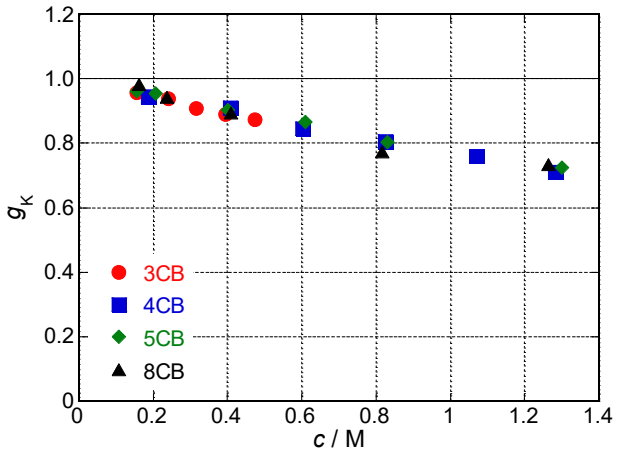

Fig. 3.5. Dependence of the Kirkwood factor, g_K, on c for the 3CB–cH, 4CB–cH, 5CB–cH and 8CB–cH systems.

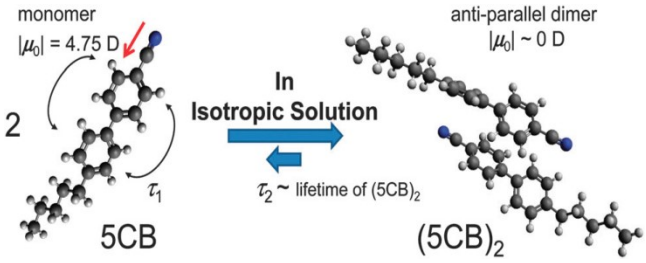

Fig. 3.6. Schematic depiction of the chemical reaction between monomeric *n*CB and anti-parallel dimeric $(n\text{CB})_2$; n = 5 in this depiction.

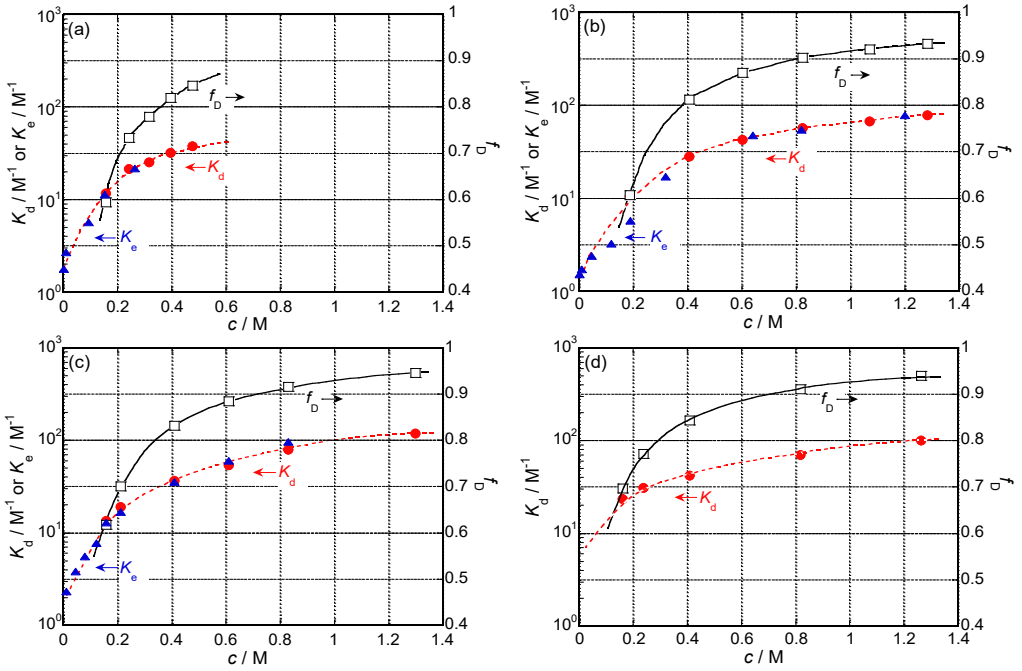

Fig. 3.7. Dependence of the equilibrium constants, K_d (anti-parallel dimers; circles) and K_e (excimers; triangles), on c for the 3CB–cH (a), 4CB–cH (b), 5CB–cH (c) and 8CB–cH (d) systems. The c dependence of the anti-parallel dimer mole fractions, f_D (=1 − [nCB]c^{-1}; squares), are also plotted. Lines are guide to the eye.

A proportionality constant, α_D, defined as $\varepsilon_2 = \alpha_D[D]$ was also evaluable *via* an equation $\alpha_D = 2\varepsilon_2 (c - [M])^{-1}$. The relationship $\alpha_M > \alpha_D/2$ is responsible for the relationship $g_K < 1$ in all the nCB–cH systems examined, as was the case for the 5CB–Bz and 8CB–Bz systems.[24]

3.3.2. Steady-state fluorescence behavior

Under extremely dilute conditions, the nCB molecules are expected to be isolated and behave as individual molecules in the nCB–cH systems. The fluorescence emission spectra ($I_{EM}(\lambda)$ vs. λ) upon excitation at 274 nm normalized by the emission intensities at 324 nm for the 5CB–cH and 8CB–cH systems over the concentration range from 1.0×10^{-6} (1.1×10^{-6}) to 1.0×10^{-3} (1.1×10^{-3}) M are shown in Fig. 3.8(a), as a typical result. The obtained emission spectra of both systems are essentially independent of the concentration and the number of alkyl chains (excluding the small peaks observed at 310 nm), suggesting that the spectra represent emission from nCB monomers. Fig. 3.8(b) shows the excitation spectra ($I_{EX}(\lambda)$ vs. λ) of the 5CB–cH and 8CB–cH systems recorded at the emission wavelength of 324 nm for the same concentrations as in Fig. 3.8(a) normalized by the intensities at the peak wavelength of 274 nm. Weak alkyl chain length dependence is observed, and

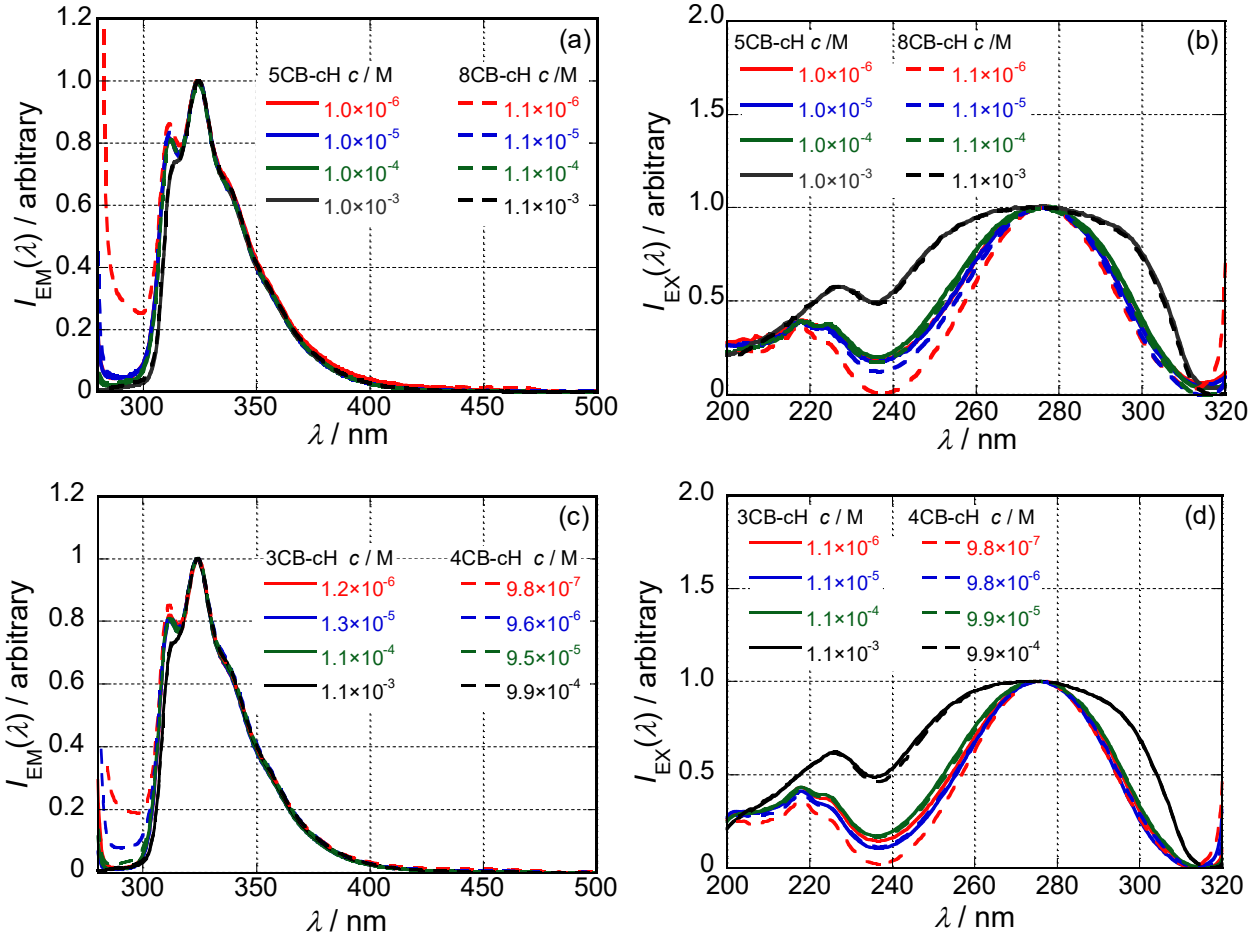

Fig. 3.8. Fluorescence emission spectra ($I_{EM}(\lambda)$ vs. λ) normalized by the intensities at 324 nm for the 5CB–cH and 8CB–cH (a), and 3CB–cH and 4CB–cH (c) systems at concentrations ranging from 1×10^{-6} to 1×10^{-3} M (excitation at 274 nm), and fluorescence excitation spectra ($I_{EX}(\lambda)$ vs. λ) normalized by the intensities at 274 nm (b) for the same systems in (a), and (d) for the same systems in (c) (emission monitored at 324 nm).

more notably, the spectra become broader with an increase in *c*. These observations reveal that the fluorescence behavior of the *n*CB molecules substantially deviates from an expected linear response with changing concentration because of self-absorption approximately at 310 nm, even in dilute cH solutions in the absence of an excimer. Similar dependence of fluorescence emission and excitation spectra at dilute concentrations was observed for 3CB–CH and 4CB–cH systems (Fig. 3.8(c) and (d)). Fluorescence emission spectra of the 5CB–cH system at moderate to high concentrations (1.0×10^{-2} to 1.30 M) upon excitation at 274 nm normalized to the emission peak intensities are shown in Fig. 3.9(a). The magnitude of the fluorescence peak found at 324 nm, which corresponds to the monomer emission, clearly decreased and a new peak at 380–390 nm remarkably increased

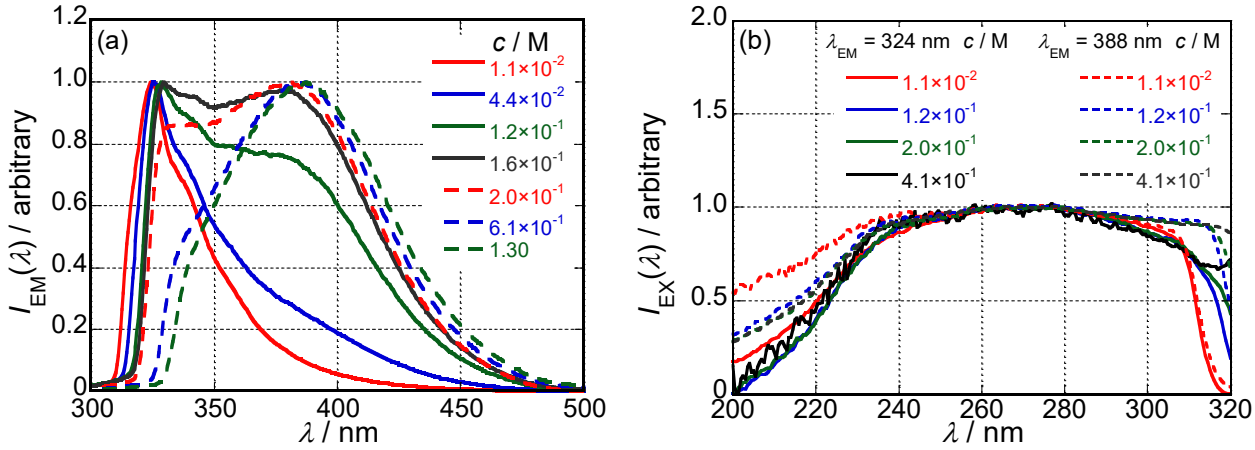

Fig. 3.9. (a) Fluorescence emission spectra, $I_{EM}(\lambda)$ vs. λ, normalized by the peak intensities for the 5CB–cH systems at concentrations ranging from 1.1×10^{-2} to 1.30 M (excitation at 274 nm) and (b) fluorescence excitation spectra, $I_{EX}(\lambda)$ vs. λ, normalized by the peak intensities at 274 nm for the same systems in (a) (emission monitored at 324 and 388 nm).

with an increase in *c*. Because the fluorescence emission wavelength of the new peak agreed well with that reported in the literature as excimer emission in the pure, neat 5CB,[17–19] this new fluorescence peak was attributed to the excimer emission signal. Excitation spectra normalized by the peak at 270 nm for the monomer and excimer emissions at 324 and 388 nm, respectively, are shown in Fig. 3.9(b). The dependence of the excitation spectra on the emission wavelength is not strong, whereas the dependence on *c* is considerable. The excitation spectra became broader with an increase in *c*. These observations suggest that there exist two types of excimers, each possessing different excitation spectra. The first type of excimer is an ordinary excimer generated by a contact between an excited monomer and a ground state monomer, which should possess the same excitation spectra as a monomer and is mainly observed in a system consisting of repulsive monomer molecules. The second type excimer is classified as another excited chemical species that is generated by the excitation of a ground state dimer formed by inter-molecular attractive interactions. These types of interactions are characteristic of a system with dipole–dipole interactions like those in the 5CB–cH system.[17,34] In seminal fluorescence spectroscopic studies on *n*CB carried out in the pure, neat state, classification of excimers was considered but was not taken into account in an explicit manner.[17–19] Because 5CB–cH system here demonstrated excitation spectra rather different from those of the monomers, as observed in Fig. 3.8(b), a large amount of excimers generated in the system are likely to be excited ground state dimers. Essentially, the same concentration dependence of fluorescence emission and excitation spectra was also observed in the

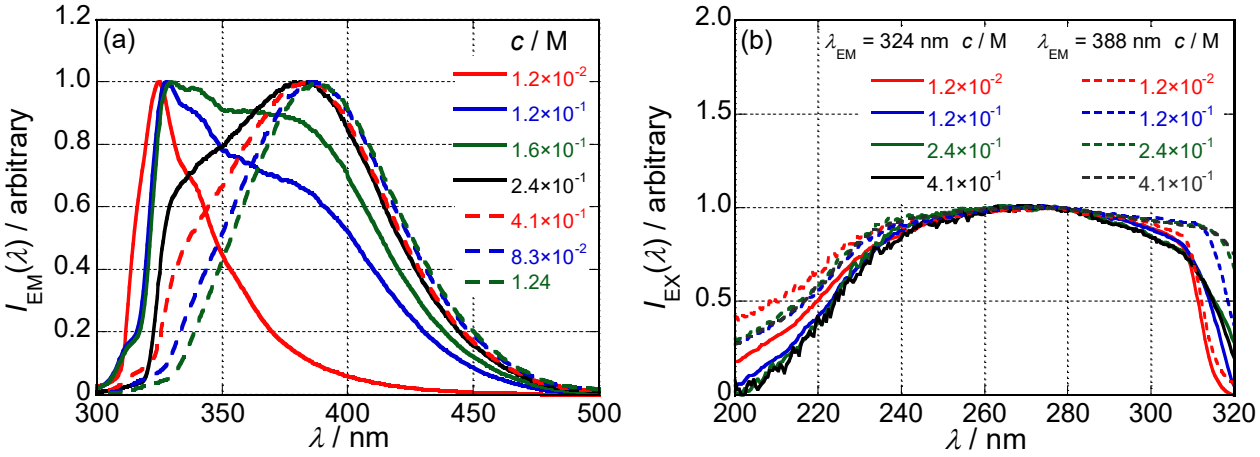

Fig. 3.10. (a) Fluorescence emission spectra, $I_{EM}(\lambda)$ vs. λ, normalized by the peak intensities for the 8CB–cH systems at concentrations ranging from 1.2×10^{-2} to 1.24 M (excitation at 274 nm) and (b) fluorescence excitation spectra, $I_{EX}(\lambda)$ vs. λ, normalized by the peak intensities at 274 nm for the same systems in (a) (emission monitored at 324 and 388 nm).

8CB–cH system at moderate to high concentrations, as observed in Fig. 3.10(a) and (b).

Here, the author assumes that the *n*CB molecules possess only two states, monomers and excimers (including ground state dimers), in the *n*CB–cH systems examined. In this scenario, the fluorescence emission spectra should remarkably alter depending on the distribution of monomers and excimers because both monomers and excimers have the same excitation peak wavelength of 274 nm. Moreover, emission spectra normalized by the total amount of effectively excited species in the examined system should have an isosbestic point between the monomer and excimer emission wavelength that is independent of the distribution of monomers and excimers. However, the total amount of effectively excited species was not known precisely in this study because of the very large c range that exceeded the region of linear dependence on c due to strong absorption at the front face of the sample and self-absorption by the *n*CB molecules. Fortunately, the fluorescence emission spectra at $c = 2.0 \times 10^{-1}$M demonstrated a clear minima at close to 350 nm as observed in Fig. 3.9(a). Thus, 350 nm was used as the isosbestic point.

If the isosbestic point is known for a standard monomer and excimer, ($I^{Std}_{EM,M}(\lambda)$ and $I^{Std}_{EM,E}(\lambda)$), emission spectra of a given solution can be determined by multiplying the normalized monomer and excimer emission spectra, $I_{EM,M}(\lambda)$ and $I_{EM,E}(\lambda)$, by a correction factor. The normalized emission spectra, $I_{EM}(\lambda)$, of a sample solution can then be described as $I_{EM}(\lambda) = f_M^* I^{Std}_{EM,M}(\lambda) + f_E^* I^{Std}_{EM,E}(\lambda)$, where $f_M^* + f_E^* = 1$. If the wavelength at isosbestic point, λ_{iso}, is not correctly selected, the relationship $f_M^* + f_E^* = 1$ will not be satisfied. Fig. 3.11 shows the values of $f_M^* + f_E^*$ calculated for several trial

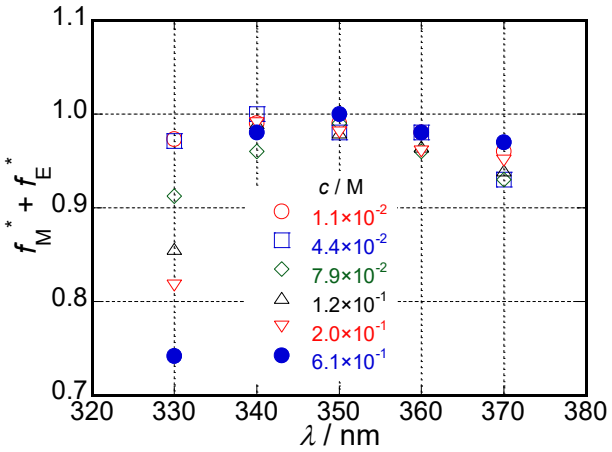

Fig. 3.11. Wavelength dependence of the total fractions of monomers and excimers, $f_M^* + f_E^*$, calculated by assuming each λ value as the isosbestic point for the 5CB–cH system at several c values.

isosbestic point wavelengths, 340, 350, 360 and 370 nm, for the 5CB–cH system at several concentrations. The relationship $f_M^* + f_E^* = 1$ was best satisfied at 350 nm, revealing that the isosbestic point is near 350 nm in the 5CB–cH system. As typical results, Fig. 3.12(a)–(c) shows the fluorescence emission spectra of the 3CB–cH, 4CB–cH and 5CB–cH systems, respectively, in the moderate to high concentration regime, which were re-normalized by the emission intensities at λ_{iso}(= 350 nm): $I_{EM}^{350}(\lambda)$. It seems that the monomers dominate the system at $c < ca.\ 1 \times 10^{-2}$ M, whereas excimers dominate at $c > ca.\ 8 \times 10^{-1}$ M. Because the shape of the emission spectra at approximately 330 nm was reductively influenced by a self-absorption phenomenon due to the overlapping of the emission and excitation spectra (*cf.* Fig. 3.9(a) and (b)), deconvolution of the fluorescence emission spectra near this wavelength into their constituent monomer and excimer components is inaccurate. However, at wavelengths longer than 340 nm, this analysis was reasonably performed by a curve fitting procedure using the emission spectra at $c = 1.1 \times 10^{-2}$ and 1.30 M as the standard emission spectra of the monomer, $I_{EM,M}^{Std}(\lambda)$, and the excimer, $I_{EM,E}^{Std}(\lambda)$, respectively, for the 5CB–cH system. Then, a ratio of the fraction of excited monomers to that of excited excimers, $f_M^* f_E^{*-1}$, which is identical to the value of $[M^*](2[D^*])^{-1}$, was approximately determined, where an asterisk denotes excited state. Then, the determined $[M^*](2[D^*])^{-1}$ value at each c permitted evaluation of the equilibrium constant (K_e) for the chemical reaction between monomers and excimers *via* eqn (3.3) (*cf.* Fig. 3.6). In addition, the ratio of the concentration of excimer to that of excited monomer for steady-state fluorescence system $[D^*]_{ss}/[M^*]_{ss}$ (= $f_E^*/2f_M^*$) was also determined. The obtained K_e value for the 3CB–cH, 4CB–cH and 5CB–cH systems is also

shown in Fig. 3.7(a)–(c), respectively, as a function of c. The agreement between K_d and K_e strongly suggests that the anti-parallel dimer and excimers (including the excited ground state dimers) are identical chemical species.

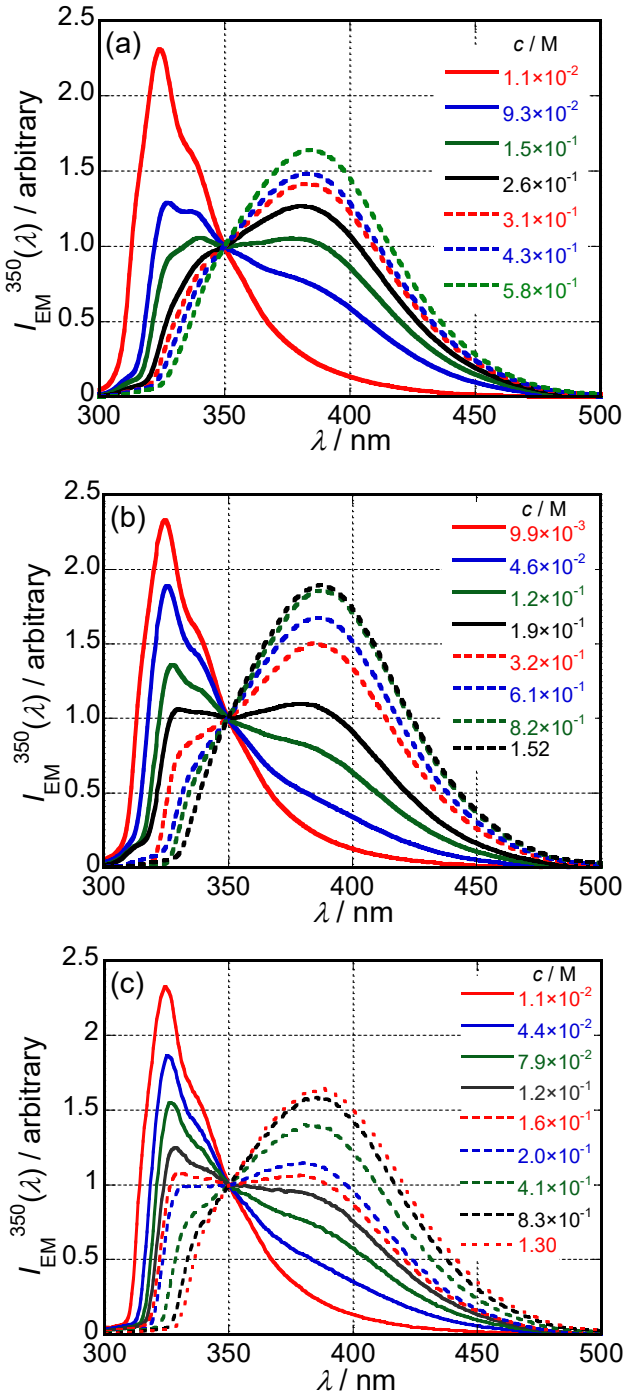

Fig. 3.12. Fluorescence emission spectra, $I_{EM}^{350}(\lambda)$ vs. λ, re-normalized by intensities at 350 nm for the 3CB–cH (a), 4CB–cH (b) and 5CB–cH (c) systems at the moderate to high concentrations (excitation at 274 nm).

In the 8CB–cH system, the influence of the concentration on the emission spectra in the moderate to high concentration regime was much stronger than that of the other nCB–cH systems. Thus, the emission intensities at around λ_{ex} = 350 nm were strongly reduced due to self-absorption (*cf.* Fig. 3.10(a)) in the concentrated regime such that K_e evaluation was not performed. However, the author believes that the same excimer formation process governed by the chemical equilibrium shown in Fig. 3.6 (*cf.* eqn (3.3)) holds in the 8CB–cH system based on the results obtained from the other nCB–cH system.

3.3.3. Time-resolved fluorescence behavior

Figure 3.13 shows the fluorescence decay curve of 5CB–cH at extremely dilute solution (c = 1.8 × 10^{-6} M) as a typical result, in which only monomer emission is to be observed since 5CB molecules are expected to be isolated. The decay curves were fitted to single exponential functions: $I(t) = A\exp(-t/\tau_M)$, where A and τ_M denote the amplitude and the lifetime of nCB in extremely dilute solution, respectively. The obtained τ_M values were ~1.1 ns irrespective of the length of alkyl chain, n.

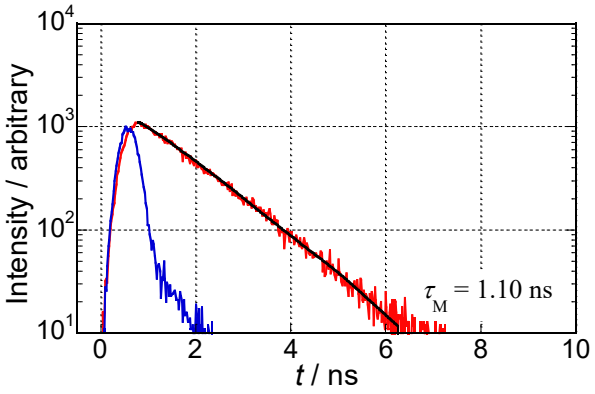

Fig. 3.13. Fluorescence decay of 5CB–cH at c = 1.8 × 10^{-6} M (red solid line). The instrumental response function (IRF) for the excitation laser pulse is also shown (blue solid line). The χ_R^2 value was 1.10.

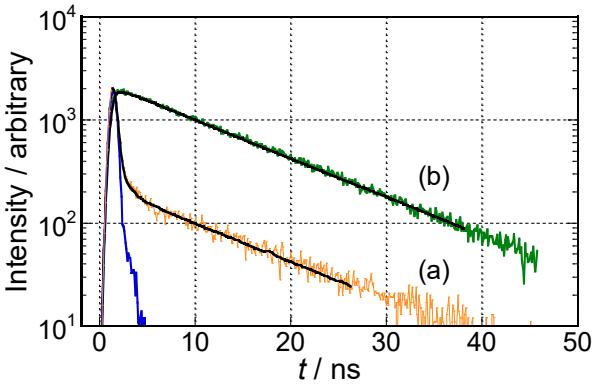

Fig. 3.14. Fluorescence decay profiles obtained for 5CB–cH system in the monomer (a) (305–345 nm) and excimer (b) (430–480nm) regions at c = 0.30 M. The IRF is also shown (blue solid line). The χ_R^2 values were 1.15 and 1.26, respectively.

The typical monomer and excimer fluorescence decay profiles of 5CB–cH at c = 0.30 M are shown in Fig. 3.14. The observed wavelength regions were 305–345 nm and 430–480nm for the monomer and excimer fluorescence emission, respectively. In the monomer emission a fast-decaying component and a slow-decaying component were observed, while a fast-rise component as well as the slow-decaying component was observed in the excimer emission. According to a model described subsequently, the rise and decay curves were fitted to a bi-exponential function in the form of $I(t) = A_f\exp(-t/\tau_f) + A_s\exp(-t/\tau_s)$, where subscripts f and s indicate the first and slow components, respectively. For 3CB, 4CB and 5CB, lifetimes of τ_f (250–630 ps) and τ_s (10–13 ns) were obtained. Dependence of the lifetimes on c for the 3CB–cH, 4CB–cH and 5CB–cH systems are shown in Fig. 3.15(a)–(c). These rate constant values vary with the phases. Tamai *et al.*[35,36] carried out the picosecond time-resolved fluorescence measurement of

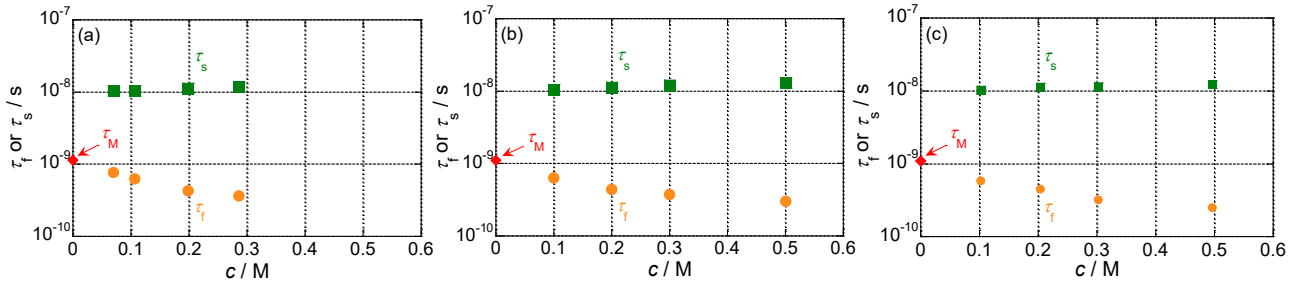

Fig. 3.15. Concentration dependence of the fluorescence lifetimes τ_f and τ_s for the 3CB–cH (a), 4CB–cH (b) and 5CB–cH (c) systems.

4-cyano-4′-octylbiphenyl (8OCB) in various phases, whose molecular structure is similar to that of *n*CB. They estimated the monomer fluorescence lifetime of 8OCB to be τ_M = 1.1 ns in dilute *n*-hexane solution (~ 10^{-5} M), which is in good agreement with that of obtained here, and excimer one to be 8.7 ns at 5 × 10^{-1} M. They regarded the decay curves of neat 8OCB as roughly bi-exponential to obtain lifetimes of τ_f= 0.09 ns and τ_s= 8.0 ns in nematic phase, and τ_f= 0.14 ns and τ_s = 10.0 ns in smectic A phase. Abe *et al.*[19] also estimated the lifetimes of 5CB in nematic phase to be τ_f = 0.5 ns and τ_s = 14 ns.

Figure 3.16 shows the normalized time-resolved fluorescence spectra for 5CB–cH at two different concentrations. The spectrum around 400 nm, or excimer emission band, gradually increases in intensity with lapse of the time accompanying the emission around 330 nm (monomer emission) which is observed immediately after the excitation. Attention must be directed toward the higher concentration one (0.50 M), in which the excimer emission intensity is significantly higher in the short time region than that observed in the diluter one. This result strongly suggests that there are not only *ordinary* excimers but preformed excimers paired in the ground state, which is consistent with the DR measurement result. The similar time dependences of fluorescence emission spectra are obtained for 3, 4 and 8CB–cH systems.

Scheme 3.1 shows the kinetic model for the excimer formation according to the modified Birks' model proposed by Ikeda *et al.*,[17,37,38] in which the ground-state association of *n*CB molecules is taken into consideration. Here, M^* and D^* are the excited monomer and dimer, respectively, k_a and

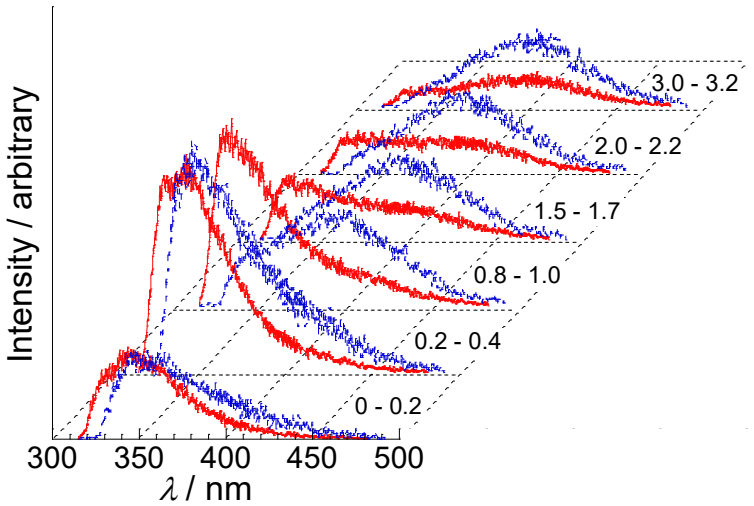

Fig. 3.16. Time-resolved normalized fluorescence spectra for 5CB–cH system at two different concentrations: 0.10 M (red solid lines) and 0.50 M (blue broken lines). The numbers in this figure denote the delay time in ns after excitation pulse.

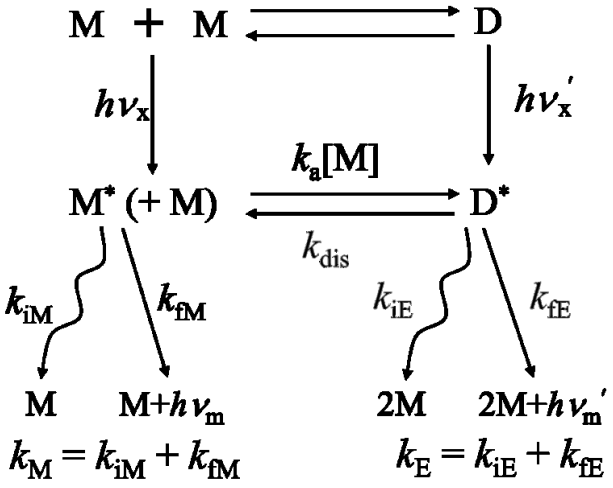

Scheme 3.1. Kinetic model for the excimer formation.

k_d are the excimer formation and dissociation rate constants, [M] is the monomer concentration in the ground state, and k_{iM}, k_{fM}, k_{iE} and k_{fE} denote the non-radiative and radiative rate constants of M^* and D^*, respectively. The respective sums of the radiative and non-radiative rate constants of monomer and excimer are expressed as $k_M = k_{iM} + k_{fM}$ and $k_E = k_{iE} + k_{fE}$.

According to this model, the time evolution of monomer $I_M(t)$ and excimer $I_E(t)$ fluorescence intensities are given by

$$I_M(t) = \frac{k_{fM}}{\lambda_f - \lambda_s}\{A_{Mf}\exp(-\lambda_f t) + A_{Ms}\exp(-\lambda_s t)\} \quad (3.4)$$

$$I_E(t) = \frac{k_{fE}}{\lambda_f - \lambda_s}\{A_{Ef}\exp(-\lambda_f t) + A_{Es}\exp(-\lambda_s t)\}, \quad (3.5)$$

where

$$A_{Mf} = (X - \lambda_s)[M^*]_0 - k_{dis}[D^*]_0 \quad (3.6)$$

$$A_{Ms} = -(X - \lambda_f)[M^*]_0 + k_{dis}[D^*]_0 \quad (3.7)$$

$$A_{Ef} = -k_a[M][M^*]_0 - (X - \lambda_f)[D^*]_0 \quad (3.8)$$

$$A_{Es} = k_a[M][M^*]_0 + (X - \lambda_s)[D^*]_0 \quad (3.9)$$

$$\lambda_f, \lambda_s = \frac{1}{2}\left\{(X + Y) \pm \sqrt{(X - Y)^2 + 4k_a[M]k_{dis}}\right\} \quad (3.10)$$

$$X = k_a[M] + k_{iM} + k_{fM} = k_a[M] + k_M \quad (3.11)$$

$$Y = k_{dis} + k_{iE} + k_{fE} = k_{dis} + k_E, \quad (3.12)$$

and $[M^*]_0$ and $[D^*]_0$ are initial concentration of M^* and D^*, respectively. The results are then analyzed using following relationships obtained from eqns (3.6)–(3.12)

$$X = (A_M\lambda_f - A_E\lambda_s)/(A_M - A_E) \quad (3.13)$$

$$k_a[M] = X - k_M \quad (3.14)$$

$$k_{dis} = -(1/k_a[M])(X - \lambda_f)(X - \lambda_s) \quad (3.15)$$

$$\frac{[D^*]_0}{[M^*]_0} = \frac{A_M(X - \lambda_f) + (X - \lambda_s)}{k_{dis}(A_M + 1)}. \quad (3.16)$$

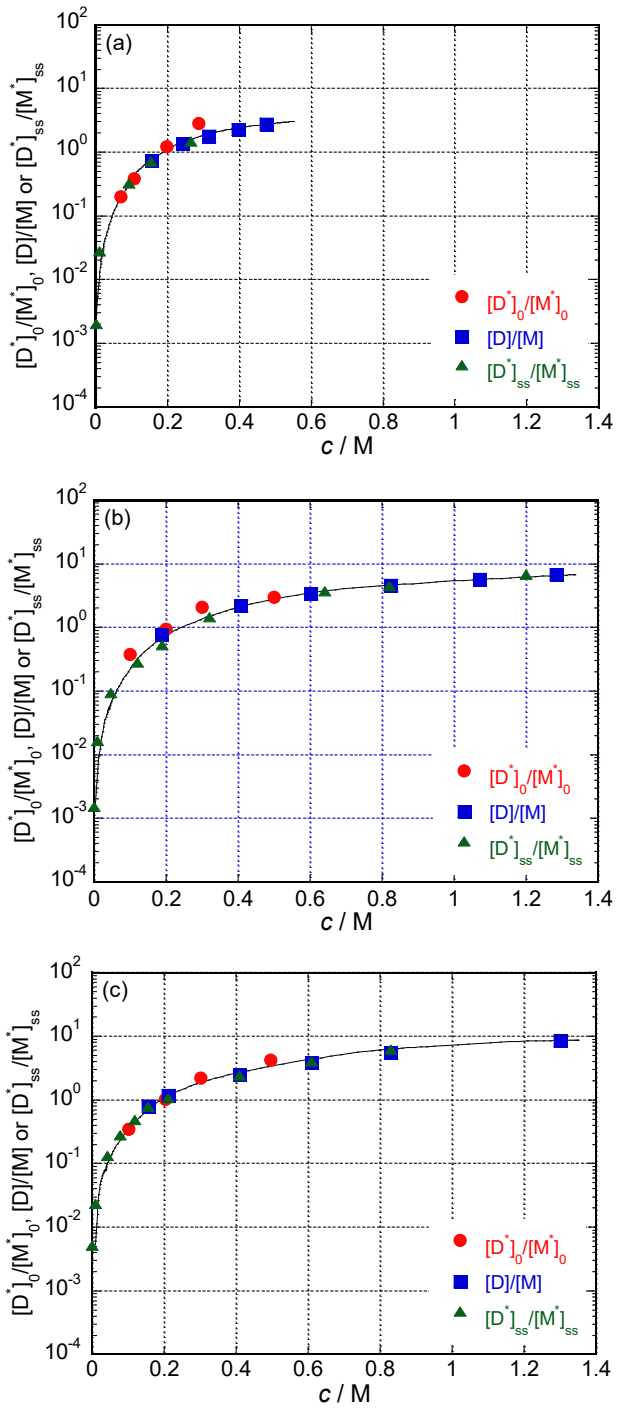

Fig. 3.17. Dependence of the concentration ratios, $[D]/[M]$, $[D^*]_{ss}/[M^*]_{ss}$ and $[D^*]_0/[M^*]_0$ on c for the 3CB–cH (a), 4CB–cH (b) and 5CB–cH (c) systems. Lines are guide to the eye.

By substituting experimental values of A_M (= A_{Mf}/A_{Ms}), A_E (= A_{Ef}/A_{Es}), λ_f (= τ_f^{-1}), λ_s (= τ_s^{-1}) and k_M (= τ_M^{-1}) into eqns (13)–(16), the excimer dissociation rate constant, k_{dis}, and the ratio of concentration of excimer to that of monomer formed at t = 0, $[D^*]_0/[M^*]_0$, are evaluated as a function of concentration, c.

Figure 3.17 shows dependence of the concentration ratio of excimer to that of monomer at t = 0, $[D^*]_0/[M^*]_0$ on c for the 3CB–cH (a), 4CB–cH (b) and 5CB–cH (c) system. The $[D^*]_0/[M^*]_0$ values are worthy of comparing with reference values obtained in DR and steady-state FE measurements though it is practically impossible to obtain the equilibrium constant from time-resolved analyses like K_e and K_d. The corresponding ratios, $[D]/[M]$ and $[D^*]_{ss}/[M^*]_{ss}$, obtained in DR and steady-state FE measurements, respectively, are also shown in Fig. 3.17. Close agreement among obtained values of $[D^*]_0/[M^*]_0$, $[D]/[M]$ and $[D^*]_{ss}/[M^*]_{ss}$ suggest again that anti-parallel dimer and excimers are identical chemical spices.

The reciprocal of the excimer dissociation rate constant τ_{dis} (= k_{dis}^{-1}) is equivalent to the excimer lifetime. Hence, one can associate τ_{dis} with the anti-parallel dimer lifetime τ_2 obtained in DR measurements to characterize the dimerization behavior in grand- and excited-state. Figure 3.18 shows the dependence of the τ_{dis} value on c for the nCB–cH systems (n = 3, 4 and 5) and corresponding τ_2 values are shown together. The obtained τ_{dis} values (*ca.* 40 ns) are 100 times as

large as τ_2 values (*ca.* 400 ps). The noticeable discordance between τ_{dis} and τ_2 values presumably due to the difference in the electronic property of the *n*CB molecules in the ground- and excited-state. Previous study has shown that the angle between the phenyl ring planes of a 5CB molecule was about 30–38° in the ground state, while it was 0° in the excited state.[39,40] The dipole moment of the excited *n*CB molecule, hence, substantially increases due to the charge localization. The results of quantum chemical calculation (CNDO/S) on cynanobiphenyl (CB) model compounds in the gas phase have shown that dipole moment of the planer CB molecule in the excited state (S_1) was 8.3 D.[41] These changes in electronic property mentioned above seem to enhance the interaction between the *n*CB molecules in excited state than that of in the ground state. Jones and Vullev[42] have confirmed such ground- and excited-state aggregation properties for a pyrene derivative in aqueous media. In their study, for the pyrene chromophore in the ground state, the monomer–dimer equilibrium constant of 150 M^{-1} was obtained for pyrenebutanoate in alkaline water using NMR methods. The excimer formation constant in water, on the other hand, was determined to be 1.6×10^4 M^{-1}, which was about 100-fold larger than the ground state dimerization constant, by the use of time-resolved emission spectroscopy.

Tamai *et al.*[35,36] determined the excimer dissociation rate constants of the 8OCB liquid crystal to be 2.0×10^9 s^{-1} in a nematic phase and to be 1.2×10^9 s^{-1} in a smectic A phase (the reciprocals are 500 ps and 833 ps, respectively). Although the presence of preformed dimer was not considered in their analyses, these values are reasonably in accord with the τ_2 value. The probability is that this is because the temporal resolution in this study is not high enough. Nevertheless, the author believes that excimer has longer lifetime in some degree than anti-parallel dimer reflecting stronger

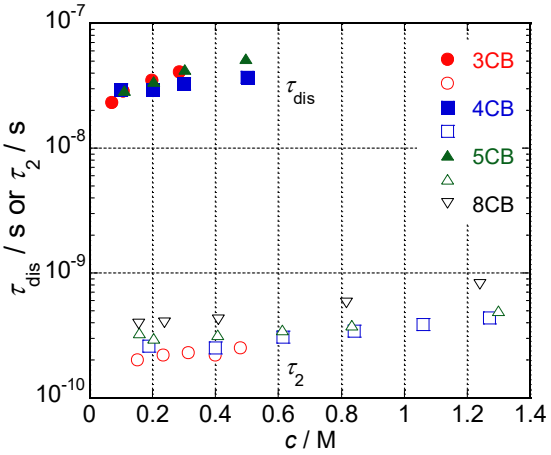

Fig. 3.18. Dependence of the reciprocal of excimer dissociation rate τ_{dis} on c for the 3CB–cH, 4CB–cH and 5CB–cH systems. The c dependence of the relaxation time τ_2 is also plotted.

molecular interaction in the excited state. A detailed analysis on ground- and excited-state aggregation properties will be presented in a future study.

Although the deconvolution fittings did not work well in the 8CB–cH system due to the strong influence of self-absorption on the fluorescence decay profiles, one can safely predict that 8CB exhibits dimer formation behavior similar to the other *n*CB compound examined.

3.4. Conclusions

Liquid crystal forming 4-cyano-4′-pentylbiphenyl and 4-cyano-4′-octylbiphenyl, and not forming 4-cyano-4′-propylbiphenyl and 4-cyano-4′-butylbiphenyl form anti-parallel dimers, even in isotropic cyclohexane solutions irrespective of the alkyl chain length. The formation of anti-parallel dimers is well described as a chemical equilibrium between monomers and dimers, and the equilibrium moves toward dimer formation with an increase in the concentration. These anti-parallel dimers could then be necessary for the appearance of the nematic liquid crystalline phase at higher concentrations and also in the pure, neat state.

Two types of molecular dynamic processes were dielectrically observed in the isotropic cyclohexane solution for all the species. A fast relaxation mode was assigned to a rotational relaxation mode of monomeric molecules, and a slow relaxation mode was attributed to dissociation of the anti-parallel dimers. The slow mode increased the magnitude of the relaxation in proportion to the anti-parallel dimer formed with increasing concentration.

The formation of the anti-parallel dimer in the isotropic solution was also evaluable using fluorescence techniques because the dimer exhibited a clear excimer emission at a wavelength longer than that of the monomer emission. The concentration dependence of the equilibrium constant of the anti-parallel dimer formation process determined using fluorescence techniques demonstrated fairly good agreement with that determined by the dielectric methods. Evidently, the dimers formed in isotropic solution are identical chemical species to the anti-parallel dimers as detected by the dielectric relaxation experiments.

The aggregation properties in ground- and excited-state were examined by time-resolved fluorescence analyses. The dimer dissociation rate constant in the excited state was considerably smaller than that in the ground state. There is every possibility of the excimer having longer lifetime than that of the anti-parallel dimer.

3.5. References

[1] J. A. Castellano, The Story of Liquid Crystal Displays and the Creation of an Industry, World Scientific, Singapore, 2005.

[2] H. Kawamoto, *Proc. IEEE*, 2002, **4**, 460.

[3] G. H. Heilmeier, L. A. Zanoni and L. A. Barton, *Proc. IEEE*, 1968, **56**, 1162.

[4] R. Williams, *J. Phys. Chem.*, 1963, **39**, 382.

[5] G. W. Gray and S. M. Kelly, *J. Mater. Chem.*, 1999, **9**, 2037.

[6] P. J. Collings and M. Hird, *Introduction to Liquid Crystals: Chemistry and Physics*, Taylor & Francis, London, 1997, p. 51.

[7] G. W. Gray, K. J. Harrison and J. A. Nash, *Electron. Lett.*, 1973, **9**, 130.

[8] W. Haasel, Z. X. Fan and H. J. Müller, *J. Chem. Phys.*, 1988, **89**, 3317.

[9] S. Gierlotka, P. Lambooy and W. H. de Jeu, *Europhys. Lett.*, 1990, **12**, 341.

[10] A. J. Leadbetter, R. M. Richardson and C. N. Colling, *J. Phys., Colloq.*, 1975, **36**, C1-37.

[11] J. S. Foster and J. E. Frommer, *Nature*, 1988, **333**, 542.

[12] D. P. E. Smith, H. Hörber, C. Gerber and G. Binnig, *Science*, 1989, **245**, 43.

[13] W. Haase, H. Paulus and R. Pendzialek, *Mol. Cryst. Liq. Cryst.*, 1983, **100**, 211.

[14] J. Jadżyn and G. Czechowski, *Phys. Rev. E*, 2003, **67**, 041705.

[15] I. Zgura, R. Moldovan, T. Beica and S. Frunza, *Cryst. Res. Technol.*, 2009, **44**, 883.

[16] G.V. Vani, *Mol. Cryst. Liq. Cryst.*, 1983, **99**, 21.

[17] T. Ikeda, S. Kurihara and S. Tazyke, *J. Phys. Chem.*, 1990, **94**, 6550.

[18] Y. P. Piryatinskiĭ and O. V. Yaroshchuk, *Opt. Spectrosc.*, 2000, **89**, 860.

[19] K. Abe, A. Usami, K. Ishida, Y. Fukushima and T. Shigenari, *J. Korean Phys. Soc.*, 2005, **46**, 220.

[20] H. Fukunaga, J. Takimoto and M. Doi, *J. Chem. Phys.*, 2004, **120**, 7792.

[21] D. A. Dunmur, G. R. Luckhurst, M. R. de la Fuente, S. Diez and M. A. Peréz Jubindo, *J. Chem. Phys.*, 2001, **115**, 8681.

[22] Y. Ono and T. Shikata, *J. Am. Chem. Soc.*, 2006, **128**, 10030.

[23] Y. Satokawa and T. Shikata, *Macromolecules*, 2008, **414**, 2908.

[24] T. Shikata and M. Minamoto, *Nihon Reoroji Gakkaishi*, 2014, **42**, 197.

[25] A. Ghanadzadeh and M. S. Beevers, *J. Mol. Liq.*, 2003, **102**, 365.

[26] J. D. Kirkwood, *J. Chem. Phys.*, 1937, **7**, 911.

[27] T. I. Shabatina, E. V. Vovk, G. N. Andreev, A. Y. Bogomolov and G. B. Sergeev, *J. Struct.*

Chem., 1998, **39**, 318.

[28] I. B. Berlman, *Handbook of Fluorescence Spectra of Aromatic Molecules*, Academic Press, New York and London, 2nd edn, 1971, ch. 4.

[29] S. Urban, B. Gestblom and R. Dąbrowski, *Phys. Chem. Chem. Phys.*, 1999, **1**, 4843.

[30] S. K. Kundu, S. Okudaira, M. Kosuge, N. Shinyashiki and S. Yagihara, *J. Chem. Phys.*, 2008, **129**, 164509.

[31] T. Shikata and N. Sugimoto, *Phys. Chem. Chem. Phys.*, 2011, **13**, 16542.

[32] T. Shikata, N. Sugimoto, U. Sakai and J. Watanabe, *J. Phys. Chem. B*, 2012, **116**, 12605.

[33] T. Shikata, Y. Sakai and J. Watanabe, *AIP Adv.*, 2014, **4**, 067130.

[34] P. Reynders, W. Kuehnle, A. Klaas and K. A. Zachariasse, *J. Am. Chem. Soc.*, 1990, **112**, 3929.

[35] N. Tamai, I. Yamazaki, H. Masuhara and N. Mataga, *Chem. Phys. Lett.*, 1984, **104**, 485.

[36] N. Tamai, I. Yamazaki, H. Masuhara and N. Mataga, "Picosecond Time-Resolved Fluorescence Spectra of Liquid Crystal : Cyanooctylbiphenyls," in Ultrafast Phenomena IV, D.H. Auston and K.B. Eisenthal, eds., pp. 355–358, Springer, Berlin, 1984

[37] J. B. Birks, *Rep. Prog. Phys.*, 1975, **38**, 903.

[38] J.B. Birks, Photophysics of Aromatic Molecules, Ch. 7, Wiley-Interscience, New York, 1971

[39] S. Sinton and A. Pines, *Chem. Phys. Lett.*, 1980, **76**, 263.

[40] G. Celebre, M. Longeri, E. Sicilia and J. W. Emsley, *Liq. Cryst.*, 1990, **7**, 731.

[41] A. M. Klock, W. Rettig, J. Hofkens, M. van Damme and F. C. De Schryver, *J. Photochem. Photobiol. A*, 1995, **85**, 11.

[42] G. Jones, II and V. I. Vullev, *J. Phys. Chem. A*, 2001, **105**, 6402.

Chapter 4 Anti-parallel Dimer Formation of Ethylene Carbonate in Solution

4.1. Introduction

Ethylene carbonate (EC), which is a five-membered ring shaped carbonate, has been widely used as a typical high permittivity chemical component in electrolyte liquids in many commercial lithium ion secondary batteries.[1–5] EC has also been used as a dipolar aprotic chemical component of reacting liquids for various types of chemical reactions that require highly polar conditions.[6,7] Because the melting point of EC, 36–37 °C, is slightly higher than room temperature, EC is typically used in solution form where it is dissolved in other low melting point liquids for use in applications at room temperature. For example, for electrolyte liquids employed in lithium ion batteries, EC is dissolved in dimethyl carbonate (DMC), possessing a lower meting point of 24 °C.

It is still unclear if EC forms dimers in its liquid state and in solution.[8–14] Several studies using vibrational spectroscopic experimental techniques, such as infrared absorption (IR) and Raman scattering (RS) measurements,[8–11] indicate that EC forms dimers ($(EC)_2$) in an anti-parallel conformation with respect to the electric dipole moments due to the strong dipole–dipole interactions because of its dipole moment, which is larger than 4 D. The results from ab initio quantum chemical calculations have also predicted the formation of $(EC)_2$ in the anti-parallel conformation in the gaseous state, and this conformation has a much more stable formation energy than the dimer where the dipoles are in a series configuration.[11,12] Nevertheless, a dielectric investigation demonstrated the absence of specific intermolecular interactions between EC molecules.[13]

A recent pioneering IR study of EC dimer formation performed using supersonic jet expansion methods indicated that monomeric EC molecules possess only a single C=O stretching vibrational band. However, the dimer, $(EC)_2$, exhibits C=O vibration bands sharply split into two frequencies due to a Fermi resonance effect.[14] This discovery is consistent with the observation of both the C=O vibration and the Fermi resonance effect between the C=O vibration mode (ν_2) and the first overtone of the ring breathing vibration mode ($2\nu_7$) in the pure liquid state containing the anti-parallel dimers.[10,15] In addition, these results would also be helpful for the precise population analysis of $(EC)_2$ based on the IR and Raman data for EC in the molten state and in solution. However, no quantitative discussion of the anti-parallel dimer formation of EC has been previously reported even though it is essential for improving the performance of lithium ion batteries.

Dielectric spectroscopic (DS) measurements are highly sensitive for the detection of the presence of anti-parallel dimers *via* the evaluation of the orientational correlation factor of dipole moments, which is quantified as the ratio of the square of the apparent dipole moment ($\boldsymbol{\mu}_{app}^2$) to that of the intrinsic one ($\boldsymbol{\mu}_0^2$) for a tested compound and is called the Kirkwood factor ($g_K = \boldsymbol{\mu}_{app}^2\boldsymbol{\mu}_0^{-2}$).[16,17] When the g_K values are smaller than unity, the tested compound has a tendency to form anti-parallel dimers in the system.[16] The $|\boldsymbol{\mu}_0|$ value of 4.87D[18] for EC, which has been widely reported, was recently determined again using dielectric techniques in a benzene (Bz) solution.[19] However, the determination of the magnitude of $|\boldsymbol{\mu}_0|$ for EC is difficult due to the formation of anti-parallel dimers bearing a total dipole moment of approximately zero due to a dipole–dipole interaction caused by its large dipole moment, even in vapor phase experiments using microwave techniques.[14] Then, a $|\boldsymbol{\mu}_0|$ value of 5.2–5.5 D for EC was determined using careful microwave techniques.[20] This $|\boldsymbol{\mu}_0|$ value has been confirmed by ab initio quantum chemical calculations[21,22] and is much larger than that previously determined by *ca.* 0.5 D. Therefore, the conclusion that EC does not form dimers based on DS measurements is doubtful and should be reconsidered using the newly determined and correct $|\boldsymbol{\mu}_0|$ value.

Ab initio quantum chemical calculations to inspect the formation of heterodimers between EC and DMC (EC–DMC) were performed in a vacuum.[12] Because the obtained result showed finite but lower binding energies for EC–DMC than those for anti-parallel EC dimer, $(EC)_2$, it was concluded that EC molecules behave freer in DMC solution than in a pure liquid state of EC (at higher temperature than 40 °C) as reported by Klassen *et al.*[9,12] If EC–Bz heterodimers possess less binding or interaction energies than those for EC–DMC ones, EC molecules probably form much more anti-parallel dimers, $(EC)_2$, in Bz solution than in DMC.

To improve the performance of electrolyte liquids contained in lithium ion secondary batteries, the efficiency of tested polar molecules, such as EC and propylene carbonate (PC), to lithium ions has so far been mainly investigated.[9,23] However, the literature has provided evidence that EC and PC molecules form intermolecular association such as anti-parallel dimers as described above.[912,23] If EC molecules form the anti-parallel dimers, $(EC)_2$, in electrolyte liquids of lithium ion secondary batteries, there should be at least two basic chemical reactions controlled by each equilibrium process such as $2EC \leftrightarrow (EC)_2$ and $nEC + Li^+ \leftrightarrow Li^+(EC)_n$, where n means the coordination number of EC to Li^+. Seeking important factors to improve performance of electrolyte liquids in lithium ion secondary batteries, full understanding of the chemical equilibrium process, $2EC \leftrightarrow (EC)_2$, should be essential. A comparison between the efficiency of anti-parallel dimer formation in a relatively

good solvent, DMC, which has been used in many commercial lithium ion batteries, and that in a not so good solvent, Bz, would be considerably helpful for understanding of the mechanism of anti-parallel dimer formation of EC in liquid state.

In this study, RS measurements were performed using EC solutions dissolved in Bz and DMC at room temperature to investigate the concentration dependence of the population of monomeric EC and $(EC)_2$. Then, the chemical equilibrium constant (K_d^{RS}) for the formation of anti-parallel dimers, $(EC)_2$, was evaluated based on the RS data as a function of the concentration assuming a simple chemical process, $2EC \leftrightarrow (EC)_2$. The dependence of the solvent species, such as Bz and DMC, on the values of K_d^{RS} is also discussed to provide information that may be useful for improving the performance of lithium ion secondary batteries.

4.2. Experimental

Materials

Highly purified ethylene carbonate, EC (>99.0%), benzene, Bz (>99.5%), and dimethyl carbonate, DMC (>98.0%), were purchased from the Tokyo Chemical Industry Co., Ltd. (Tokyo) and used without further purification. The concentration of EC in the Bz solution ranged from 6.3×10^{-2} M (0.62 wt%) to 6.0 M (48.7 wt%), and the concentration in the DMC solution ranged from 1.5×10^{-1} M (1.2 wt%) to 11.5 M (80.0 wt%).

Methods

The total Raman scattering (RS) spectra (total scattering intensities ($I(wn)$) vs the Raman shift (wn in the unit of cm^{-1})) were recorded at room temperature (*ca.* 25.0 °C) using an XploRA Plus confocal Raman microscope (Horiba, Ltd., Kyoto) in spectroscope mode equipped with a Nd:YAG laser system emitting a green light source at a wavelength of 532 nm and a multi-pass liquid cell. The system was operated at a resolution of 3.15 cm^{-1}. The sample solution was poured into a conventional rectangular quartz cuvette of 1 cm × 1 cm in size that was placed in the multi-pass liquid cell. In the wn range from 1760 to 1820 cm^{-1} discussed in this study, the obtained Raman spectra, $I(wn)$, well correspond to the products of the spectra for the square of polarizability changes of EC molecules and their number density.

4.3. Results and discussion

4.3.1. EC/Bz system.

The Raman scattering spectra for the EC/Bz system, which ranged from c = 0 M (Bz) to 6.01 M in a Raman shift regime corresponding to the C=O stretching vibrational mode, 1740 < wn < 1860 cm^{-1}, are shown in Fig. 4.1(a). Because the solvent, Bz, has no significant vibrational signals in the wn region except for a very weak signal observed at 1765 cm^{-1}, all the signals observed in Fig. 4.1(a) correspond to those from the EC molecules. From an overview of the concentration dependence of the spectra, $I(wn)$, shown in Fig. 4.1(a), EC has at least three vibrational signals located at 1773, 1795–1800, and 1815 cm^{-1}, and the magnitudes of these signals varied as the concentration (c) increased. EC does not exhibit any signals at 1773 and 1795–1800 cm^{-1} but does exhibit a signal at a higher Raman shift of 1815 cm^{-1} when c is less than 0.2 M. The relative intensities of the two lower Raman shift signals compared to that of the higher Raman shift signal at 1815 cm^{-1} increased with increasing c. Therefore, the vibrational mode observed at 1815 cm^{-1} corresponds to the C=O stretching mode of the monomeric EC molecule.

To confirm the three constituent vibrational modes for $I(wn)$ in Fig. 4.1(a), we carried out a curve fitting procedure that decomposed $I(wn)$ into three vibrational modes ($I_j(wn)$; j = 1, 2, and 3). Figure 4.1(b) shows the wn dependence of $I(wn)$ for a EC/Bz solution at c = 3.43 M along with the fitted (solid line) curve resulting from the summation of three constituent Lorentz-type scattering functions, $I_j(wn) = (I_j\delta_j/\pi)((wn - wn_j)^2 + \delta_j^2)^{-1}$ (dotted lines), with the strength intensities (I_j ; j =

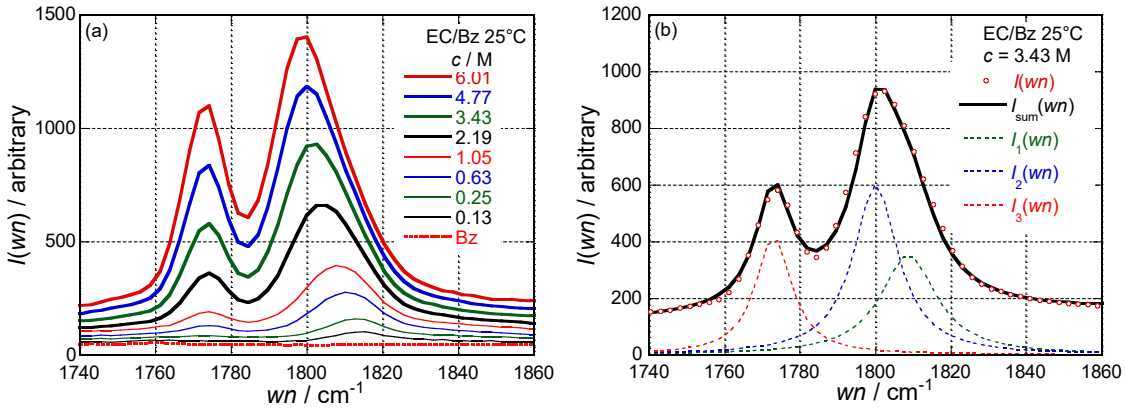

Fig. 4.1. (a) Raman scattering spectra, $I(wn)$, as a function of the Raman shift, wn, for the EC/Bz system at several concentrations and at 25 °C. (b) The fitted spectrum (solid line) for the EC/Bz solution at c = 3.43 M. The three constituent signal components (dotted lines) are also shown.

1, 2, and 3 from the highest wavenumber), characteristic Raman shifts (wn_j) and half-width values ($2\delta_j$) shown in the figure as a typical example. Reasonable agreement between $I(wn)$ and the fitted curve ($I_{sum}(wn) = I_1(wn) + I_2(wn) + I_3(wn)$) indicates that the RS spectra for the EC/Bz system in the C=O stretching regime are composed of the three vibrational modes described above. This reasonable agreement between the $I(wn)$ data and the fitted curves *via* the same fit procedure was confirmed for the other EC/Bz solutions examined in this study.

Figure 4.2(a) shows the c dependence of the characteristic Raman shift, wn_j, and half width values, $2\delta_j$, and Fig. 4.2(b) shows the respective strengths, I_j, determined by the curve fitting procedure for the EC/Bz system. Because the values of wn_j and $2\delta_j$ are weakly affected by the value of c, the basic characteristics of each vibrational mode are not altered by c. Although the relative ratio of I_2 to I_3 was maintained at a constant value of *ca.* 1.8 irrespective of the c value, the ratio of I_2 (or I_3) to I_1 strongly depended on the c value. This observation indicated that the j = 2 and 3 vibrational modes resulted from the same chemical species. Based on the IR experimental results on the EC molecules obtained using the monomeric EC dominated jet spectrum method, no evidence was observed for pronounced Fermi resonance in monomeric EC molecules, but a single C=O stretching vibrational signal was observed.[14] However, using the heated jet spectrum method, the anti-parallel dimers ($(EC)_2$) exhibited two distinct vibrational signals: a C=O stretching vibrational signal shifted toward a lower energy and an additional signal caused by the Fermi resonance effect at a substantially lower Raman shift than that of the C=O stretching mode.[14] Based

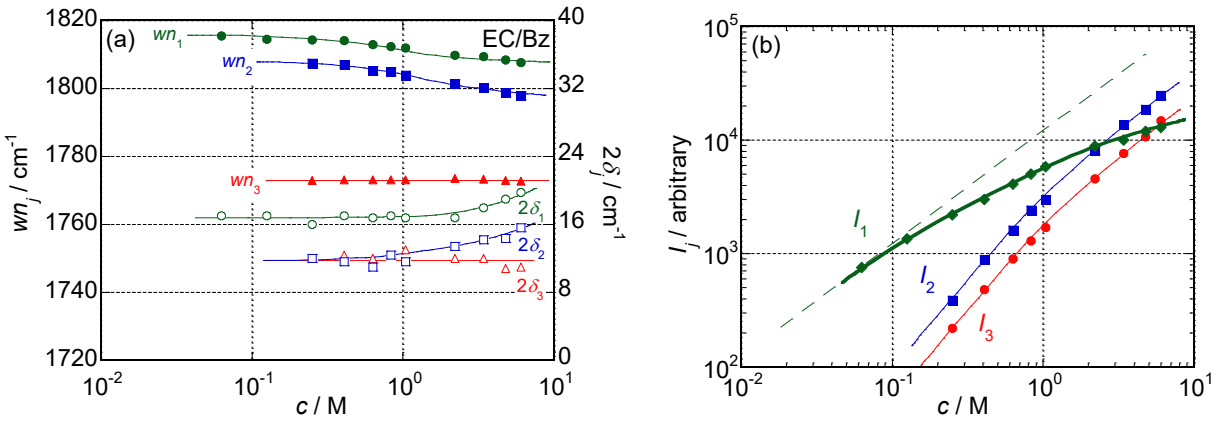

Fig. 4.2. Concentration, c, dependence of the (a) Raman shift, wn_j, and half-width values, $2\delta_j$, and (b) signal strength, I_j, of the three constituent modes for the EC/Bz system at 25 °C. Solid lines are guides to the eye. A thin broken line in (b) means the linear relationship between I_1 and c found only in a dilute regime.

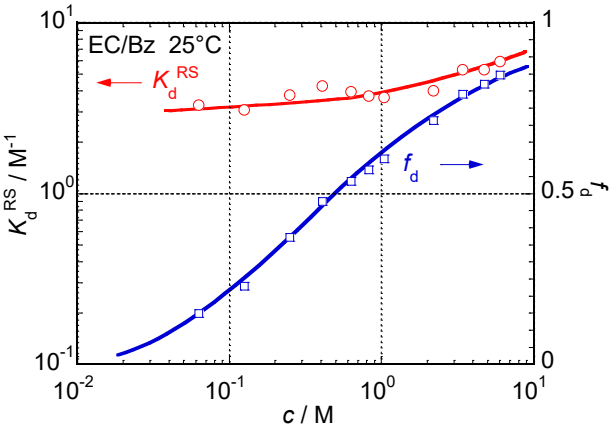

Fig. 4.3. Concentration, c, dependence of the obtained equilibrium constants for anti-parallel dimer formation, K_d^{RS}, and the molar fraction of anti-parallel dimers, f_d, for the EC/Bz systems at 25 °C. Solid lines are guides to the eye.

on these results, the two vibration modes, j = 2 and 3, in the EC/Bz system correspond to C=O stretching and the Raman resonance modes of the formed anti-parallel dimers, respectively. However, the j =1 vibrational mode, which has a strength, I_1, that was proportional to c only in an extremely dilute regime in the manner $I_1 = \alpha \cdot c$, where $\alpha = ca.\ 1.4 \times 10^4\ M^{-1}$ (a thin broken line in Fig. 4.2(b)), is a proportional constant, was attributed to the C=O stretching vibrational mode of monomeric EC molecules. Then, the concentration of monomeric EC ([EC]) was evaluated using the following relationship $[EC] = I \cdot (\alpha)^{-1}$, even in a concentration range where additional vibrational modes, j = 2 and 3, were observed.

Fortunato *et al.*[15] also assigned the vibrational bands observed at 1798 and 1773 cm^{-1} found in liquid state EC at 50 °C to the C=O stretching mode and the Fermi resonance mode between the C=O stretching (ν_2) and ring breathing ($2\nu_7$) modes of EC molecules, respectively. However, since most EC molecules form anti-parallel dimers in the bulk EC liquid, their assignments should be corrected to be the C=O stretching and the Fermi resonance mode of anti-parallel dimers, $(EC)_2$.

Ab initio quantum chemical calculations suggested the presence of a trimer of EC molecules possessing a binding energy comparable to that of the anti-parallel dimer and a unique cyclic-type structure in dipoles.[12] If EC trimers bearing such a cyclic structure exist in the system examined, rather different Raman spectrum for C=O stretching vibration mode than that of the anti-parallel dimers would be observed. However, the obtained Raman spectra were reasonably decomposed into three modes, and the vibration modes, j = 2 and 3, observed at lower Raman shifts demonstrated the identical concentration dependence originated by the same chemical species, i.e. the anti-parallel dimer. Consequently, a monomeric EC molecule and an anti-parallel dimer are major chemical

species to be considered in this study.

Since the concentration of EC, c, was altered widely in this study, electric permittivity substantially heightened at high c values in both the solutions examined. Then, a change in the electric permittivity possibly alters the values of wn_j and $2\delta_j$ slightly. Moreover, an increase in the number densities of EC and anti-parallel dimers, $(EC)_2$, in itself would subtly influence the structure of anti-parallel dimers, *e.g.* the separation between two constituent EC molecules. Then, it is likely that the values of wn_j and $2\delta_j$ for the anti-parallel dimer are slightly affected by concentration change as observed in Fig. 4.2(a).

Here, the author simply assumes a chemical equilibrium process for the anti-parallel dimer formation of EC: $2EC \leftrightarrow (EC)_2$. Then, the equilibrium constant for this chemical process is expressed as $K_d^{RS} \equiv [(EC)_2]/[EC]^2$. According to the chemical process, because the relationship $c = [EC] + 2[(EC)^2]$ holds, the concentration of anti-parallel dimers is given by the following equation: $[(EC)_2] = (c - [EC])/2$. Therefore, the equilibrium constant (K_d^{RS}) can be calculated from the I_1 data as a function of the concentration (c) as follows:

$$K_d^{RS} \equiv (c - [EC]) \cdot [EC]^{-2}/2 = (\alpha/2) \cdot (\alpha c - I_1) \cdot (I_1)^{-2} \qquad (4.1)$$

Here, the K_d^{RS} value was determined from the I_1 data shown in Fig. 4.2(b) for the EC/Bz system and is shown as a function of c in Fig. 4.3. A mole fraction of dimer forming EC molecules given by $f_d = 1 - I_1 \cdot (\alpha c)^{-1}$ is also shown in Fig. 4.3. Over the entire c range studied, the K_d^{RS} value slightly depended on the c value, and increased from *ca.* 3.0 M^{-1} (at c = 0.13 M) up to *ca.* 6.0 M^{-1} (c = 6.01 M). In a dilute regime, such as $c < 0.1$ M, the dimer forming fraction, f_d, was less than 0.2. In a c range higher than 3.0 M, most ($f_d > 0.8$) of the EC molecules existed as anti-parallel dimers, as observed in Fig. 4.3.

Because I_2 and I_3 should be proportional to $[(EC)_2]$ (*i.e.*, $I_2 = \beta[(EC)_2]$ and $I_3 = \gamma[(EC)_2]$), the proportional constants, β and γ, can be expressed by the following relationship: $\beta = 2I_2 \cdot \{c - I_1 \cdot (\alpha)^{-1}\}^{-1}$ and $\gamma = 2I_3 \cdot \{c - I_1 \cdot (\alpha)^{-1}\}^{-1}$. These approximately constant values β, *ca.* 1.0×10^4 M^{-1}, and γ, *ca.* 5.6×10^3 M^{-1}, were obtained irrespective of the c value, which confirms the assumed basic chemical process for the anti-parallel dimer formation.

4.3.2. EC/DMC system

For the RS data of the EC/DMC system, the same analytical procedure used in the EC/Bz system worked well. However, because the DMC solvent exhibited a strong C=O stretching vibrational signal with a Raman shift of *ca.* 1753 cm^{-1}, which is close to that of the EC molecules shown in Fig. 4.4(a), the C=O signal corresponding to DMC was eliminated from the total RS spectra, assuming its intensity was proportional to the concentration of DMC. Figure 4.4(b) shows the dependence of the modified RS spectrum ($I_{mod}(wn)$) on *wn* of the EC/DMC solution at c = 5.30 M as a typical example where the C=O stretching signal corresponding to EC, which was observed at 1753 cm^{-1}, was precisely eliminated. The modified RS spectrum ($I_{mod}(wn)$) has a similar appearance to $I(wn)$ of EC/Bz shown in Fig. 4.1(b). Therefore, the idea that the vibrational spectra in the Raman shift range are composed of three Lorentz-type scattering functions was also accepted in the EC/DMC system. Figure 4.4(b) also shows the fitted (solid line) curve resulting from the summation of three constituent Lorentz-type scattering functions (dotted lines). The reasonable agreement between $I_{mod}(wn)$ and the fitted curve ($I_{sum}(wn)$) confirmed the validity of the three-component idea. This reasonable agreement between the $I_{mod}(wn)$ and fitted curves was also obtained for all the studied EC/DMC solutions.

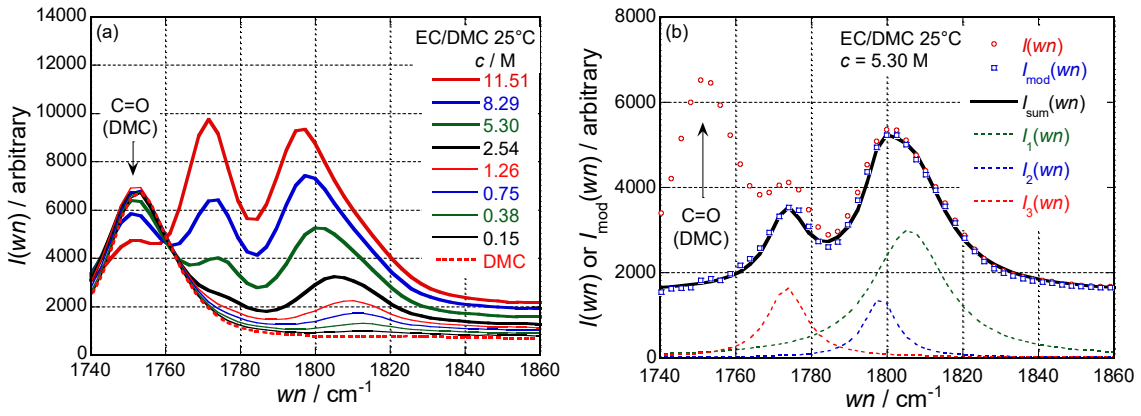

Fig. 4.4. (a) Raman scattering spectra as a function of the Raman shift, *wn*, for the EC/DMC system at several concentrations and at 25 °C. (b) The fitted spectrum (solid line) to the modified Raman scattering spectrum, $I_{mod}(wn)$, without the contribution of C=O stretching signal of DMC for the EC/DMC solution at c = 5.30 M. The three constituent signal components (dotted lines) are also shown.

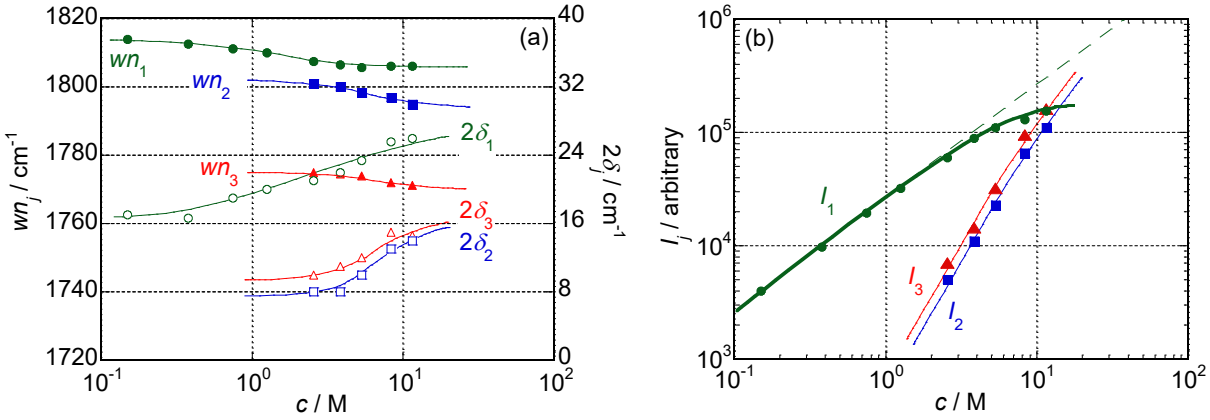

Fig. 4.5. Concentration, c, dependence of the (a) Raman shifts, wn_j, and half-width values, $2\delta_j$, and (b) signal strength, I_j, of the three constituent modes for the EC/DMC system at 25 °C. Solid lines are guides to the eye. A thin broken line in (b) means the linear relationship between I_1 and c in a dilute regime.

Figures 4.5(a) and 4.5(b) show the c dependencies of the characteristic Raman shifts, v_j, and half width values, $2\delta_j$, and of the strengths, I_j, respectively, which were determined by the curve fitting procedure for the EC/DMC system. The c dependence of wn_j was not strong in the EC/DMC system. The I_2 to I_3 ratio was maintained at a constant value of *ca.* 0.7 irrespective of the c value, and the I_2 (or I_3) to I_1 ratio was dependent on the c value, which was also observed in the EC/Bz system.

Figure 4.6 shows the dependence of the K_d^{RS} value on c, which was determined from the I_1 data in the EC/DMC system *via* eqn 4.1 using an α value of 2.63×10^4 M^{-1}, evaluated from the c dependence of I_1 (a thin broken line) shown in Fig. 4.5(b). The mole fraction of dimer forming the EC molecules (f_d) is also included in Fig. 4.6. In a concentration range of $c < 3.0$ M, K_d^{RS} exhibited a nearly constant value of *ca.* 0.03 M^{-1} with a slightly increasing trend with increasing c. However, in the other c range of $c > 3.0$ M, K_d^{RS} substantially increased as c increased. Corresponding to the c dependence of K_d^{RS}, the value of f_d substantially increased from 0.1 ($c < 3.0$ M) to 0.5 ($c = 11.5$ M). Because less than 10% of the EC molecules exist as anti-parallel dimers even at a c value of 3.0 M in the EC/DMC (Fig. 4.6), this behavior is markedly distinctive from the behavior observed in the EC/Bz system (*ca.* 70% at $c = 3.0$ M, as seen in Fig. 4.3). Therefore, the c dependence of K_d^{RS} for the EC/DMC system is different from that for the EC/Bz system. The slightly polar DMC may act as a much better solvent for EC than nonpolar Bz. DMC can dissolve many more EC molecules in a molecularly dispersed shape compared to Bz. In addition, because nearly constant β (*ca.* $3.9 \times 10^3 M^{-1}$) and γ (*ca.* 5.7×10^3 M^{-1}) values were obtained irrespective of the c value, the validity of the assumed basic chemical process of the anti-parallel dimer formation was also confirmed for the

EC/DMC system.

Based on a comparison of the wn_j and $2\delta_j$ values in a higher c region for the EC/Bz and EC/DMC systems shown in Figs. 4.2(a) and 4.5(a), all the wn_j values for the EC/DMC system are a few cm^{-1} smaller. In contrast, the $2\delta_1$ and $2\delta_3$ values of the EC/DMC system are larger than those of the EC/Bz system. In addition, the $I_2 > I_3$ relationship observed in the EC/Bz system was reversed in the EC/DMC system, as shown in Figs. 4.2(b) and 4.5(b). These results indicate that the structures of the anti-parallel dimers, $(EC)_2$, formed in the two systems are not identical. Presumably, some characteristic structural parameters, such as the mean separation between two EC molecules, are slightly different.

As described in the introduction, dielectric spectroscopic, DS, measurements can detect the presence of anti-parallel dimers of a tested compound. The value of the intrinsic dipole moment, $|\boldsymbol{\mu}_0|$, of EC, which is required to calculate the Kirkwood factor, g_K, is useful for discussion of anti-parallel dimer formation, and this value was recently determined precisely using a microwave technique[20] and ab initio calculations.[21,22] Therefore, the equilibrium constant of anti-parallel dimer formation of EC (K_d^{DS}) can be determined in some media, including Bz and DMC, *via* DS techniques. In chapter 5, the author will report the values of K_d^{DS} for the EC/Bz and EC/DMC systems and compare the values of K_d^{DS} and K_d^{RS} to confirm that EC forms anti-parallel dimers in solution and that the equilibrium of the dimer formation is controllable by choosing the solvent species and tuning the EC composition in the solution.

The performance of lithium ion secondary batteries is influenced by electric conductivity due to Li^+ cations being solvated by several EC molecules in the electrolyte liquids in these batteries.

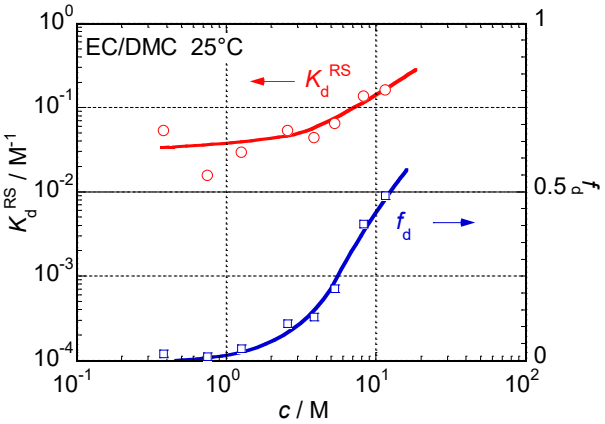

Fig. 4.6. Concentration, c, dependence of the obtained equilibrium constants for anti-parallel dimer formation, K_d^{RS}, and the molar fraction of anti-parallel dimers, f_d, for the EC/DMC systems at 25 °C. Solid lines are guides to the eye.

Therefore, a different chemical process occurring between Li^+ cations and EC molecules that possesses a different equilibrium constant should be considered in these batteries, which is closely related to the chemical process of anti-parallel dimer formation, $2EC \leftrightarrow (EC)_2$, that has been extensively discussed in this study.

4.4. Conclusions

Ethylene carbonate (EC), which has been widely used as a main dipolar component of electrolyte liquids in many commercially available lithium ion secondary batteries, forms anti-parallel dimers ($(EC)_2$) in solutions consisting of pure solvents, such as benzene (Bz) and dimethyl carbonate (DMC), at room temperature. The tendency of anti-parallel dimer formation for EC was precisely quantified by the value of the equilibrium constant of the $2EC \leftrightarrow (EC)_2$ chemical process using Raman scattering spectroscopic experiments. The equilibrium constant was dependent on the solvent species and the EC composition in solution, and EC formed more anti-parallel dimers in nonpolar Bz than in slightly polar DMC, as schematically described in Fig. 4.7.

The strong Raman band observed at approximately 1800 cm^{-1} was split into a signal assigned to the C=O stretching of monomeric EC molecules (1810–1815 cm^{-1}) and two signals related to anti-parallel dimers as follows: a C=O stretching band (1800–1810 cm^{-1}) and an additional Fermi resonance one (1773 cm^{-1}) caused by the formation of anti-parallel dimers in the studied solutions.

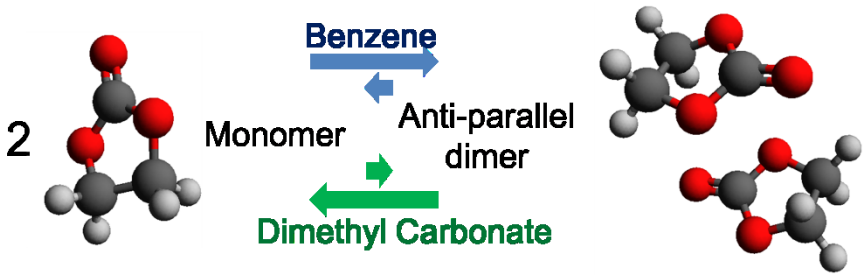

Fig. 4.7. Schematic depiction of the chemical reaction between monomeric EC and anti-parallel dimeric $(EC)_2$.

4.5. References

[1] J.-M. Tarascon, M. Armand, *Nature*, 2001, **414**, 359.

[2] P. G. Bruce, S. A. Freunberger, L. J. Hardwick, J.-M. Tarascon, *Nat. Mater.*, 2012, **11**, 19.

[3] D. Aurbach, M. D. Levi, E. Levi, A. Schechter, *J. Phys. Chem. B*, 1997, **101**, 2195.

[4] K. Takei, N. Terada, K. Kumai, T. Iwahori, T. Uwai, T. Miura, *J. Power Sources*, 1995, **55**, 191.

[5] D. Aurbach, B. Markovsky, A. Shechter, Y. Ein-Eli, H. Cohen, *J. Electrochem. Soc.*, 1996, **143**, 3809.

[6] A.-A. G. Shaikh, S. Sivaram, *Chem. Rev.*, 1996, **96**, 951.

[7] B. Schäffner, F. Schäffner, S. P. Verevkin, A. Börner, *Chem. Rev.*, 2010, **110**, 4554.

[8] G.Fini, P. Mirone, B. Fortunato, *J. Chem. Soc., Faraday Trans. 2*, 1973, **69**, 1243.

[9] B. Klassen, R. Aroca, M. Nazri, G. A. Nazri, *J. Phys. Chem. B*, 1998, **102**, 4795.

[10] W. Schindler, T. W. Zerda, J. Jonas, *J. Chem. Phys.*, 1984, **81**, 4306.

[11] P. D. Vaz, P. J. A. Ribeiro-Claro, *Struct. Chem.*, 2005, **16**, 287.

[12] Y. Wang, P. B. Balbuena, *J. Phys. Chem. A*, 2001, **105**, 9972.

[13] R. Payne, I. E. Theodorou, *J. Phys. Chem.*, 1972, **76**, 2892.

[14] F. Kollipost, S. Hesse, J. J. Lee, M. A. Suhm, *Phys. Chem. Chem. Phys.*, 2011, **13**, 14176.

[15] B. Fortunato, P. Mirone, G. Fini, *Spectrochim. Acta, Part A*, 1971, **27**, 1917.

[16] G. Oster, J. G. Kirkwood, *J. Chem. Phys.*, 1943, **11**, 175.

[17] T. Shikata, N. Sugimoto, *Phys. Chem. Chem. Phys.*, 2011, **13**, 16542.

[18] R. Kempa, W. H. Lee, *J. Chem. Soc.*, **1958**, 1936.

[19] Y. Chernyak, *J. Chem. Eng. Data*, 2006, **51**, 416.

[20] J. L. Alonso, R. Cervellati, A. D. Esposti, D. G. Lister, P. Palmieri, *J. Chem. Soc., Faraday Trans. 2*, 1986, **82**, 357.

[21] K. D. Jordan, F. Wang, *Annu. Rev. Phys. Chem.*, 2003, **54**, 367.

[22] L. B. Silva, L. C. G. Freitas, *THEOCHEM*, 2007, **806**, 23.

[23] M. G. Giorgini, K. Futamatagawa, H. Torii, M. Musso, S. Ceromo, *J. Phys. Chem. Lett.*, 2015, **6**, 3296.

Chapter 5 A Dielectric Spectroscopic Study of Ethylene Carbonate in Solution

5.1. Introduction

A five-membered ring carbonate, ethylene carbonate (EC), has been widely used as a high permittivity chemical component in the electrolyte liquids of many commercial lithium ion secondary batteries.[1–5] EC and its derivatives have also been used as dipolar aprotic solvents for various chemical reactions that require polar conditions.[6,7] EC is usually dissolved in other liquids possessing low melting points (T_m) for many practical applications at room temperature because the T_m of EC, *ca.* 40 °C, is higher than room temperature. A solution of EC in dimethyl carbonate (DMC) bearing T_m = 24 °C has been widely used as an electrolytic liquid in lithium ion secondary batteries.

Some vibrational spectroscopy studies employing infrared absorption (IR) and Raman scattering (RS) techniques[8–12] have demonstrated that EC forms dimers ($(EC)_2$) in an anti-parallel conformation because of strong dipole–dipole interactions. The dipole moment of EC is greater than 4 D, which is the reason for the strong dipole–dipole interactions. Several ab initio quantum chemical calculations have predicted the formation of $(EC)_2$ in the anti-parallel conformation in the gaseous state; the anti-parallel conformation has a more stable formation energy than that of a dimer keeping the two dipoles in a parallel configuration.[11,13]

An IR study using supersonic jet expansion methods has clearly revealed that monomeric EC molecules show a single sharp C=O stretching vibrational band, while the anti-parallel dimers $(EC)_2$ present doublet C=O vibrational bands that are clearly split into two frequencies because of a Fermi resonance effect.[14] This discovery is consistent with the well-known observation of both the C=O stretching vibration and the Fermi resonance effect between the C=O vibrational mode ($\nu 2$) and the first overtone of the ring breathing vibrational mode ($2\nu_7$) in the pure liquid state of EC containing the anti-parallel dimers.[10,15] These investigations are useful for a population analysis of $(EC)_2$ based on the IR and Raman data for EC in the molten state and in solution. Although information about intermolecular association formation is essential for improving the performance of lithium ion batteries, there is very little quantitative discussion about the anti-parallel dimer formation of EC. A previous study using RS techniques has clearly demonstrated the presence of anti-parallel dimers in solutions of benzene (Bz) and DMC.[12] The populations of monomeric EC and dimeric $(EC)_2$ were first successfully evaluated as functions of the concentration of EC based on the RS data analysis,

which determined the difference in C=O vibration bands between the monomer and the dimer.[12] The EC concentration dependence of the equilibrium constant K_d^{RS} for anti-parallel dimer formation at room temperature was newly evaluated *via* RS spectrum analysis, assuming a chemical process 2EC ↔ $(EC)_2$. Moreover, it has clearly been demonstrated that the value of K_d^{RS} is highly dependent on the species of solvent.

On the other hand, dielectric spectroscopic (DS) studies have demonstrated that there are no specific intermolecular interactions between EC molecules, such as the anti-parallel dimer formation caused by the strong dipole–dipole interaction.[12,16] Because DS measurements are highly sensitive to the magnitude of dipole moments, the amount of anti-parallel dimers is also evaluable through quantification of the orientational correlation factor of dipole moments, which is defined as the ratio of the square of the apparent dipole moment ($\boldsymbol{\mu}_{app}^2$) to that of the intrinsic dipole moment ($\boldsymbol{\mu}_0^2$) for an examined substance ($g_K = \boldsymbol{\mu}_{app}^2 \boldsymbol{\mu}_0^{-2}$) and is called the Kirkwood correlation factor.[17,18] When an examined substance possesses a g_K value smaller than unity, it has a tendency to form anti-parallel dimers in the system.[17] More than seven decades ago, the $|\boldsymbol{\mu}_0|$ value of 4.87 D[19] for EC was reported and has been widely used. A value for EC, which is very close to 4.87 D, was recently reported again *via* a dielectric study in a benzene (Bz) solution.[20] However, it has been noted that the determination of the magnitude of $|\boldsymbol{\mu}_0|$ for EC is quite difficult due to the formation of anti-parallel dimers, even in vapor phase experiments using microwave techniques. These dimers possess a total dipole moment of approximately zero due to a strong dipole–dipole interaction that is caused by large dipole moment of the isolated molecule.[14] Eventually, a value of 5.2–5.5 D for the $|\boldsymbol{\mu}_0|$ of EC was determined *via* careful experimental techniques using microwave spectrospcopy.[21] This $|\boldsymbol{\mu}_0|$ value has also been confirmed by several ab initio quantum chemical calculations[22,23] and is markedly greater than the value previously determined by dielectric techniques. Therefore, the conclusion that EC does not form anti-parallel dimers, which resulted from (classical) DS studies, is highly doubtful and should be reconsidered using the precisely determined correct $|\boldsymbol{\mu}_0|$ value.

In this study, DS measurements were performed in EC solutions with (non-polar) Bz and (slightly polar) DMC as the solvents at room temperature to investigate the concentration dependence of the population of monomeric EC and/or the anti-parallel dimer $(EC)_2$. Then, the determination of the chemical equilibrium constant (K_d^{DS}) for $(EC)_2$ formation was based on the DS data as a function of concentration, while assuming a simple dimer formation chemical process, 2EC ↔ $(EC)_2$. The dependence of the solvent species on the values of K_d^{DS} was also discussed to provide useful

information for improving the performance of lithium ion secondary batteries. Moreover, the author would like to compare the values of K_d^{DS} and K_d^{RS} to validate the idea that EC forms anti-parallel dimers by the simple chemical process.

5.2. Experimental

Materials

Highly purified ethylene carbonate, EC (>99.0%); benzene, Bz (>99.5%); and dimethyl carbonate, DMC (>98.0%) were purchased from Tokyo Chemical Industry Co., Ltd. (Tokyo) and used without further purification. The concentration of EC in the Bz solution ranged from 6.3×10^{-2} M (0.6 wt%) to 6.0 M (49 wt%), and the concentration in the DMC solution ranged from 1.24 M (10 wt%) to 11.51 M (80 wt%). Solution samples were prepared by weight, and molarity concentrations were calculated assuming the proportionality of density in prepared solution.

Methods

Dielectric spectroscopic (DS) measurements were performed over a wide frequency range from 50 MHz to 3 THz at room temperature, *ca.* 25.0 °C. Two systems were used to perform DS measurements over such a wide frequency range. A dielectric probe kit 85070E was equipped with network analyzer N5230C, ECal module N4693A, and performance probe 05 (Agilent Technologies, Santa Clara, USA), and was used for dielectric relaxation measurements over a frequency range from 50 MHz to 50 GHz (3.14×10^8–3.14×10^{11} s^{-1} in angular frequency (ω)). Real and imaginary (loss) parts (ε' and ε'') of electric permittivity were automatically calculated from reflection coefficients measured by the network analyzer *via* a program supplied by Agilent Technologies. A three-point calibration procedure using *n*-hexane, 3-pentanone, and water as the standard materials was performed prior to all the dielectric measurements.[18] Details for the three-point calibrating procedure used in this study have been described elsewhere.[18] Depending on the magnitude of ε'', the determined ε'' data in a frequency range lower than 500 MHz (3.14×10^9 s^{-1}) were scattered and out of reliability especially for dilute samples. In that case, only the ε'' data in the frequency range higher than 500 MHz possessing sufficient reliability were accepted.

A terahertz spectrometer (C12068-2, Hamamatsu Photonics K.K., Hamamatsu) was employed to perform DS measurements in a higher frequency range from 100 GHz to 3 THz (6.28×10^{11}–1.88×10^{13} s^{-1} in ω). This terahertz range spectrometer is basically a time-domain reflectometer possessing a femtosecond laser pulse unit at a wavelength of 780 nm as pumping (emitting) and probing

(detecting) light sources. The instrument was also equipped with a silicon-crystal prism for terahertz attenuated total reflection (ATR) spectroscopy for liquid samples (especially for liquid samples bearing a high absorption in the terahertz range, such as water), in which terahertz wave emitter and detector modules are combined in a single piece with the ATR prism. In these systems, dielectric measurements were performed at a temperature of T = 25 °C (accuracy of ±0.1 °C) using a temperature control unit made with a Peltier device. The uncertainty of the used THz spectrometer was less than 5.0% over the measuring frequency range in accordance with a specification given by Hamamatsu Photonics K.K.

5.3. Results and Discussion

5.3.1. EC/Bz System

Some typical dielectric spectra (ε' and ε'' vs. ω) for the EC/Bz system, which ranged from c = 0 M (Bz) to 4.78 M over a wide frequency region up to $\omega = 1.88 \times 10^{13}$ s^{-1}, are shown in Fig. 5.1. The solvent Bz has no significant dielectric dispersion in the ω region except for a small resonance-type peak[24] that was barely observed and only then in the imaginary part of the data (ε''_{Bz}) near $\omega = 8 \times 10^{12}$ s^{-1}. Therefore, all of the signals were observed in a moderate to concentrated c data range, as seen in Fig. 5.1, and correspond to dielectric dispersions generated by the EC molecules. Very recently, it has been reported that Bz, a typical non-polar liquid, exhibits a small but obvious resonance-type dielectric dispersion in the THz range, and a discussion on the origin of this dielectric dispersion was presented.[24] Because the terahertz range spectrometer used in this study was designed for dielectric measurements of highly absorbing liquid samples, such as water and alcohols, the obtained ε'' data for Bz were too small to be detected precisely and were considerably scattered. However, the presence of a weak dielectric dispersion in pure Bz was clearly confirmed even in the rather scattered data shown in Fig. 5.1.

The Cole–Cole[25] and Cole–Davidson[26] equations useful to describe the distribution of dielectric relaxation modes were applied to (so-called Cole–Cole) plots between ε' and ε'' data to determine the type of the distribution of dielectric relaxation modes. The fit of the Cole–Cole equation to the data for the EC/Bz system seemed insufficient especially at moderate to high c values. On the other hand, the Cole–Davidson equation was reasonably fit and asymmetric broadening factors (β) for the equation were determined successfully depending on the c value for the system. The determined value of β varied from 0.80–0.85 (c = 0.10 M) to 0.74 (c = 4.78 M) for the EC/Bz system as shown in Fig. 5.1. The reason for the reasonable applicability of the Cole–Davidson equation[26] at higher

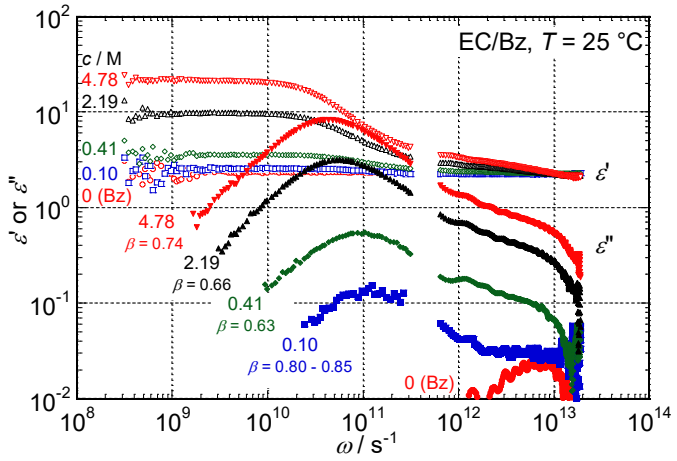

Fig. 5.1. Typical dielectric spectra ε' and ε'' vs. ω of the EC/Bz system for several concentrations from 0 to 4.78 M and at 25 °C. The values of β represent asymmetric broadening factors determined *via* the Cole–Davidson equation[26] for each spectrum

concentrations is the evidential presence of minor relaxation modes at frequencies higher than that for the major relaxation mode, which will be described as modes 1 and 2 later. In this study, the Debye-type relaxation model containing necessary numbers of relaxation modes was employed to describe the distribution of relaxation modes in both the EC/Bz and EC/DMC systems.

From an overview of the concentration dependence of the dielectric spectra shown in Fig. 5.1, it is evident that EC has at least two Debye-type dielectric relaxations at $\omega = 4.0 \times 10^{10}$ and 1.0×10^{11} s^{-1} in the lower ω range, and that the magnitudes of these relaxation modes altered as the concentration c was changed. When the c value decreased to a highly dilute value of 0.10 M, EC exhibited a quite small dielectric relaxation mode at $\omega = 4.0 \times 10^{10}$ s^{-1}, but did exhibit a relaxation mode only at $\omega = 1.0 \times 10^{11}$ s^{-1}. The relaxation intensity observed at $\omega = 4.0 \times 10^{10}$ s^{-1} relative to that at $\omega = 1.0 \times 10^{11}$ s^{-1} appears to grow with increasing c. Then, it is likely that the relaxation mode observed at the higher $\omega = 1.0 \times 10^{11}$ s^{-1} corresponds to a rotational relaxation mode of the isolated monomeric EC molecules in Bz. The origin of the relaxation mode observed at the lower frequency of $\omega = 4.0 \times 10^{10}$ s^{-1} is an open question at present. One of the proposed, but not established, assignments is a dissociation process of the anti-parallel dimers $(EC)_2$, which bear a total dipole moment of zero due to the cancelling anti-parallel dipole configuration, and demonstrates a dielectric relaxation process at the onset of dimer dissociation.[18,27–29] Such an assignment for the slower dielectric relaxation mode, which is called a dissociation model in this study, has also been given to the dissociation process of anti-parallel dimers in typical polar liquids such as dimethylsulfoxide, benzonitrile, nitrobenzene and 4-cyano-4′-alkybiphenyls, and

equilibrium constants for the anti-parallel dimer formation in the polar liquids were evaluated *via* the population analysis of each component, which resulted from DS data.[18,27–29]

All of the obtained dielectric spectra were decomposed into three Debye-type relaxation modes and a resonance-type mode, as given by eqn 5.1, *via* curve-fit procedures,

$$\varepsilon' = \sum_{j=1}^{3} \frac{\varepsilon_j}{1+\omega^2\tau_j^2} + \frac{E_1\omega_1^2\left(\omega_1^2-\omega^2\right)}{\left(\omega_1^2-\omega^2\right)^2+\omega^2\gamma_1^2} + \varepsilon_{\infty 0}$$
$$\varepsilon'' = \sum_{j=1}^{3} \frac{\varepsilon_j\omega\tau_j}{1+\omega^2\tau_j^2} + \frac{E_1\omega_1^2\omega\gamma_1}{\left(\omega_1^2-\omega^2\right)^2+\omega^2\gamma_1^2} \qquad (5.1)$$

where ε_j and τ_j represent the Debye-type relaxation strength and time of mode j, and where E_1, ω_1, and γ_1 represent resonance strength, frequency and damping factor, respectively. The results of the decompositions for two samples at c = 0.10 and 4.78 M are shown in Figs. 5.2(a) and 5.2(b) as typical examples of dilute and concentrated samples. In Fig. 5.2(a), the dielectric loss difference ($\Delta\varepsilon'' = \varepsilon'' - \varepsilon''_{Bz}$) is shown instead of the sample ε'' to demonstrate the (pure) dielectric contribution of EC in the dilute Bz solution with c = 0.10 M. Because the real part (ε'_{Bz}) of pure Bz has very little dispersion dependent ω, one does not have to modify the ε' data of the system, as was done for ε''. The obtained dielectric (difference) spectra were reasonably decomposed into three Debye-type relaxation processes that were observed at $\tau_1 = 5.0 \times 10^{-13}$ s, $\tau_2 = 9.0 \times 10^{-12}$ s, and $\tau_3 = 2.0 \times 10^{-11}$ s and at a relatively sharp resonance mode at $\omega_1 = 1.5 \times 10^{13}$ s^{-1}, as shown in Fig. 5.2(a). Because the

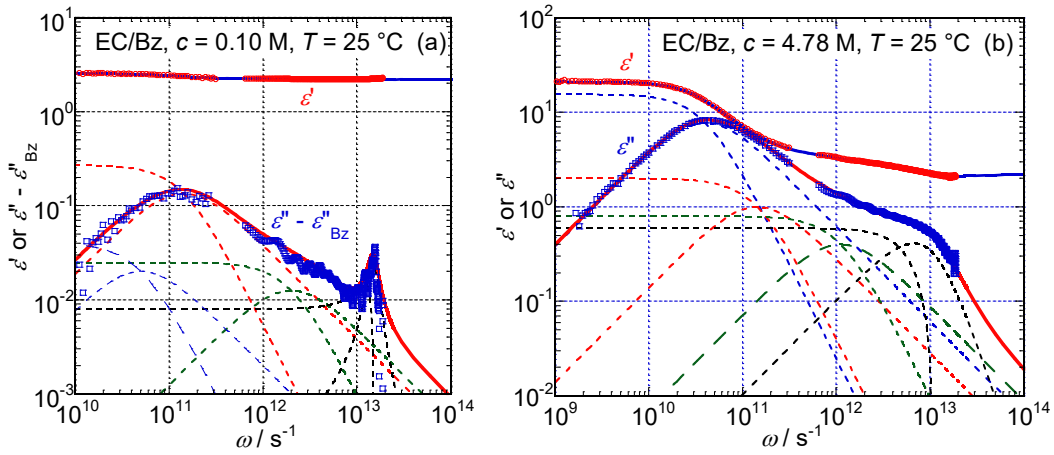

Fig. 5.2. The fitted (solid lines) and experimental dielectric spectra for the EC/Bz system at c = 0.10 M (a) and 4.78 M (b). The constituent Debye-type relaxation and resonance-type components (dotted lines) are also shown. In the case of (a), a differential dielectric loss curve $\varepsilon'' - \varepsilon''_{Bz}$ is shown as an experimental plot to emphasize the essential contribution of EC molecules in dilute Bz solutions.

concentration of c = 0.10 M was too low to form an appreciable amount of anti-parallel dimers, even in Bz,[12] the dielectric parameters of modes j = 1 and 2 are of those for isolated monomeric EC molecules. According to previous vibrational spectroscopic studies,[30] a ring puckering vibrational mode of EC is observable at *ca.* 4.1 × 10^{13} s^{-1} (*ca.* 215 cm^{-1}), therefore, the relatively sharp resonance-type mode observed at ω_1 = 1.5 × 10^{13} s^{-1} (80 cm^{-1}) is attributed to the librational mode of EC in Bz.[15] The observed major and minor relaxation modes are assigned to an overall rotational mode and a fast in plain relaxation process with a small amplitude of isolated EC molecules. The reason for the deviation of fit curve from ε'' data observed in a frequency range higher than ω = 1.5 × 10^{13} s^{-1} seen in Fig. 5.2(a) would be the neglect of an inertia effect in the Debye-type relaxation mode in a high frequency range, which is necessary for more quantitative consideration.[31]

As shown in Fig. 5.2(b), in the concentrated regime with c = 4.78 M, the dielectric contribution of Bz is small and negligible. Consequently, the obtained dielectric spectra essentially demonstrate the contribution of (pure) EC molecules. The three relaxation modes τ_1 = 9.0 × 10^{-13} s, τ_2 = 7.0 × 10^{-12} s, and τ_3 = 2.5 × 10^{-11} s and a broad resonance-type mode at ω_1 = 1.05 × 10^{13} s^{-1} were necessary to reproduce the dielectric spectra. In this solution, EC exists as a mixture of monomeric EC molecules and anti-parallel dimers, and the additional τ_3 relaxation mode is attributed to the contribution of the dimers, as described above. Then, the dielectric parameters of the fastest Debye-type relaxation mode (j = 1) and the resonance-type ω_1 mode for a moderate to concentrated Bz solution are the average values of the monomeric EC and the anti-parallel dimers $(EC)_2$, which depend on the EC concentration c. Here, one might easily conclude that isolated monomeric EC molecules (*cf.* Fig. 5.2(a)) possess a much sharper resonance-type librational mode than EC molecules forming anti-parallel dimers $(EC)_2$.

If one knows the exact intrinsic magnitude of the dipole moment, $|\boldsymbol{\mu}_0|$, for an EC molecule, then the determined dielectric parameters, such as ε_0 (= ε_1 + ε_2 (+ ε_3) + ε_∞) and ε_∞ (= ε_0 + E_1), allow one to calculate the Kirkwood correlation factor, g_K, for the EC/Bz solution as a function of c *via* eqn 5.2,

$$g_K = \frac{9(\varepsilon_0 - \varepsilon_\infty)(2\varepsilon_0 + \varepsilon_\infty)\varepsilon_v k_B T}{\varepsilon_0(\varepsilon_\infty + 2)^2 10^{-3} c N_A \boldsymbol{\mu}_0^2} \qquad (5.2)$$

where $10^{-3}c$, N_A, ε_v, and k_BT represent the molar concentration of molecules in units of mol cm^{-3}, Avogadro's number, the electric permittivity in a vacuum and the product of the Boltzmann constant and the absolute temperature, respectively.[17] A value of $|\boldsymbol{\mu}_0|$ = 5.2 D provided the relationship g_K = 1,

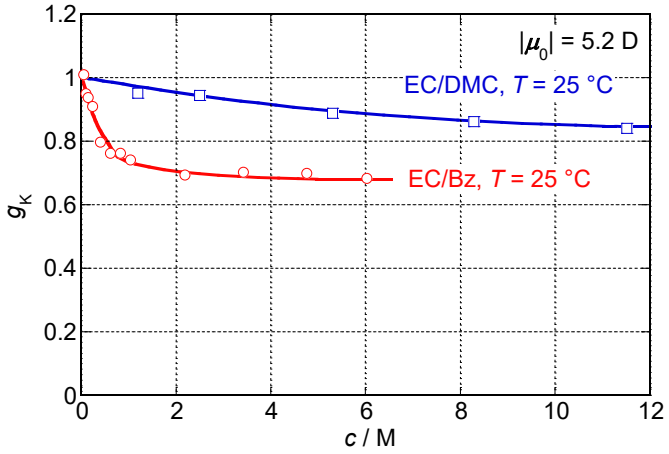

Fig. 5.3. Concentration c dependence of the Kirkwood correlation factors g_K for the EC/Bz and EC/DMC systems.

obtained by extrapolation to c = 0, which means there was no orientational correlation between the dipoles of the EC molecules. Therefore, the c dependence of g_K was calculated assuming the $|\boldsymbol{\mu}_0|$ value and is shown in Fig. 5.3. The value of $|\boldsymbol{\mu}_0|$ = 4.8–4.9 D,[19,20] which has been widely accepted so far, provided an illogical relationship, where $g_K \approx 1.2$ at c = 0. Thus, the value of $|\boldsymbol{\mu}_0|$ = 5.2 D, which coincides well with that determined by careful microwave experiments,[21] seems to be correct for EC in the isolated monomeric state. The g_K value close to 0.7, which was obtained in a c range higher than 2.0 M (Fig. 5.3), strongly suggests that the EC molecules possess an anti-parallel interaction between their dipoles and form the anti-parallel dimers, $(EC)_2$, especially in the moderate to concentrated range.

The c dependence of Debye-type relaxation times and strengths, τ_j and ε_j (j = 1 to 3), for the EC/Bz solution is shown in Figs. 5.4(a) and 5.4(b). The value of τ_2, which was *ca.* 9×10^{-12} s and possessed a weak c dependence, suggests that the rotational relaxation time of monomeric EC molecules in Bz is hardly influenced by an increase in c. In the simplest case, the rotational relaxation time of solute molecules is proportionally controlled by the product of the effective hydrodynamic volume of a solute molecule and the viscosity of solvent liquid.[32] However, it is well known that the rotational relaxation time of solute molecules is proportional to the macroscopic viscosity of solution, when the concentration of a solute molecule is rather high. Because the solubility of EC in Bz is not high, *ca.* 6.1 M (50 wt%) at 25 °C, the examined concentration range in this study seems to be that the rotational relaxation time of monomeric EC molecules is simply proportional to the viscosity of Bz. In the EC/Bz system, viscosities were determined at 25 °C using an Ubbelohde-type capillary viscometer to be *e.g.*, 0.61, 0.66, and 0.84 mPa s at c = 0.1, 1.0, and

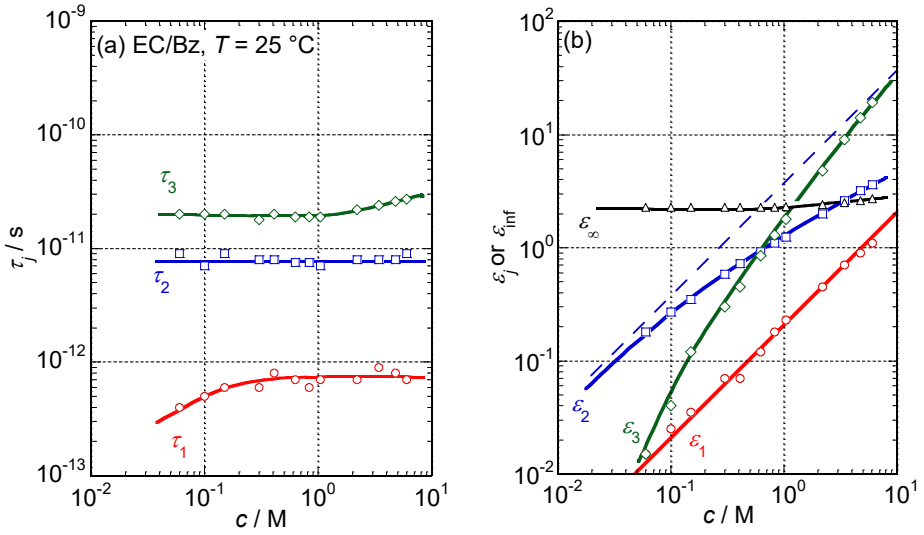

Fig. 5.4. Concentration c dependence of the relaxation times τ_j (j = 1 to 3) (a) and strengths ε_j (j = 1 to 3 and ∞) (b) of the constituent relaxation modes for the EC/Bz system at 25 °C. A broken line in (b) represents a constant of proportionality, α = 3.9, for the relationship $\varepsilon_2 = \alpha \cdot c$ in the dilute regime.

4.8 M, respectively, and were not so dependent on the concentration c. This observation reveals that the rotational relaxation mode of EC molecules is simply controlled by the inner viscosity essentially identical to the solvent, Bz, viscosity: *ca.* 0.60 mPa s.[33] Dielectric data showing the constant τ_2 value of *ca.* 9×10^{-12} s as seen in Fig. 5.4(a) confirmed such consideration. The value of τ_3 was *ca.* 2×10^{-11} s and weakly dependent on c. According to the previously proposed dissociation model,[18,27–29] the value of τ_3 corresponds to the lifetime of anti-parallel dimers $(EC)_2$ formed in the EC/Bz system. Then, the magnitudes of relaxation strengths ε_2 and ε_3 are related to the populations of monomeric EC molecules and the formed dimers. Therefore, an ε_3 that is markedly smaller than ε_2 and the proportionality between ε_2 and c confirmed that in the dilute c range seen in Fig. 5.4(b) the EC molecules exist mainly in the form of monomeric EC. On the other hand because the value of ε_3 appears to be proportional to c in the concentrated regime, as seen in Fig. 5.4(b), the amount of anti-parallel dimers is proportional to c in this range in accordance with the dissociation model.[18,27–29]

It is worth noting that the fastest relaxation mode, j = 1, was assigned to a small amplitude fast relaxing mode at $\tau_1 \approx 8 \times 10^{-13}$ s, which slightly increased and approached a constant value with increasing c, for each EC molecule belonging to either the isolated monomeric or the anti-parallel dimeric state. Then, ε_1 is clearly proportional to c over the entire examined c range and is proportional irrespective of the formation of anti-parallel dimers, as seen in Fig. 5.4(b).

The ε_2 value was proportional to c only in the dilute regime as $\varepsilon_2 = A \cdot c$, where A = 3.9 M^{-1} is a constant of proportionality given by the (broken) straight line drawn in Fig. 5.4(b). For an initial approximate method, this proportional relationship was used to quantify the population of monomeric EC molecules. Then, the concentration of isolated monomeric EC ([EC]) was evaluated using the relationship [EC] = ε_2 $(A)^{-1}$ even in a moderate to concentrated regime in which an additional relaxation mode, j = 3, was clearly observed. Here, the author simply assumes a chemical equilibrium process for the anti-parallel dimer formation of EC: 2EC ↔ $(EC)_2$. Then, the equilibrium constant for this process is given as $K_d^{DS} \equiv [(EC)_2] \cdot [EC]^{-2}$. Because the relationship c = [EC] + 2[$(EC)_2$] holds in the chemical process, the concentration of anti-parallel dimers is given by the equation [$(EC)_2$] = (c − [EC])/2. Consequently, the equilibrium constant K_d^{DS} can be calculated from the magnitude of dielectric strength ε_2 as a function of the concentration, c,

$$K_d^{DS} \equiv \frac{A(Ac - \varepsilon_2)}{2\varepsilon_2^2}. \qquad (5.3)$$

Here, K_d^{DS} was determined from the ε_2 data seen in Fig. 5.4(b) for the EC/Bz system and is shown as a function of c in Fig. 5.5(a). Whereas, the mole fraction of dimer forming EC molecules given by $f_d = 1 - \varepsilon_2 \cdot (Ac)^{-1}$ is shown in Fig. 5.5(b). Over the c range examined, K_d^{DS} showed a weak c dependence and a constant value of *ca.* 3 M^{-1} in the moderate to concentrated range. The dimer forming mole fraction, f_d, was less than 0.1 in the low c range, while more than 80% of the EC molecules existed as anti-parallel dimers in the c range higher than 3.0 M, as observed in Fig. 5.5(b).

Moreover, the value of ε_3 should be proportional to [$(EC)_2$] as given by $\varepsilon_3 = B[(EC)_2]$ in accordance with the dissociation model.[18,27–29] Then, the proportionality constant B can be described as $B = 2\varepsilon_3 \cdot \{c - \varepsilon_2 \cdot (A)^{-1}\}^{-1}$ irrespective of the c value. However, the calculated B values were not constant, but varied from *ca.* 4.1 M^{-1} (at c = 1.0 M) to 7.6 M^{-1} (at c = 6.0 M). Because this non-constant B value is illogical, one concludes that the first approximate analytical method using a constant A value is inadequate.

In accordance with eqn 5.2, when the value of ε_∞ in an examined system alters, the dielectric increment $\varepsilon_0 - \varepsilon_\infty$ is not observed as a constant value even if both the g_K and c are kept constant. Nevertheless, one can calculate the concentration of monomeric EC molecules [EC] from the experimental ε_2 and ε_∞ values *via* eqn 5.2 by assuming the contribution of the monomeric EC only under the condition of g_K = 1. Here, the author proposes the second method to evaluate K_d^{DS} and f_d as functions of c. By substituting the constants of g_K = 1 and $|\boldsymbol{\mu}_0|$ = 5.2 D and the value of $\varepsilon_0 = \varepsilon_2$ +

ε_∞ observed at each c examined into eqn 5.2, the value of [EC] was calculated in the units of mol cm^{-3} instead of $10^{-3}c$. Then, the K_d^{DS} and f_d that were determined by the second method were also plotted as functions of c in Fig. 5.5(a). Although A and B values were not constant over the wide c range and depended on a substantial change in the ε_∞ value, as described above, the ratio of B to A calculated in this method was kept at an approximately constant value of 1.1 over the examined c range. This result strongly suggests that the second method to evaluate K_d^{DS} and f_d is more reliable than the first one.

The K_d^{DS} value that resulted from the second approximate method showed a weak c dependence, as seen in Fig. 5.5(a). Although the difference between K_d^{DS} values that resulted from the two methods seemed small at low c, the value from the second method became three times as large as that from the first method in the high c range side, and the f_d value calculated from the second method rises at a slightly faster rate than that from the first method. However, one might claim that the essential c dependence of K_d^{DS} for EC in Bz is not a strong function of c and possesses a value of 2 to 7 M^{-1} over a wide c range.

Now, we compare the c dependence of K_d^{DS} for EC in Bz determined using the DS method in this study with that of K_d^{RS} determined using Raman spectroscopic, RS, techniques in the previous study.[12] Because the K_d^{RS} has a weak c dependence and increases from *ca.* 3 (c = 0.1 M) to 6 M^{-1} (6 M), as shown in Fig. 5.5(a), the c dependencies of K_d^{DS} and K_d^{RS} are in (semi-) quantitative agreement. Consequently, the author concludes that EC forms anti-parallel dimers and the kinetics

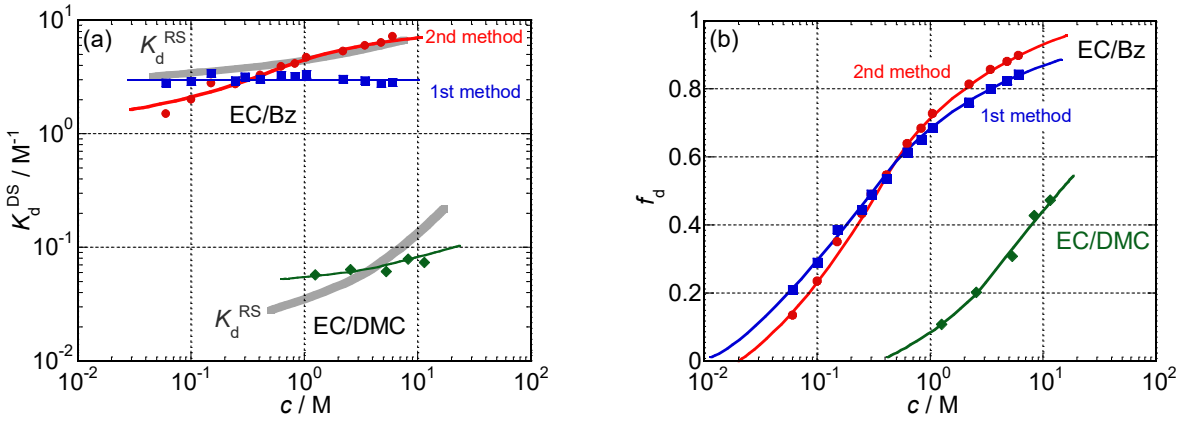

Fig. 5.5. Concentration c dependence of the obtained equilibrium constants for anti-parallel dimer formation K_d^{DS} (a) and the molar fraction of anti-parallel dimers f_d (b) for the EC/Bz and EC/DMC systems at 25 °C. Bold solid lines in (a) represent previously obtained K_d^{RS} values for both systems using Raman scattering techniques.

of the dimer forming process is governed by the equilibrium constant K_d^{DS} (and K_d^{RS}), which possesses a value ranged from 2 to 7 M^{-1} and is weakly dependent on c.

5.3.2. EC/DMC System

The dielectric spectra for the EC/DMC system, which ranged from c = 0 M (DMC) to 11.51 M over a wide frequency region up to $\omega = 1.88 \times 10^{13}$ s^{-1}, are shown in Fig. 5.6. As clearly shown in this figure, DMC possesses a marked dielectric dispersion over the entire ω range examined because of its small permanent dipole moment of 0.91 D,[34,35] which is due to a *cis–cis* conformation in liquid state. As a result, the contribution of DMC to the dielectric spectra for the EC/DMC system is not negligible, especially in a dilute regime. However, the dielectric spectra observed in the moderate to concentrated c range in Fig. 5.6 correspond to dielectric dispersions generated by EC molecules bearing a much larger dipole moment of 5.2 D. Major Debye-type relaxation modes observed at $\omega = 10^{10} - 3 \times 10^{10}$ s^{-1} increased the magnitudes of the relaxation strengths and altered the distribution of relaxation times with increasing concentration c, as was also observed in the EC/Bz system (Fig. 5.1).

The obtained dielectric spectra in the EC/DMC system were readily decomposed into three (or two) Debye-type relaxation modes and a resonance-type mode, as given by eqn 5.1, even in the case of DMC at c = 0 M. In accordance with the previous vibrational study for pure liquid DMC,[36] an O–C torsional vibrational mode can be found at *ca.* 3.8×10^{13} s^{-1} (200 cm^{-1}). Thus, the fastest resonance-type mode observed at 1.0×10^{13} s^{-1} in DMC (Fig. 5.6) was assigned to the librational mode of DMC molecules in the pure liquid state. The major and minor Debye-type relaxation modes were found at $\tau_2 = 8.5 \times 10^{-12}$ s and $\tau_1 = 1.5 \times 10^{-12}$ s, respectively, and were attributed to rotational relaxation modes around two different molecular axes. In addition to this, the minor fast τ_1 mode is possibly caused by the intramolecular motion of DMC molecules.

The decomposition results for two typical samples, a dilute sample at c = 1.24 M and the most concentrated one at c = 11.51 M, are shown in Figs. 5.7(a) and 5.7(b), together with spectra of the constituent relaxation and resonance modes. As mentioned above, the contribution of DMC to the observed dielectric spectra was not small in the case of dilute samples. To accurately quantify the dielectric spectra ($\varepsilon'_{EC}{}^{P}$ and $\varepsilon''_{EC}{}^{P}$) that resulted from (pure) EC molecules in the EC/DMC system, the c dependent dielectric contributions of (solvent) DMC were evaluated from the dielectric data ($\varepsilon'_{DMC} - \varepsilon_{DMC\infty}$ and ε''_{DMC}) of pure DMC as $\phi_{DMC} \cdot (\varepsilon'_{DMC} - \varepsilon_{DMC\infty})$ and $\phi_{DMC}\varepsilon''_{DMC}$, where ϕ_{DMC} represents the volume fraction of DMC in solution and were subtracted from the ε' and ε'' data

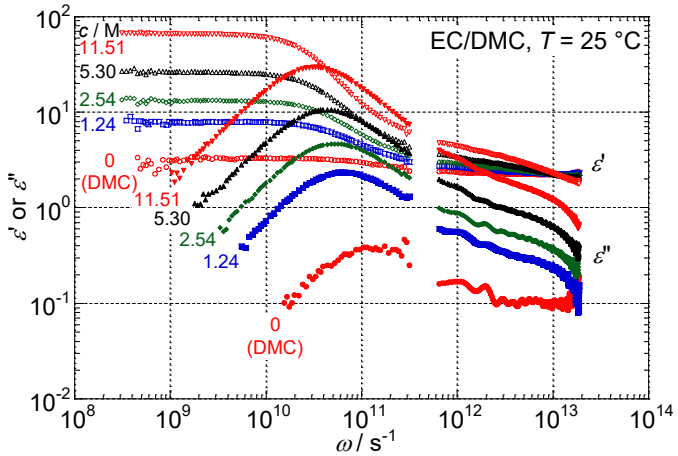

Fig. 5.6. Dielectric spectra for the EC/DMC system at several concentrations from 0 to 11.51 M and at 25 °C.

of sample solutions assuming no interaction between EC and DMC molecules. The obtained dielectric difference, $\varepsilon'_{EC}{}^{P} = \varepsilon' - \phi_{DMC}\cdot(\varepsilon'_{DMC} - \varepsilon_{DMC\infty})$ and $\varepsilon''_{EC}{}^{P} = \varepsilon'' - \phi_{DMC}\varepsilon''_{DMC}$ for a sample solution at c = 1.24 M were decomposed into two Debye-type relaxation modes and a resonance-type mode using eqn 5.1, as shown in Fig. 5.7(a). In the case of Fig. 5.7(b), the concentration of DMC, 2.87 M, was much lower than that of EC, 11.51 M, and the dielectric spectra were essentially identical to the pure contribution of EC molecules dissolved in DMC. The large dielectric dispersion observed on the lower ω side was decomposed into two distinct relaxation modes at $\tau_2 = 2.4 \times 10^{-11}$ s and $\tau_3 = 5.0 \times 10^{-11}$ s that were attributed to the contributions from the monomeric EC and the anti-parallel dimers $(EC)_2$ in accordance with the dissociation model,[18,27–29] respectively. Then, the magnitude of relaxation strength ε_2 is simply related to the population of monomeric EC, as in the case of the EC/Bz system.

The necessary parameters for the decomposition of the dielectric spectra of the EC/DMC system are shown as functions of c in Fig. 5.8(a): relaxation times, τ_j (and τ_j^{P} necessary for $\varepsilon'_{EC}{}^{P}$ and $\varepsilon''_{EC}{}^{P}$), and Fig. 5.8(b): strengths, ε_j (and ε_j^{P}). The differences between ε_j and ε_j^{P} were small at c greater than 2.5 M, while those at the lowest concentration were significant. The linear relationship between ε_1 (or ε_1^{P}) and c clearly reveals that the fast, small amplitude relaxation mode for EC molecules possesses the same relaxation strength, which is irrespective of the formation of anti-parallel dimers $(EC)_2$, as observed in the EC/Bz system. As discussed above in the EC/Bz system, the rotational relaxation τ_2 of the monomeric EC molecules is proportionally governed by the viscosity of the solvent.[32] Since the solubility of EC in DMC is markedly higher than in Bz, the concentration of EC was more widely changed in the EC/DMC system than in the EC/Bz system.

The value of τ_2 at the highest c of 11.51 M was 1.5 times as long as that observed in a low c side as seen in Fig. 5.8(a). This substantial increase in the τ_2 value with increasing c observed in the EC/DMC systems seems to be related to the rotational relaxation time of solute molecules not being simply governed by the inner viscosity identical to solvent viscosity, but has the influence of an increase in the macroscopic viscosity of solution. Moreover, it is worthy to note that the viscosities of Bz and DMC are close to each other, *i.e.*, *ca.* 0.60 and 0.59 mPa s,[33,37] respectively, at 25 °C. Then, the τ_2 of the monomeric EC should not be so much different in both the EC/Bz and EC/DMC systems, if EC molecules possess not so different effective hydrodynamic volumes in both the systems. However, the value of τ_2 for the EC/DMC is about 1.5 times as long as that of the EC/Bz system (*cf.* Fig. 5.4(a) and Fig. 5.8(a)). This observation reveals that hydrodynamic sizes of EC molecules resulted from the intermolecular interaction between EC and Bz molecules and that between EC and DMC molecules are not identical to each other. The reason for the difference in the intermolecular interaction would be caused by the presence of dipole–dipole interaction existing only between EC and DMC molecules, which will be discussed later again in the frequency dependence of a resonance-type dielectric dispersion. Moreover, the τ_1 value of EC dissolved in DMC was very little dependent on c as seen in Fig. 5.8(a). The minor relaxation mode j = 1 has been already attributed to the fast in-plane relaxation mechanism of EC molecules. This observation well corresponds to the fact that the resonance-type dielectric spectra observed were hardly

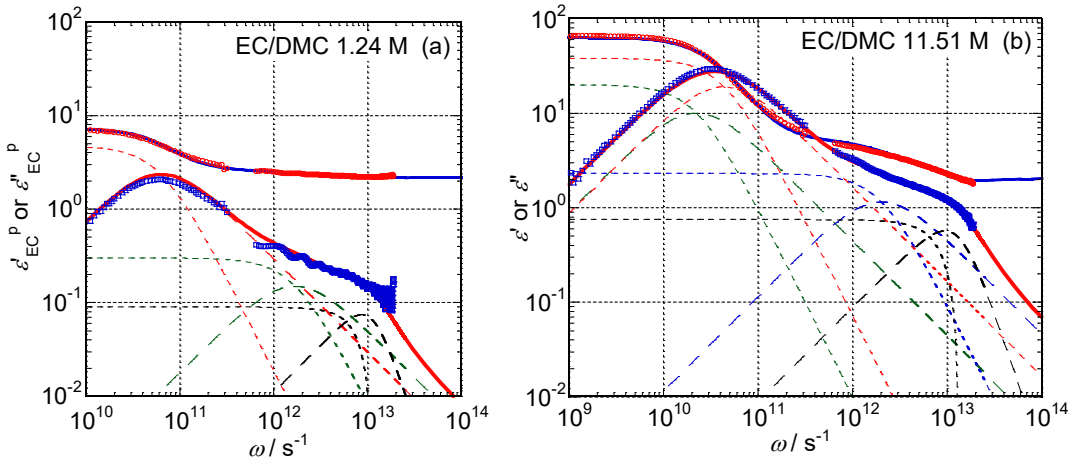

Fig. 5.7. The fitted (solid lines) and the experimental dielectric spectra for the EC/DMC system at c = 1.24 M (a) and 11.51 M (b). Constituent Debye-type relaxation and resonance-type components (dotted lines) are also shown. In the case of (a), the evaluated (pure) dielectric spectra $\varepsilon'_{EC}{}^{P}$ and $\varepsilon''_{EC}{}^{P}$ for EC molecules in the solution are shown as experimental spectra to be fitted (see text).

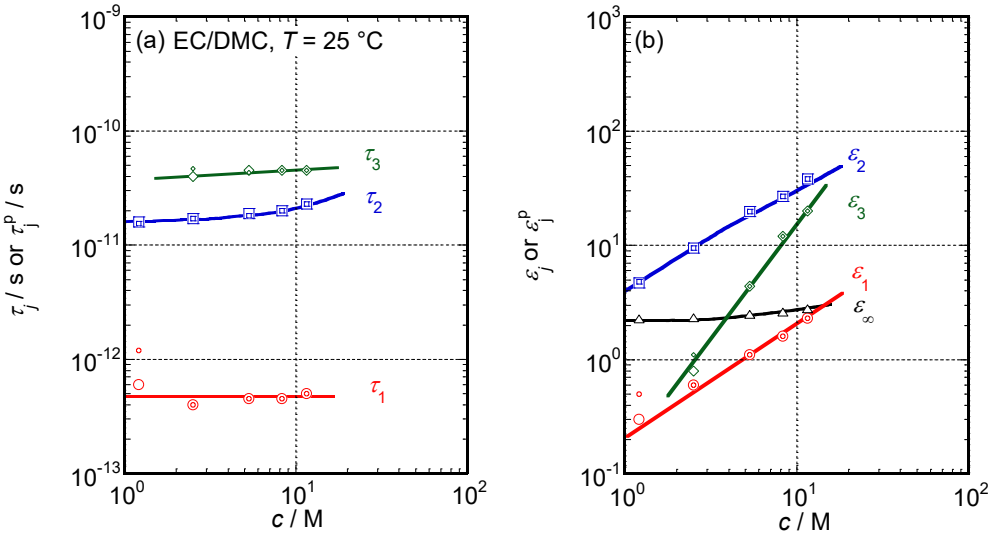

Fig. 5.8. Concentration, c, dependence of the relaxation times τ_j (j = 1 to 3) (a) and strengths ε_j (j = 1 to 3 and ∞) (b) of the constituent relaxation modes for the EC/DMC system at 25 °C. Small and large symbols represent τ_j and ε_j, and τ_j^{P} and $\varepsilon_j^{\mathrm{P}}$, which were obtained from normal dielectric spectra ε' and ε'' and from modified spectra $\varepsilon'_{\mathrm{EC}}{}^{\mathrm{P}}$ and $\varepsilon''_{\mathrm{EC}}{}^{\mathrm{P}}$ of pure EC molecules in solution, respectively.

influenced by the anti-parallel dimer formation in a high c range (*cf.* Figs. 5.7(a) and 5.7(b)).

The concentration c dependence of the Kirkwood correlation factor g_{K} for EC molecules in the EC/DMC system was calculated from the (pure) dielectric contribution of EC, by again assuming $|\boldsymbol{\mu}_0|$ = 5.2 D, is also shown in Fig. 5.3. The g_{K} value naturally approached unity by extrapolation to c = 0 M and decreased down to only 0.86 at the highest concentration, c = 11.51 M. This c dependence of the g_{K} value in the EC/DMC system, which is substantially weaker than that in the EC/Bz system, strongly reveals that the tendency for EC molecules to form anti-parallel dimers $(\mathrm{EC})_2$ in DMC is much weaker than in Bz for the same concentration.

Here, the author calculates the concentration c dependence of the equilibrium constant $K_{\mathrm{d}}^{\mathrm{DS}}$ for the anti-parallel dimer formation from dielectric data, such as ε_2 (or $\varepsilon_2^{\mathrm{P}}$) and ε_∞, for the EC/DMC system according to the same procedure based on eqn 5.3 that was used in the EC/Bz system above. In this system, the more reliable second method to calculate $K_{\mathrm{d}}^{\mathrm{DS}}$ and f_{d} described above was employed. A formula to evaluate [EC] in the units of mol cm^{-3} (instead of $10^{-3}c$) was obtained from eqn 5.2 by substituting the relationship g_{K} = 1, $|\boldsymbol{\mu}_0|$ = 5.2 D and $\varepsilon_0 = \varepsilon_2$ (or $\varepsilon_2^{\mathrm{P}}$) + ε_∞. Then, the values of [EC] and also A were determined at each c examined. The obtained c dependence of $K_{\mathrm{d}}^{\mathrm{DS}}$ is also shown in Fig. 5.5(a) to compare with that for the EC/Bz system. Moreover, the dimer forming mole

fraction of EC molecules f_D in the EC/DMC system is also plotted in Fig. 5.5(b). Because the K_d^{DS} of the EC/DMC system is smaller than that of the EC/Bz by almost two orders of magnitude, the efficiency of anti-parallel dimer formation in DMC is significantly lower than in Bz over the c range examined. The markedly low f_D value in DMC, when compared with that in Bz at the same c (Fig. 5.5(b)), also strongly confirms the lower dimer formation efficiency of EC molecules in DMC.

It is worthy to note that the ratio of B to A, which represent the constants of proportionality relating ε_3 and $[(EC)_2]$ in accordance with the dissociation model,[18,27–29] and ε_2 and [EC], respectively, was a constant value of *ca.* 1.1 irrespective of c. This constant ratio strongly confirms the validity of the assumed basic dimer formation kinetics, $2EC \leftrightarrow (EC)_2$ and that of the analytical procedure used in this study. On the other hand, the equilibrium constant for dimer formation K_d^{RS} that was previously determined using RS for the EC/DMC system changes from 0.04 M^{-1} (c = 3 M) to 0.15 M^{-1} (c = 11 M), depending on the c values, as indicated in Fig. 5.5(a).[12] Because the agreement between the c dependencies of K_d^{DS} and K_d^{RS} seems reasonable, the validity of the anti-parallel dimer forming process assumed in this study is strongly confirmed. Consequently, the author might conclude that EC forms anti-parallel dimers in solution and that the equilibrium of the dimer formation is controllable by choosing the solvent species and tuning the composition.

It is interesting to compare the ω dependencies of the dielectric spectra for EC molecules dissolved in Bz and DMC as they pertain to isolated monomeric EC. Monomeric EC molecules demonstrated a resonance-type of dielectric dispersion in the high ω range for Bz (*cf.* Fig. 5.2(a)) that was sharper than in DMC (*cf.* Fig. 5.7(a)). Although EC molecules are in the same isolated monomeric state in both solvents, some detailed structural conditions related to molecular motions should be different. Because DMC is a slightly polar molecule, there exists a dipole–dipole interaction between EC and DMC molecules. However, there is no dipole–dipole interaction between EC and Bz. Therefore, the interaction time between EC and DMC molecules would be substantially longer than that between EC and Bz. The reason for the broad resonance-type of dielectric dispersion found in the EC/DMC system might be related to long intermolecular interactions and contacts, which generate more events.

It has been well known that the performance of lithium ion secondary batteries is highly influenced by the electrical conductivity of Li^+ cations that are solvated by several numbers of EC molecules in the electrolyte. Therefore, another important chemical process between Li^+ cations and EC molecules that possesses a different equilibrium constant should be considered when concerned with batteries, which is closely related to the chemical process of anti-parallel dimer formation

discussed in this study.

5.4. Conclusions

Ethylene carbonate (EC) is widely used as a dipolar component of electrolytic liquids in many lithium ion secondary batteries and forms anti-parallel dimers ($(EC)_2$) in solutions of pure solvents, such as benzene (Bz) and dimethyl carbonate (DMC), at room temperature. The tendency for anti-parallel dimer formation was accurately evaluated by the equilibrium constant of the chemical process $2EC \leftrightarrow (EC)_2$ using dielectric spectroscopic techniques. The equilibrium constant was remarkably dependent on the solvent species but weakly dependent on the concentration of EC in solution, and the values obtained here agreed reasonably well with an equilibrium constant that was previously determined by Raman scattering techniques. EC molecules formed significantly more anti-parallel dimers in non-polar Bz than in slightly polar DMC at the same concentration, as schematically described in Fig. 5.9.

The dielectric spectra for EC molecules in solutions of both Bz and DMC demonstrated two distinct Debye-type relaxation modes in the frequency region lower than 10^{12} s^{-1}. A faster relaxation mode was assigned to the rotational process of isolated monomeric EC molecules. The chemical equilibrium constant for anti-parallel dimer formation was precisely evaluable from the magnitude of the relaxation strength for the fast relaxation mode that was related to the amount of monomeric EC molecules.

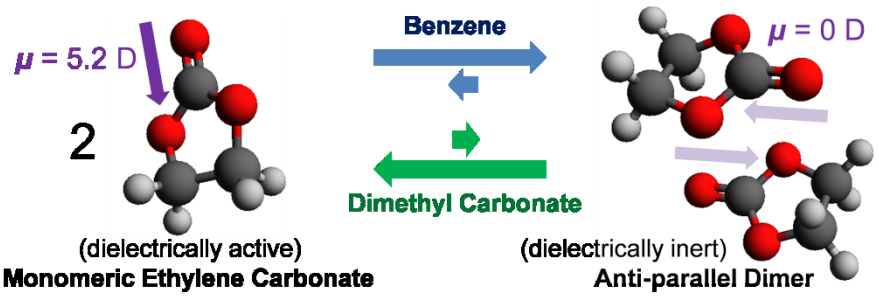

Fig. 5.9. Schematic depiction of the chemical reaction between monomeric EC and anti-parallel dimeric $(EC)_2$.

5.5. References

[1] J.-M. Tarascon, M. Armand, *Nature*, 2001, **414**, 359.

[2] P. G. Bruce, S. A. Freunberger, L. J. Hardwick, J.-M. *Tarascon, Nat. Mater.* 2012, **11**, 19.

[3] D. Aurbach, M. D. Levi, E. Levi, A. Schechter, *J. Phys. Chem. B*, 1997, **101**, 2195.

[4] K. Takei, N. Terada, K. Kumai, T. Iwahori, T. Uwai, T. Miura, *J. Power Sources*, 1995, **55**, 191.

[5] D. Aurbach, B. Markovsky, A. Shechter, Y. Ein-Eli, H. Cohen, *J. Electrochem. Soc.*, 1996, **143**, 3809.

[6] A.-A. G. Shaikh, S. Sivaram, *Chem. Rev.*, 1996, **96**, 951.

[7] B. Schäffner, F. Schäffner, S. P. Verevkin, A. Börner, *Chem. Rev.*, 2010, **110**, 4554.

[8] G.Fini, P. Mirone, B. Fortunato, *J. Chem. Soc., Faraday Trans. 2*, 1973, **69**, 1243.

[9] B. Klassen, R. Aroca, M. Nazri, G. A. Nazri, *J. Phys. Chem. B*, 1998, **102**, 4795.

[10] W. Schindler, T. W. Zerda, J. Jonas, *J. Chem. Phys.*, 1984, **81**, 4306.

[11] P. D. Vaz, P. J. A. Ribeiro-Claro, *Struct. Chem.*, 2005, **16**, 287.

[12] S. Takabatake, N. Sagawa, T. Shikata, *Bull. Chem. Soc. Jpn.*, 2016, **89**, 237.

[13] Y. Wang, P. B. Balbuena, *J. Phys. Chem. A*, 2001, **105**, 9972.

[14] F. Kollipost, S. Hesse, J. J. Lee, M. A. Suhm, *Phys. Chem. Chem. Phys.*, 2011, **13**, 14176.

[15] B. Fortunato, P. Mirone, G. Fini, *Spectrochim. Acta, Part A*, 1971, **27**, 1917.

[16] R. Payne, I. E. Theodorou, *J. Phys. Chem.*, 1972, **76**, 2892.

[17] G. Oster, J. G. Kirkwood, *J. Chem. Phys.*, 1943, **11**, 175.

[18] T. Shikata, N. Sugimoto, *Phys. Chem. Chem. Phys.*, 2011, **13**, 16542.

[19] R. Kempa, W. H. Lee, *J. Chem. Soc.*, **1958**, 1936.

[20] Y. Chernyak, *J. Chem. Eng. Data*, 2006, **51**, 416.

[21] J. L. Alonso, R. Cervellati, A. D. Esposti, D. G. Lister, P. Palmieri, *J. Chem. Soc., Faraday Trans. 2*, 1986, **82**, 357.

[22] K. D. Jordan, F. Wang, Annu. *Rev. Phys. Chem.*, 2003, **54**, 367.

[23] L. B. Silva, L. C. G. Freitas, *THEOCHEM*, 2007, **806**, 23.

[24] C. Rønne, K. Jensby, B. J. Loughnane, J. Fourkas, O. F. Nielsen, S. R. Keiding, *J. Chem. Phys.*, 2000, **113**, 3749.

[25] K. S. Cole, R. H. Cole, *J. Chem. Phys.*, 1941, **9**, 341.

[26] D. W. Davidson, R. H. Cole, *J. Chem. Phys.*, 1951, **19**, 1484.

[27] T. Shikata, N. Sugimoto, Y. Sakai, J. Watanabe, *J. Phys. Chem. B*, 2012, **116**, 12605.

[28] T. Shikata, Y. Sakai, J. Watanabe, *AIP Adv.*, 2014, **4**, 067130.

[29] S. Takabatake, T. Shikata, *Phys. Chem. Chem. Phys.*, 2015, **17**, 1934.

[30] J. R. Durig, J. W. Clark, J. M. Casper, *J. Mol. Struct.*, 1970, **5**, 67.

[31] D. A. Turton, K. Whynne, *J. Chem. Phys.*, 2008, 128, 154516.

[32] P. Debye, *Phys. Z.*, 1912, **13**, 97.

[33] *Handbook of Chemistry and Physics*, 74th ed., ed. by R. L. David, CRC Press, Roca Raton, 1993, pp. 6195.

[34] J.-M. Thiebaut, J.-L. Rivail, J.-L. Greffe, *J. Chem. Soc., Faraday Trans. 2*, 1976, **72**, 2024.

[35] S. K. Reddy, S. Balasubramanian, *J. Phys. Chem. B*, 2012, **116**, 14892.

[36] H. Bohets, B. J. van der Veken, *Phys. Chem. Chem. Phys.*, 1999, **1**, 1817.

[37] A. Rodríguez, J. Canosa, A. Domínguez, J. Tojo, *J. Chem. Eng. Data*, 2003, **48**, 146.

Chapter 6 Summary and Conclusions

In this thesis, the author investigated anti-parallel dimer formation behavior of some highly polar molecules in solution.

In chapter 3, the formation of anti-parallel dimers of liquid crystal forming 4-cyano-4′-alkyl biphenyls (*n*CB, *n* = 5 (pentyl) and *n* = 8 (octyl)) and also not forming ones (*n* = 3 (propyl) and *n* = 4 (butyl)) was confirmed in an isotropic cyclohexane solution (*n*CB–cH). In addition to high frequency dielectric relaxation (DR) measurements up to 50 GHz, steady-state fluorescence emission (FE) experiments in the wavelength range from 280 to 500 nm, and picosecond time-resolved FE measurements were carried out to investigate the molecular dynamics of the *n*CB molecules. The DR spectra of solutions at intermediate to high concentrations were comprised of two dynamic modes. A fast mode with a relaxation time of *ca.* 90 ps was assigned to the free rotations of monomeric *n*CB molecules. The slow mode with a relaxation time of *ca.* 400 ps was attributed to the dissociation process of the anti-parallel dimers ((*n*CB)$_2$). The Kirkwood factor (g_K), a measure of the orientational correlation between the dipole moments of the cyano groups, was markedly less than unity for the slow mode, which demonstrated the formation of anti-parallel dimers, (*n*CB)$_2$. The equilibrium constant for anti-parallel dimer formation in an isotropic solution, *i.e.*, for the reaction, 2*n*CB ↔ (*n*CB)$_2$, which was determined *via* the DR data increased with an increase in the concentration of *n*CB. Under extremely dilute conditions, a sharp fluorescence emission signal attributed to the *n*CB monomer was observed at 324 nm in FE spectrum measurements. However, at the moderate to high concentrations used in the DR measurements where the slow mode was clearly observed, a broad FE signal at 388 nm was observed, which was assigned to excimer emission (including emission from the excited ground state dimers). The relative intensity of the excimer emission to the monomer emission significantly increased with an increase in the concentration. Moreover, the equilibrium constant for the excimer formation reasonably agreed with that for the anti-parallel dimer formation evaluated by the DR data. A lifetime of the excimer, *i.e.*, the reciprocal of the excimer dissociation rate constant was determined to be *ca.* 40 ns *via* time-resolved FE measurements, indicating that the lifetime of the anti-parallel dimer in the excited state is considerably longer than that of in the ground state. Consequently, the results of the FE measurements evidently revealed that excimers of *n*CB and the (*n*CB)$_2$ dimers formed in isotropic solution are identical chemical species.

In chapter 4, the equilibrium constants for the anti-parallel dimer formation of ethylene carbonate

(EC) in solutions of pure solvents, *i.e.*, benzene (Bz) and dimethyl carbonate (DMC), were quantitatively determined at room temperature (25 °C) and various concentrations using Raman scattering (RS) experiments. The strong C=O stretching vibrational band of EC observed at approximately 1800 cm^{-1} split into a monomeric EC signal, and signals assigned to anti-parallel dimers ($(EC)_2$) in the examined solutions. From the concentration dependence of the C=O stretching vibrational signal intensities, the equilibrium constants (K_d^{RS}) of the formation of $(EC)_2$ in the solutions were determined assuming a chemical process, $2EC \leftrightarrow (EC)_2$. Moreover, the fact that the equilibrium constant, K_d^{RS}, substantially depends on the species in the solvent and on the EC composition strongly manifests that the choice of a solvent effectively governs the anti-parallel dimer formation and consequently influences the performance of lithium ion secondary batteries.

In chapter 5, the formation of anti-parallel dimers ($(EC)_2$) of EC in solution is discussed in detail *via* dielectric data determined over a frequency range up to 3 THz. Two major dielectric processes have been identified in both Bz and DMC solutions. The relaxation times were *ca.* 8 and *ca.* 20 ps in Bz, and *ca.* 20 and *ca.* 40 ps in DMC solution for the two relaxation processes, respectively. The population of monomeric EC was evaluated from the strength of the faster relaxation mode assigned to the rotational mode of monomeric EC. Equilibrium constants (K_d^{DS}) for the $(EC)_2$ formation in the two solvents were determined as functions of the concentration at room temperature assuming a process, $2EC \leftrightarrow (EC)_2$. The libration of EC molecules was observed as a sharper resonance signal at *ca.* 1.5×10^{13} s^{-1} when they existed as monomeric EC rather than in the form of $(EC)_2$ in Bz, whereas the signal was not so sharp in DMC. The fact that the determined K_d^{DS} values depended on the solvent; 3–7 M^{-1} in Bz and 0.05–0.1 M^{-1} in DMC, reveals that the choice of solvent governs the efficiency of $(EC)_2$ formation. The K_d^{DS} showed reasonable agreement with the previously determined equilibrium constants, K_d^{RS}, using Raman scattering techniques.

In conclusion, tendency to form anti-parallel dimer of highly polar molecules and its solvent dependence was quantitatively evaluated. Hence, the effects of anti-parallel dimer formation upon the structure of their solutions were revealed, and these results provided the valuable information for the solution structure which will be useful to improve solution properties for practical application.

List of Publications

[1] S. Takabatake, T. Shikata, Evidence of anti-parallel dimer formation of 4-cyano-4′-alkylbiphenyls in isotropic cyclohexane solution, Physical Chemistry Chemical Physics, Vol. 17, Issue 3, 1934-1942, 2015 Jan

[2] S. Takabatake, N. Sagawa, T. Shikata, Quantitative Antiparallel Dimer Formation Analysis of Ethylene Carbonate in Solution, Bulletin of the Chemical Society of Japan, Vol. 89, Issue 2, 237-242, 2016 Feb

[3] N. Sagawa, S. Takabatake, T. Shikata, A Dielectric Spectroscopic Study of Ethylene Carbonate in Solution, Bulletin of the Chemical Society of Japan, Vol. 89, Issue 9, 1018–1025, 2016 Sep